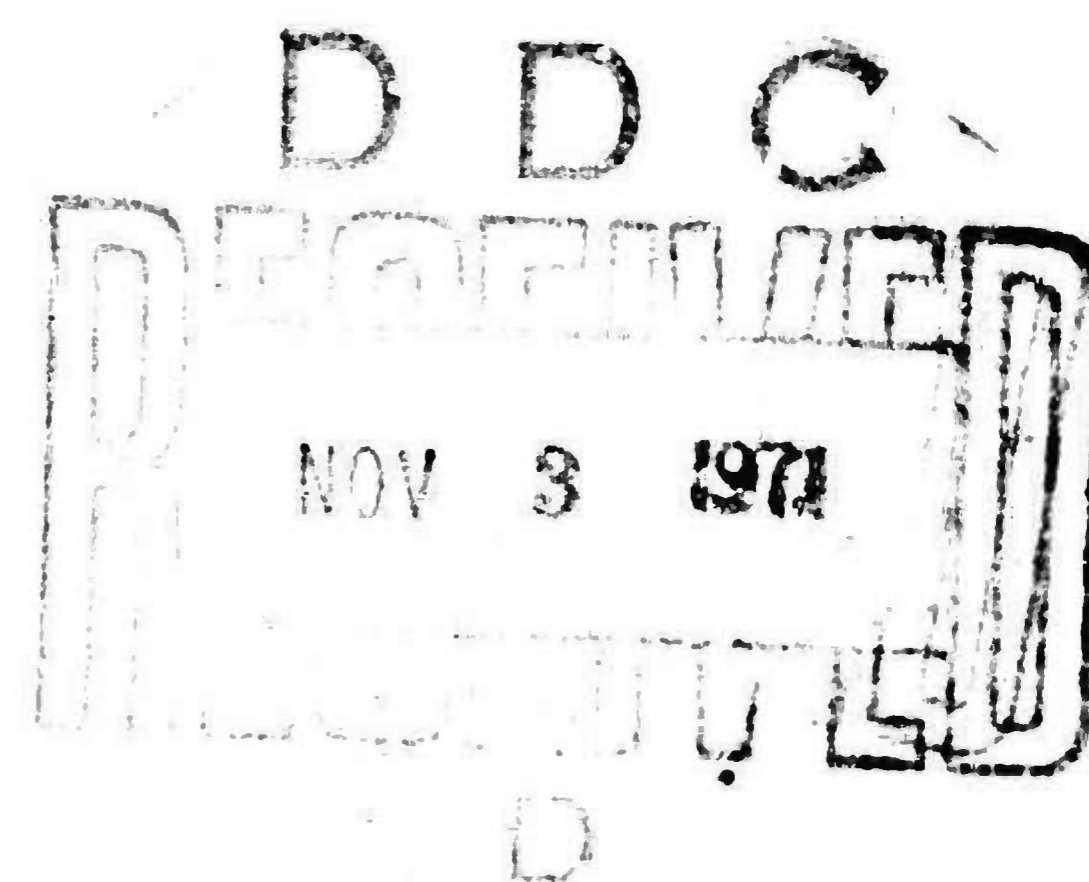AD732027

September 1971

URS 7028-1

Final Report

SIMULATION OF UNDERWATER NUCLEAR BURSTS AT SHALLOW DEPTHS WITH EXPLODING WIRES (U)

Prepared for
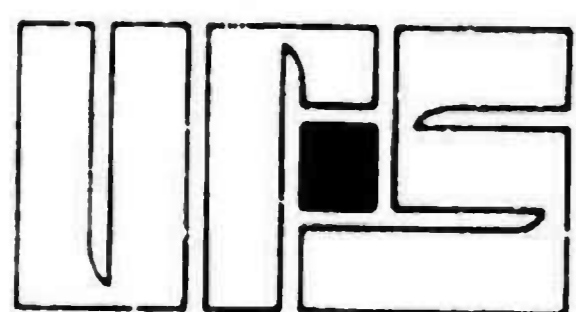
OFFICE OF NAVAL RESEARCH
Department of the Navy
Arlington, Virginia 22217

Contract No. N00014-71-C-0137
NR 089-071/8-31-70(418)

by A.R. Kriebel

DDC

NOV 3 1971

urs research company • 155 bovet road • san mateo, california 94402

DOCUMENT CONTROL DATA - R & D .

(Security classification of title, body of abstract and indexing annotation must be entered when the overall report is classified)

1. ORIGINATING ACTIVITY (Corporate author)	2a. REPORT SECURITY CLASSIFICATION
URS Research Company 155 Bovet Road San Mateo, California 94402	UNCLASSIFIED
	2b. GROUP

3. REPORT TITLE

SIMULATION OF UNDERWATER NUCLEAR BURSTS AT SHALLOW DEPTHS WITH WIRES

4. DESCRIPTIVE NOTES (Type of report and inclusive dates)

Final Report

5. AUTHOR(S) (First name, middle initial, last name)

A.R. Kriebel

6. REPORT DATE	7a. TOTAL NO. OF PAGES	7b. NO. OF REFS
September 1971	135	8

8a. CONTRACT OR GRANT NO.	9a. ORIGINATOR'S REPORT NUMBER(S)
N00014-71-C-0137	URS 7028-1
b. PROJECT NO.	
c.	9b. OTHER REPORT NO(S) (Any other numbers that may be assigned this report)
d.	

10. DISTRIBUTION STATEMENT

Reproduction in whole or in part is permitted for any purpose of the United States Government.

11. SUPPLEMENTARY NOTES	12. SPONSORING MILITARY ACTIVITY
	Office of Naval Research

13. ABSTRACT

Fifty four nearly identical bridge wires were exploded in a vacuum tank near the surface of deep water and in water as shallow as 0.1 in. The deeply submerged wires produced steam bubbles about 4.1 in. in diameter so that the equivalent TNT charge weight was approximately 0.86×10^{-4} lb. The atmospheric pressure was reduced to half the normal value for some of the tests to prevent the column walls from tapering inward. The cavities and water columns were photographically recorded, and the surface waves were measured with a new type of magnetic wave gage.

A distinct upper critical depth effect was observed for the exploding wires, and it was caused by the fact that two types of cavities were produced, those that flared open and those that sprayed upward.

The wave trains calculated from the cavities produced by the wire explosions near the surface of deep water correlate well with the wave gage records, but only about 1 percent of the cavity energy propagated away as surface waves so that all the calculated wave heights were reduced by a factor of about 10 to account for frictional losses associated with the collapsing cavities. The factor is much larger than for large bursts.

14. KEY WORDS	LINK A		LINK B		LINK C	
	ROLE	WT	ROLE	WT	ROLE	WT
water waves						
underwater explosions						
blast simulation						
wave prediction methods						
experimental water wave tank						

CONTENTS

IIE 7028-1

TABLES

ILLUSTRATIONS

ILLUSTRATIONS, cont.

ILLUSTRATIONS, cont.

ILLUSTRATIONS, cont.

ACKNOWLEDGEMENTS

NOMENCLATURE

A_{max} maximum bubble radius (ft)

D_{col} maximum column diameter (ft)

D_{max} maximum cavity diameter (ft)

d   depth of burst (ft)

E_o energy released by explosion (ft-lb)

E_c gravitational energy in initial expanded cavity (ft-lb)

g   gravitational constant (ft/sec^2)

H   peak wave height, trough to crest (ft)

P_a atmospheric pressure (psf, atm, or ft or H_2O)

P_d detonation pressure (psf or atm)

R   wave gage range (ft)

R_c horizontal radius of fully expanded cavity (ft)

R_{col} maximum column radius (ft)

R_o radius of TNT charge (ft)

t   time (sec)

W   equivalent TNT charge weight (lb)

Y   yield of burst (kt = $2 \times 10^6 W_N$)

Z   atmospheric plus hydrodynamic heads at the depth of burst (ft of H_2O)

η_m peak wave amplitude from undisturbed surface (ft)

ρ water density

μ water viscosity

$()_{1,2}$ value of () at first and second wave gage

Section 1
INTRODUCTION

The tests described here are a continuation of a series of experiments
designed and analyzed by URS Research Company, and conducted at the Shock
Hydrodynamic Facility of Engineering - Physics Company (EPCO). The program
is sponsored jointly by the Defense Nuclear Agency (DNA) and the Office of
Naval Research (ONR). The previous test data reported in Ref. 1 consisted of
41 nearly identical wires exploded at heights from 4 in. above to 4 in. below
the surface of a tank of water about 3 ft deep by 6 ft in diameter and under
normal atmospheric pressure. The wire length was about 0.15 in. which
corresponds roughly with the diameter of the equivalent sphere of TNT. The
deeply submerged wires produced spherical bubbles with a maximum diameter
of about 4.1 in. for which the equivalent TNT charge weight is 0.039 gm. The
measured data consisted of:

a. Very high speed photography of the initial expansion of the water
cavities, plumes, water shock waves, and air shock waves

b. Photography of a wave gage board showing the water surface wave
trains at a range of 18 in., and

c. Water shock wave measurements with three miniature piezoelectric
pressure transducers.

A distinct upper critical depth (UCD) effect was observed at a wire depth
of burst of 0.06 in. for which the water surface waves were over twice as
high as those measured for surface bursts or for depths exceeding 0.09 in.
This was the first time that the UCD effect had been observed for other than
HE explosions and under conditions where the hydrodynamic causes of the
effect could be studied in detail to check the results of previous theoretical
analysis (e.g., Ref. 2). It was found that the surface waves scaled reasonably
well with those obtained previously with HE charges ranging in yield from
$1/2$ to 10^6 lbs of TNT, and that the wave trains also agreed reasonably well
with those calculated from the initial cavity shape by the Kranzer-Keller
theory after an energy loss coefficient was incorporated to account for fric-
tional losses associated with the collapse of the cavity.

1

The main purposes of the additional tests to be described here were to:

1. Obtain slower and longer duration photography of the motion of the water cavity to determine the cause for the upper critical depth

2. Reduce the atmospheric pressure to half the normal value to better simulate the hydrodynamics of underwater nuclear bursts in deep water

3. Use electronic surface wave gages recently invented, patented, and developed at EPCO

4. Reduce the water depth and atmospheric pressure to scale three nuclear bursts and one Mono Lake HE test.

A total of 43 shots with 11 additional repeat shots were fired near the surface of deep water (with the depth of burst less than 0.2 in.) and in shallow water (ranging in depth between 0.073 and 5.50 in.).

Section 2
TEST FACILITY, INSTRUMENTATION, AND SCALING PROCEDURE

2.1 TEST FACILITY

The test facility was essentially the same as described in Ref. 1, and
only supplementary information will be given here. The tank is practically
cylindrical, 6 ft in diameter by 6 ft long, with the axis vertical, and nearly
half filled with water. Each exploding bridge wire is welded to the ends of
two prongs (or needles about 1 1/4 in. long and spaced about 1 8 in. apart).
These project from the end of a 1/2 in. diameter cylindrical probe as shown
in the following sketch.

← 1/2 in. dia probe

#40 Nichrome wire ≃ .003 in. diameter
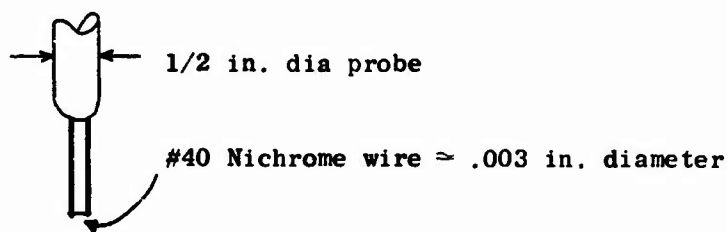
Sketch A - Configuration of Exploding Bridge Wire

The nominal electrical discharge for all of the tests originated from a 15
microfarad capacitor charged to 15 kv. The stored electrical energy was
1690 joules = 404 calories = 1240 ft-lb, corresponding to the energy released
by a TNT charge weighing 0.404 gm = 0.89×10^{-3} lb.

The energy delivered to the water was calculated in Ref. 1 from well-
known equations relating the radius of a submerged expanded bubble to the
explosive yield. For 11 wires exploded between 1 and 4 in. below the water
surface under normal atmospheric pressure, the maximum radius of the
expanded bubble ranged between 1.87 and 2.26 in. (or 2.07 ± 10 percent as shown
in Table 2 of Ref. 1). This corresponded with an average nuclear yield of 0.046
gm (or a TNT yield of 0.039 gm) as given by Eqs. (1) and (2) of Ref. 1. Thus the
equivalent TNT yield is less than one-tenth as large as that corresponding to
the stored electrical energy, and most of the stored energy is dissipated in
the electrical circuit and switch.

3

It is interesting to note that the diameter of the equivalent TNT sphere is 0.14 in., which is roughly equal to both the length of the exploding bridge wire and the diameter of the sphere of plasma shown in the earliest photographs of the explosion (e.g., Fig. 7, Ref. 1). For all of the tests the exploding wires were located near the center of the tank. Normally, the wire axis was horizontal and the probe axis extended vertically upward from the wire, as shown in the previous sketch. However, a few tests were run with other orientations, specifically to determine the effect of the probe on the test results.

The air in the upper half of the tank was at normal atmospheric pressure for about half of the tests, but the others were run at one-half atmosphere to improve the simulation of large explosions at shallow depth.

A false bottom was added to the facility for some of the recent tests to reduce the effective water depth and simulate one large HE and three nuclear explosions, as described in Subsection 4.5. The bottom consisted of a 3/4-in. thick aluminum plate with the configuration shown in the following sketch. Two wave gages were positioned just beyond the edge of the plate as indicated at ranges of 10 and 20 in. For all of the tests in deep water (without the plate), the gage ranges were 9 and 18 in.

2.2 INSTRUMENTATION

The instrumentation was expanded and improved for the recent test series in the following ways. In addition to the Dynafax (35 mm) framing camera running at 25,000 frames per second, the cavity was photographed by a Redlake (16 mm) camera running at 2,500 frames per second to record the collapse and subsequent motions of the water cavity as well as its initial expansion and the generation of air and water shock waves. Both cameras viewed the cavity by means of a beam splitter and a schlieren optical system which projected a 9.5 in. diameter beam of light across the tank horizontally. The water surface waves were measured with two magnetic wave gages rather than by photography of a wave gage board as before. Each gage consisted of two vertical cylinders protruding through the water surface. The cylinders were spaced

4
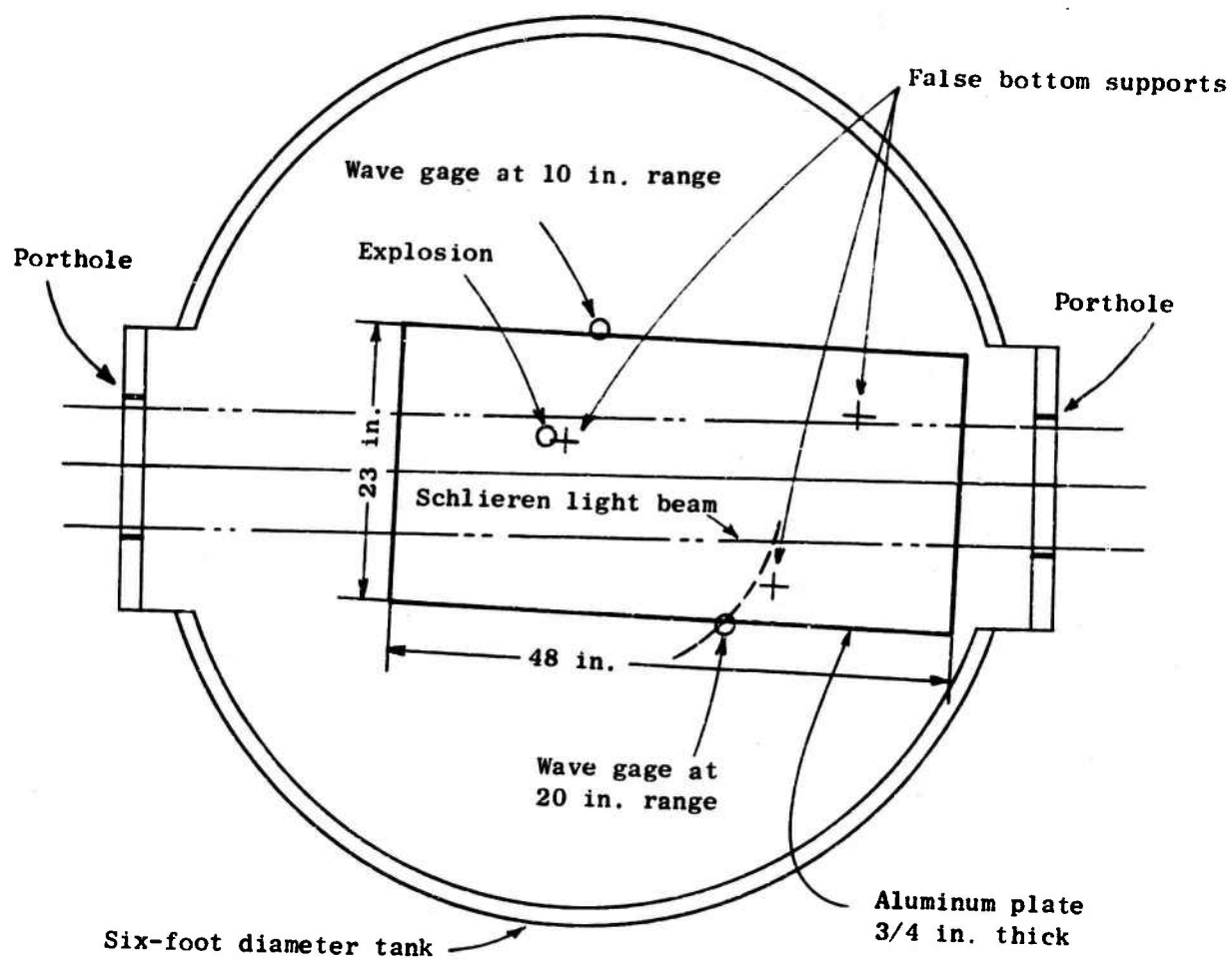
Sketch B - Configuration of False Bottom and Wave Gages

5

11/16 in. apart. The active cylinder had a spiral winding of insulated wire
to produce a magnetic field and finally a DC voltage proportional to the
location of the water surface. The outer diameter of this cylinder was 0.160
in., and the other cylinder was an 1/8-in. diameter rod. The output voltage
was linear with water displacement and the sensitivity was one volt per inch
of water displacement.

The gage calibration was independent of both the meniscus of the water
surface at the gage and the presence of the aluminum bottom plate. To back-up
these wave gages, a wave rod projecting through the water surface at a range
of 15 in. was photographed by a 16 mm Bolex camera running at 64 frames per
second. The movies were not required since the wave gages performed extremely
well, which was fortunate since the jitter and resolution of these movies made
them difficult to interpret. Hence the Bolex data will not be reported here.

The water shock waves were not measured during the recent tests reported
here since the depth of burst was so shallow that the shock front was reduced
by "anomalous" surface reflection except directly beneath the explosion as
shown in Ref. 1.

In summary, the useful measured data for each of the 54 shots consists of
two schlieren movies of the cavity taken at 2500 at 25,000 frames per second
and two surface wave gage records.

2.3 SCALING PROCEDURE

To simulate the full-scale tests in shallow water the objective was to
duplicate the geometric shapes of the water surface at the "initial" times
when the cavities were fully expanded to radius R_c and nearly motionless.
The water surface wave pattern should then scale geometrically at corresponding
times (when gt^2/R_c is the same for the full-scale and model tests). This
scaling procedure corresponds with the Kranzer-Keller theory for wave generation,
although the initial cavities are not actually completely motionless and the
water is not perfectly inviscid as assumed. The inviscid approximation
appears to cause a far greater effect on the predicted wave trains, although

6

the effects of viscosity do seem to be confined mainly to early times when
the cavity collapses into a few spilling breakers (within about five
cavity radii).

It appears that most of the gravitational (or stored) energy in the
initial cavity is lost to friction during this time, so that the energy in
the wave trains is much less than that in the initial cavity, as will be
shown. Furthermore, the data will indicate that a larger fraction of the
energy is lost for very small bursts, as might be expected since the Reynolds
number is smaller. However, this is not perfectly evident a priori, since
much of the frictional loss appears to be due to the hydrodynamic instability
of the steep waves generated at short range which causes them to spill over
(or break down) to the maximum stable height, and this limiting height does
scale geometrically in both shallow and deep water (as shown in Ref. 4).
Fortunately, the data indicate that the frictional effects can be accounted
for fairly well by the use of a loss coefficient which is Reynolds number
dependent and which simply reduces the height of all the waves by a constant
factor for a given burst. This loss coefficient is equivalent to the use of
a shallow "psuedo" cavity shape with reduced energy in deep water. For
bursts near the surface of deep water the maximum cavity depth is actually
nearly equal to its radius and much deeper than for the "psuedo" cavity shape.
This shape corresponds theoretically with the measured wave trains only if
the real effects of hydrodynamic instability and viscosity are neglected in
the theory. In shallow water where the cavity sweeps over the bottom, there
is no psuedo cavity shape equivalent to the frictional loss coefficient.

In order to obtain the geometric shapes of the full-scale cavities in
the laboratory tests, the tests were repeated at both normal atmospheric
pressure and 1/2 atmosphere. The reason for the reduction in pressure was
not to attempt to satisfy the requirements of true dynamic similitude
(described in Subsection 5.1), since this requires a much harder vacuum
which would cause the water to flash into steam. Rather, the objective was
to prevent the water column which rises above the expanded cavity from
collapsing inward. This causes the columns for small bursts to be conical

7

in shape rather than cylindrical as observed for large explosions at Mono Lake and CROSSROADS-Baker. The data reported by Hudson show that reduction of the pressure to half normal is sufficient to prevent the column walls from collapsing inward for small HE bursts scaled to Baker (Ref. 7). The present data indicate that this is also true for any water depth if the depth of burst is small, but that a harder vacuum is required for exploding wires than for HE explosions.

To scale the geometric shape of the initial cavities, A_{max} scaling was used, where the depth of burst and water depth are scaled in proportion with the radius of the maximum bubble radius upon its first expansion. This technique is well established for scaling the surface effects of deeply submerged bursts, and it is reasonably accurate for shallow bursts since the expanded cavities of shallow bursts (even in shallow water) are approximately equal to the bottom half of the hypothetical bubble truncated by the bottom (Ref. 5). However, one of the results of the current study is an improved scaling technique for very shallow bursts which will be described in Subsection 5.1.

The following empirical relationships (from the sources cited in Ref. 1) were used to relate the bubble radius A_{max} (ft) to the equivalent TNT charge weight W (lb), energy release E_o(ft-lb), and radius R_o(ft)

$$W^{1/3} = 7.32 \ R_o \tag{1}$$

$$E_o = 1.43 \times 10^6 \ W \tag{2}$$

$$A_{max} = 12.6 \ (W/Z)^{1/3} \tag{3}$$

Z(ft) = hydrostatic + atmospheric head

= d(ft) + 34 for normal atmospheric pressure and fresh water

8

For nuclear bursts

$$A_{max} = 11.9 \left(\frac{W_N}{Z} \right)^{1/3} = 1500 \left(\frac{Y}{Z} \right)^{1/3} \tag{4}$$

In summary, the technique used here to simulate the generation of surface waves is to scale all lengths (e.g., depth of burst, water depth, and gage range) in proportion to the radius of the fully expanded cavity R_c, to reduce the atmospheric pressure until the water column is cylindrical, and to adjust the measured wave heights by an empirical loss coefficient which depends on the Reynolds number $\left(\rho R_c^2 / \mu t \text{ or } \rho^2 R_c^3 g / \mu^2 \right)$. The cavity radius R_c was taken equal to the bubble radius A_{max} given by Eqs. (3) and (4) to scale the tests described here, but a better approximation for very near surface bursts is given by Eq. (9), as will be described in Subsection 5.1. The data to be given show that this procedure is reasonably accurate for a reduction in yield of over 12 orders in magnitude, or a reduction in R_c by over three orders of magnitude (from 400 ft for CROSSROADS-Baker to 0.4 ft for the exploding wire).

Section 3
PRESENTATION OF DATA

The test conditions and the resulting cavity diameter and peak wave height are listed in Tables 1 through 3. The first 16 tests in Table 1 were in deep water under normal atmospheric pressure. For tests 17 through 26 (Table 2) the atmospheric pressure was reduced to half the normal value. All the tests in shallow water (27 through 42) are given in Table 3. Each of the shallow water tests was repeated either two or three times. The last shot, 43, was fired to show the bubble from a deeply submerged explosion.

3.1 CAVITIES

The 16-mm films taken at 2500 frames/sec were projected onto a flat surface and tracings were made of the outline of the cavity and water column at 50-frame intervals (1/50 sec) until after the cavity was fully expanded. The results are given in Figs. 1 through 45 where the actual spacing between the two vertical lines is 5.06 in. and the actual diameter of the porthole is 9.50 in. For the tests in deep water, the diameter of the fully expanded cavity D_{max} (when the depth of the cavity was maximum) usually occurred at about the 150th frame or about 0.07 sec after the explosion. The outline of the cavity when it was considered to be "fully expanded" is shown by the heavier lines in Figs. 1 through 26, and the measured values of D_{max}, the largest horizontal diameter of these "expanded" cavities, are indicated in the figures and in Table 1. For the submerged shots at normal atmospheric pressure (e.g., shot 7), there was water jet impingement on the bottom of the cavity before it became fully expanded, which produces some uncertainty in the determination of D_{max}. However, this condition occurred only for shots 7 through 16. In shallow water D_{max} is nearly equal to the maximum diameter of the water column D_{col}, but in deep water D_{col} is about 35 percent larger than D_{max}, as will be described later.

The 35-mm film strips taken at 25,000 frames/sec were essentially the same as those shown in Fig. 7 of Ref. 1, and hence they will not be reported here.

11

Preceding page blank

3.2 SURFACE WAVES

The surface wave gage records measured at two horizontal ranges are shown in Figs. 46 through 86 with the scales of time and water level indicated in each figure. The measured peak wave heights η_m are listed in Tables 1 through 3. For the tests in deep water these values correspond with the maximum absolute value of the measured displacement of the water from its undisturbed level (either the height of a crest or the depth of a trough, whichever was largest in the gage record). The value of η_m is nearly equal to half the maximum amplitude of the first lobe of the wave envelope, since there were several sinusoidal wave peaks in the first lobe (and the peak waves were near the lobe maxima). For the tests in shallow water, however, there were only a few nonsymmetric wave crests in the wave envelope and the indicated values of η_m correspond to half the maximum measured wave height (trough to crest).

Although succeeding lobes in the wave envelopes appear in the wave gage records for the deep water tests (e.g., Fig. 62), these are due primarily to the inward reflection of the waves from the tank sidewalls. It can be seen that the waves traveled the 9 in. distance between the gages in about 0.4 sec, so that about 1.6 sec would be required for a wave to travel from the farthest gage to the tank wall and return. Thus only the first 1.6 sec of the wave gage record (about the duration of the first lobe of this wave envelope) is a valid record of the outgoing waves for the farthest gage.

There was a transient signal induced by the electrical discharge which normally disappeared before the peak wave was recorded (but not always, as shown by shot 2). The transient is a useful indication of the detonation time, however, as shown by the arrows on the wave records. In a few cases when anomolously large cavities and waves were generated, the recording stylus went off-scale (shots 20, 22, and 25R).

The measured values of cavity diameter, peak wave height, and their dimensionless ratio are plotted vs depth of burst in Figs. 87, 88, and 89.

12

Section 4

DESCRIPTION OF DATA AND COMPARISON WITH PREVIOUS EXPLODING WIRE DATA

The purpose of the present test series was to supplement the data
previously reported in Ref. 1 by testing under new conditions (shallow water)
and by extending the previous tests in deep water through:

a. Photography of the cavity for a longer duration

b. Orienting the probe to which the wire is mounted in different
positions to determine if the probe affects the measured results

c. Measurement of the surface waves with electronic gages, and

d. Reduction of the ambient pressure to 1/2 atmosphere to improve the
simulation of large explosions.

Several interesting results have been obtained for surface bursts and
slightly submerged bursts (near the upper critical depth) in deep water.
These results will be described next in conjunction with the data reported
previously. Then the new data obtained for explosions in shallow water will
be presented.

4.1 LONGER DURATION PHOTOGRAPHY OF CAVITIES

Several significant facts are revealed by the slower (2500 frames/sec)
photography of the cavities and plumes generated in deep water as shown in
Figs. 1 through 26. The high-speed photography gave about 150 frames at 10
times the framing rate, corresponding in time with about the first 15 frames
of the sequences shown. From the figures it is evident that the cavities
generated at shallow depths of burst were farther from being fully expanded
than estimated in Ref. 1 (from the last frame of the high-speed photography).
However, as indicated in Table 2 of Ref. 1, the cavities did become fully
expanded during the high-speed photography when the depth of burst exceeded
0.79 in. For the shallower bursts the cavities take considerably longer to
expand and they become considerably larger than indicated in Fig. 11 of Ref. 1.
This can be seen by comparison with Fig. 88, and from D_{max} in Table 1 compared

13

with Table 2 of Ref. 1. For example: at a burst depth of 0.2 in., the new value of D_{max} is 4.90 in. compared with 4.53; at 0.04 in. depth the new values are 6.37 and 6.65 in. compared with 3.42; and at zero depth the new values are 4.62 and 4.75 in. (for the probe mounted vertically upward as before) compared with 3.19 and 3.37 in.

Thus, for depths of burst between 0 and 0.2 in., the expanded cavity diameter is actually considerably larger than the values plotted in Figs. 4 and 11 of Ref. 1, and these values should be replaced by those in Table 1. This result makes the dashed curve in Fig. 11 correspond more closely with the lowest solid curve. That is, the variation of cavity radius with depth of burst for the exploding wire corresponds closely with that measured previously for miniature HE charges, except for a sharp decrease in radius with depth of burst less than 0.04 in. This decrease will be discussed in more detail later, along with the effects of reduced atmospheric pressure and probe orientation. This variation of cavity radius with depth of burst is important in scaling and in understanding the transition between the applicability of Eqs. (3) and (9).

Another interesting feature of the slower photography (not shown before in the high-speed films) is that it shows clearly the inward collapse of the walls of the water column just before the cavity becomes fully expanded. This collapse causes spike jets of water to flow both upward and downward. Thus there is jet impingement on the bottoms of the cavities shown in Figs. 7 through 16 which closely resembles that shown in Ref. 5 for 1 lb TNT charges. However, it is important to note that the collapse and impingement never occurred at zero depth of burst for the wire (Figs. 1 through 6). This result supplements the information in Ref. 5 since the minimum depth of burst reported there was 1.5 in., or about one charge radius. Furthermore, there was never any collapse and jet impingement for the tests with half the normal atmospheric pressure (Figs. 17 through 26). This shows that the expanding column walls collapse because the internal pressure drops below the normal value of atmospheric pressure. The pressure within the water column drops lower for small bursts than for large ones. This causes the walls to collapse

14

inward for the small bursts unless the atmospheric pressure is reduced, just as required for dynamic similitude in Eq. (8).

To illustrate this point let us estimate the pressure of the detonation gas within the expanded hemispherical cavity for a surface burst with the simplifying approximation that the volume of gas within the water column above the cavity is equal to that within the hemispherical cavity. In this case the detonation gases expand by a volume ratio = $(R_c/R_o)^3$. Hence the gas pressure drops from the detonation pressure P_d to a value given by

$$P_c = P_d \left(\frac{R_o}{R_c} \right)^{\gamma_d} \tag{5}$$

It will be assumed that the detonation pressure is $P_d = 10^5$ atm; that the ratio of specific heats of the detonation gas is $\gamma_d = 1.2$; that the detonation gas originally occupies a sphere of radius R_o(ft) equivalent to a TNT charge as given by Eq. (1), and finally that the cavity radius is given by Eq. (9). Substitution of these values into Eq. (5) gives the following expression for the pressure in the expanded cavity

$$P_c(\text{atm}) = 0.27 \ W^{0.30} \tag{6}$$

and the following values

W (lb)	P_c (atm)
10^{-4}	$0.27 \times 10^{-1.2} = 0.017$
1	0.27
10^4	$0.27 \times 10^{1.2} = 4.3$

15

The calculated values illustrate that the pressure drops much lower inside the expanded cavity for small explosions than for large ones.

Associated with the wall collapse and jet impingement, the expanding cavity necks down at the waterline as hypothesized in Ref. 1. This necking down increases rapidly with depth of burst (Figs. 7 through 13) until the water acutually closes over the cavity and a bubble is repelled downward from the surface (Figs. 12 and 13). However, this effect is caused by the cavity wall collapse rather than anomolous reflection of the water shock wave (as hypothesized in Ref. 1) since it did not occur at half the normal atmospheric pressure. Thus the wall collapse, jet impingement and cavity necking are associated phenomena which do not occur except for small explosions at nearly normal atmospheric pressure, (i.e., when the first parenthesized pressure ratio in Eq. (8) is smaller than some critical value). These phenomena do not occur when the atmospheric pressure is reduced, or when the cavity radius R_c is greater than the atmospheric head of 33 ft such as for the surface explosions at Mono Lake and CROSSROADS-Baker. For these large bursts the water column walls remained parallel (or cylindrical) and they did not collapse inward as did those for 1-lb charges (Refs. 5 and 6).

The maximum value of the pressure ratio required to prevent the inward collapse is probably different for HE and for bridge wire explosions since the detonation gases are entirely different in temperature, in pressure, and in their pressure-volume relationship, or ratio of specific heats. Hence the radiation losses, shock wave transmission, and finally the over-expansion to less than atmospheric pressure are different. In fact the steam produced by the wires can condense upon expansion just as for nuclear bursts. This effect appears to be particularly significant for surface bursts as will be described further in Subsection 5.1. The condensation also appears to cause the column walls to collapse inward more readily than for HE bursts as will be discussed further in Subsection 5.3.

The slower photography also gives the relationship between the diameters of the expanded cavity and the expanded columns and shows that two distinct types of cavities can be generated at the same depth of burst (which is the

16

main cause for the unrepeatability in the data in Fig. 89, as will be described in Subsection 5.2).

The relationship between the maximum column diameter D_{col} and the diameter of the fully expanded cavity D_{max} has been shown by previous under-water photography (Refs. 3, 4, and 5), but the first was obtained using oil rather than water, the second was obtained in a wedge tank with wall and ceiling interference, and the last was obtained at normal pressure with submerged charges for which the column walls collapsed inward. Therefore, the present data appear to be the first available for surface bursts with a non-collapsing column wall and condensible steam vapor inside. The two diameters and their ratio are given for seven near surface bursts in Table 4 as obtained from the dashed and heavy outlines in the figures showing the photography of these shots. The maximum column diameter occurred at about twice the time for the fully expanded cavity when the cavity had partially collapsed so that its depth was about half the maximum value. The cavity continues to rise until it becomes a mound inside the column. The mound was visible in the photography because the column walls became so thin that they ruptured and collapsed before the mound was formed. The oscillations of the water surface are shown in Figs. 31 through 34 for bursts near the surface of deep water. It is evident in Table 4 that the maximum diameter of the water column D_{col} for shallow bursts is about 35 percent greater than the diameter of the fully expanded cavity D_{max} independent of the test conditions and the way in which the cavity vents (described in Subsection 5.2).

4.2 PROBE ORIENTATION STUDY

The first six shots at zero depth in Table 1 were run to determine if the probe which supports the exploding wire affects the expansion and collapse of the water cavity. Figures 1 through 6 show that the horizontal probe position produced larger hemispherical cavities than the normal (vertically upright) probe position, and that the cavities were even smaller and distorted when the probe was mounted vertically downward. This same trend is evident for the maximum cavity diameter and peak heights listed in Table 1 for shots 1 through 6.

17

Although the foregoing six surface bursts produced column walls which tapered inward slightly, none of the columns collapsed inward as they all did for the submerged bursts under normal pressure. However, the columns for the repeat shots 5R and 6R tapered inward considerably more than for shots 5 and 6 and the cavities were also distinctly smaller. This appears to be a statistical variation (or lack of repeatability) associated with shallow bursts more than a variation in wire yield, as will be described further in Subsection 5.2.

With the probe projecting downward beneath the wire (shots 3 and 4), the cavity was distorted by the flow of water over the two prongs projecting from the probe (as shown in Figs. 3 and 4). The water shock wave was also disturbed by reflection off the end of the probe. It was decided to complete the test series with the normal upright probe position to be consistent with the previous series of tests, even though considerably larger cavities and waves were produced by the horizontal probe position (at least for the test conditions of zero depth of burst and normal atmospheric pressure).

4.3 ELECTRONIC WAVE GAGE RECORDS

The peak wave heights measured with the farthest electronic wave gage in deep water under normal pressure (η_{m_2} in Table 1) agree reasonably well with those measured previously by photography of a wave gage board (Fig. 16, Ref. 1). The upper critical depth effect is, if anything, somewhat more distinct for the new data plotted in Fig. 87, and yet more distinct at reduced pressure in Fig. 88.

The dimensionless values of wave height in Table 1 and Fig. 89 are now smaller than the comparable values in Fig. 16 of Ref. 1 because the cavity size (for the shallow shots) was actually considerably larger than previously estimated in Ref. 1. The new data in Fig. 89 show that the value of $R\eta_m/R_c^2$ is nearly constant, independent of depth of burst and ambient pressure. Since this ratio is proportional to the square root of the ratio of the energy in the wave train to that in the expanded cavity, the data indicate that the higher waves generated near the upper critical depth were caused mainly by the

18

generation of larger cavities rather than the more efficient generation of waves by cavities of the same size, as was previously believed (from the data in Fig. 16 of Ref. 1).

The new values of $R\eta_m/R_c^2$ are now also smaller in Fig. 13 of Ref. 1 which indicates that the small cavities from the exploding wires were less efficient wave generators than those from larger HE explosions. That is, for the small cavities (and low Reynolds number), a larger fraction of the cavity energy is put into frictional losses as the cavity collapses than for the much larger cavities. The values of $R\eta_m/R_c^2$ for the Mono Lake tests are probably nearly twice as large as indicated because the maximum column radius R_{col} was used as an approximation for R_c (whereas $R_{col} \simeq 1.35 R_c$). With this correction there is a consistent increase in wave-making efficiency with increasing cavity size (or Reynolds number) which will be discussed further in Subsection 5.1.

The tests at reduced pressure are believed to be the closest simulation of nuclear bursts at the upper critical depth (UCD) available, and the peak wave heights plotted in Figs. 88 and 89 appear to support the contention that the UCD effect does exist for nuclear as well as HE bursts. However, the venting of the cavities was not accurately simulated during the small scale tests. The way in which the cavity vents appears to cause the UCD effect, as described in Subsection 5.2.

In addition to the peak wave heights measured at R = 18 in., values were also obtained at R = 9 in., as shown in Table 1. Theoretically, these latter values should be twice as large as those measured at twice the range since $R\eta_m$ is a constant according to the Kranzer-Keller theory (Ref. 1). The reason that they were usually less than twice as large is probably that the closer gage was placed too near the cavity (since the cavity was larger than expected). That is, the gage range R was less than $5R_c$ so that the wave trains were not stabilized from the spilling breakers which are generated close to the collapsing cavity (Ref. 1).

19

Even though the waves were extremely small compared with full-scalc conditions, the effects of frictional damping and capillarity are believed to be negligible after the wave trains were generated in deep water since the length of the highest wave is about equal to the cavity diameter ($D_{max} \simeq 5$ in.), even in shallow water, as shown in Fig. 3 of Ref. 4. Hence they travel only a few wavelengths to the wave gages, and they are considerably longer than 1 in., which is about the longest wavelength for which capillarity has appreciable effect on gravitational waves. The effects of bottom friction may not have been entirely negligible for the shallowest water tests, however.

4.4 EFFECT OF REDUCED AMBIENT PRESSURE

The main effect of reducing the ambient pressure to half the normal value was to prevent the inward collapse of the column walls at shallow depth of burst. This was the original purpose of the reduction and the results are roughly in agreement with those previously obtained with small HE charges, as reported by Hudson (Ref. 7). However, for the deepest shots in deep water (26 and 26R), the reduction of pressure was insufficient to prevent the inward collapse. This was also true for the smallest cavities produced in shallow water (shots 38R, 39R, and 40). Hence the data indicate that a higher vacuum is required to prevent the steam-filled columns from collapsing than the columns for the HE charges.

It can be seen from Figs. 87 and 88 that the cavity diameter and peak wave height were nearly unaffected by the reduction of atmospheric pressure, in spite of the differences in the cavity wall collapse and jet impingement. However, there were a few shots at reduced pressure which produced anomolously large cavities and waves (shots 18, 19, 20, 22, and 25R in Fig. 88). These shots all vented in a distinctly different way from all the others in Fig. 88, as will be described in Subsection 5.2.

Although there was no marked change in the variation of cavity size vs depth of burst with the relatively small reduction in atmospheric pressure, a distinct change was obtained for a much larger reduction (by 1/300 with small

20

HE charges as shown in Fig. 11, Ref. 1). This change is believed to be very significant in interpreting the data, as will be described further in the next section.

Section 5
DISCUSSION OF RESULTS

### 5.1 ENERGY PARTITIONING AND CAVITY SCALING FOR SURFACE BURSTS

Formation of Cavities by Surface Bursts

The formation of a cavity by an explosion <u>at the surface of deep water</u> will be discussed next from theoretical, dimensional analysis, and experimental viewpoints. Once the formation of the cavity is thoroughly understood, its subsequent collapse and the generation of water surface waves can be predicted reasonably well from existing theory and experimental data. Essentially the problem consists of predicting the size and shape of the "motionless and fully expanded" cavity, given the initial conditions of the explosion. Even though the cavity is never perfectly motionless, high speed photography of the water cavity formed by surface bursts equivalent to 1 lb of TNT at URS and NRDL (Refs. 4 and 5) and by very small explosions in vacuum tanks at URS and EPCO (Refs. 1 and 3) have shown that a nearly motionless and hemispherical cavity surrounded by a thin lip of water is formed by near-surface bursts. Refinements and qualifications to this simple description will be added later. The fully expanded cavity is defined to occur when the depth of the cavity is maximum so that the bottom of the cavity is truly motionless. However, at this time the sides of this cavity and the surrounding lip of water (or water column) are still expanding slowly and they continue to expand to a maximum radius R_{col} which is about 35 percent greater than the depth and radius of the fully expanded cavity, R_c (as shown by the data in Table 4).

5.1.1 Theoretical Equations for Cavity Energy

The potential or gravitational energy E_c has been calculated for several cavity shapes which approximate those observed. The results are indicated below for three such shapes, where "N" below each sketch is to be substituted in Eq. (7). The last one has equal volumes in the cavity and in the elevated lip or column surrounding it, and it is probably the best approximation to the

23

observed cavity shapes when its depth is set nearly equal to its radius
($D_c = R_c$).
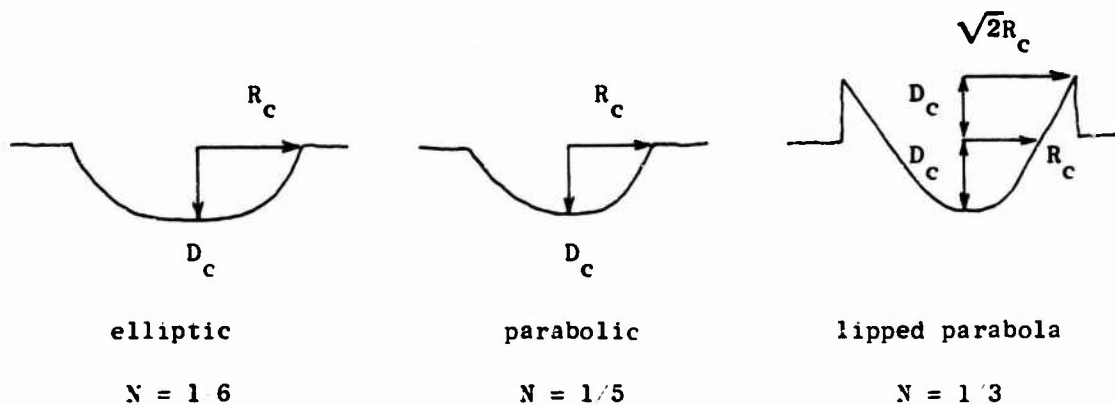
Sketch C - Theoretical Cavity Shapes

$$E_c = N\pi\rho g\, R_c^{\;2} D_c^{\;2} \tag{7}$$

Rather than giving exactly the cavity shape and its potential energy,
the main value of Eq. (7) is that it shows precisely how the size of the cavity
and its potential energy E_c scales with E_o, the energy released by the surface
burst — if all the dimensionless parameters which affect the physical event
are held fixed. In this case of true dynamic similitude, the partitioning
of released energy E_o into radiation, air blast, water shock, surface waves,
etc., will not change with the value of E_o. Thus, E_c/E_o will be a constant,
and the cavity radius R_c will be proportional to the fourth root of E_o in
accordance with "Froude scaling".

5.1.2 Dimensional Analysis

Now, by means of dimensional analysis, let us consider the dimensionless
physical parameters which must be held fixed in order to insure dynamic
similitude for surface bursts. There are a very large number of such parameters

24

if all of the possible significant effects are included, such as radiation, acoustic impedance, surface tension, viscosity, cavitation, etc. However, let us consider the effects of only two physical parameters, the atmospheric pressure P_a, and P_d the detonation pressure (or the energy density of the explosive charge or nuclear burst). For the time being, let us assume that we have spherical HE charges and that upon detonation they are instantaneously converted into spheres of a perfect gas (the detonation products) with an initial temperature T_d, an initial pressure P_d and a constant ratio of specific heats γ_d. Now let us consider how P_d and P_a must be controlled in order to insure dynamic similitude. If the dependent variable R_c is influenced by ρ, g, E_o, and P_a in addition to other physical parameters, such as those already mentioned, then dimensional analysis of this partial list of independent variables (or initial conditions) gives the following dimensionless groups (or functional relationship):

$$\frac{\rho g\ R_c^4}{E_o} \left(\frac{g\ R_c}{P_a},\ \frac{\rho g\ R_c}{P_d},\ \ldots \right) \tag{8}$$

Thus, to insure dynamic similitude such that E_c/E_o [or the first group in Eq. (8)] is a fixed constant, the two parenthesized ratios must be held fixed. Other dimensionless groupings might be chosen (e.g., the fourth root of $E_o/\rho g$ can be substituted for R_c in the parenthesized ratios to make them independent dimensionless parameters), but the form of Eq. (8) is convenient for physical interpretation. It simply shows that to insure dynamic similitude, three pressures must be held in proportion: the atmospheric pressure P_a, the detonation pressure P_d, and the hydrostatic pressure at the bottom of the expanded cavity, $\rho g\ R_c$. If this is done, then the ratio of the first and last groups $R_c^3\ P_d/E_o$ will be fixed. In this case, the ratio of the cavity radius R_c and charge radius R_o also will be fixed, since the energy released by the charge E_o is proportional to $P_d R_o^3$.

It is also evident from Eq. (8) that there is only one way to insure dynamic similitude if various size charges of the same explosive are detonated at the surface of water (so that P_a and P_d are both fixed), and that is to

25

vary the gravitational constant such that gR_c (or gR_o) remains constant. This is not practical except for small charges exploded in a centrifuged tank (such as the facility at NOL where the coriolis force on the water column would not be realistic). Therefore, let us now look at the experimental data which exist over an extremely large range of E_o, but for a bewildering variation of the large number of dimensionless groups which should actually be held fixed for dynamic similitude and Froude scaling to hold. The objective is to obtain at least a qualitative rationale to describe departures from the simple physical model just described and scaling rules for estimating the variation of R_c with E_o.

5.1.3 Experimental Data for Cavity Diameter

The primary data for the generation of cavities by explosions at a water surface are the high speed underwater photographs of:

1. Very small (fractional gram) HE charges fired in a vacuum tank (reported in Ref. 3 and described briefly in Ref. 1)

2. HE charges equivalent to 1 lb TNT spheres, fired at the apex of a wedge shaped water tank (Ref. 4)

3. HE charges equivalent to 1 lb TNT spheres (Ref. 5)

4. Exploding wires equivalent to fractional gram charges of TNT (Ref. 1).

Each of these sources of data supplies some valuable pertinent information which will be summarized here, but each source is limited in scope as indicated below.

1. Ref. 3 - Oil was used rather than water to permit a high vacuum. Hence the viscosity and compressibility of the fluid (and its shock wave) were not precisely simulated, and HE rather than nuclear detonation gases were generated.

2. Ref. 4 - The water shock wave and the venting of the cavity were not precisely simulated because of the wedge tank sidewalls and a low ceiling over the tank.

3. Ref. 5 - The minimum depth of burst was 1.5 in. or about one charge radius so that there was no surface burst. The charges in the test series were fired in an outdoor pond of water under normal

26

atmospheric pressure, so that the second group in Eq. (8) was much
smaller than for large explosions. Thus the cavity walls collapsed
inward and impinged on the bottom of the cavity. As already noted,
this effect does not occur for large explosions or for surface
bursts.

4. Ref. 1 - Tests were performed under normal atmospheric pressure, and
when the depth of burst was small, the photography ended before the
cavities were fully expanded.

Because of the foregoing shortcomings, it appears that the data reported
herein, taken with the atmospheric pressure half as large as normal, may show
the generation and collapse of a water cavity under test conditions which
simulate a nuclear surface burst better than ever before. Although the
exploding bridge wire generates a steam bubble at high pressure and temperature
as does a nuclear explosion, the gas temperature is much lower for the wire.
Furthermore, there is some vaporized metal from the wire, and the radiation
from the hot gases (or fireball) certainly does not simulate that from a
nuclear burst. Nevertheless, the steam within the expanding cavity and water
column should simulate a nuclear burst better than non-condensible HE detonation
products.

Now let us attempt to derive approximate formulae for the maximum column
radius R_{col} and the expanded cavity radius R_c for surface bursts by using all
the available data sources including Mono Lake and nuclear test data for R_{col}.
We shall start with Fig. 17 which shows the sequential shapes of the cavity
and water column for a small surface burst under half the normal atmospheric
pressure. (Repeat shot 23 is essentially identical, and so is shot 1 in Fig.
1 at normal pressure as shown in Table 4.) The maximum column radius for these
surface bursts ($R_{col} = 3.2$ in.) occurred at a time about twice as great as
that when the cavity was fully expanded to its maximum depth and when $R_c =$
2.3 in.

Let us determine how well these radii agree with Eq. (8); that is, how
well they scale with $W^{1/4}$ for bursts at the surface of deep water. The unclas-
sified data and sources are listed in Table 5, and the classified data are
added in Table A-1. The discussion here will relate to Table 5, and additional

27

comments relative to the classified data are given in the appendix. The
data sources will be discussed in the order they are listed, i.e., by
increasing yield. The purpose is to show that in accordance with Eq. (8), all
the data support the following empirical rules for the expanded cavity radius
and maximum column radius of TNT explosions at the surface of deep water.

$$R_c = 4.80W^{1/4} = 180 \ Y^{1/4} \tag{9}$$

$$R_{col} = 1.35 \ R_c = 6.50W^{1/4} = 245 \ Y^{1/4} \tag{10}$$

Although the values in Table 5 vary from these rules by factors greater than
two, these variations appear to be explainable from available experimental
information when it is used to "adjust" the values to the normalized condition
of a TNT explosion at the surface of deep water.

Looking at the data without any physical insight one would probably
conclude that there is a definite trend for $R_{col}/W^{1/4}$ to increase with yield,
so that the data actually scale with $W^{0.3}$ more closely than with $W^{1/4}$ (or
Froude scaling). However, the following adjustments appear to explain the
departures of the data from Froude scaling, which has been shown to be
precise if the test conditions could be controlled so that the governing
dimensionless groups such as those illustrated by Eq. (8) could be held
constant as required for dynamic similitude.

First, the exploding wire gave two distinct types of cavities (flared or
sprayed, as will be described in Section 5.2). The flared type appears to be
associated with small bursts which generate condensible gas and then over-
expand so that there is inflow (or blow-in) into the top of the cavity. The
sprayed cavities appear to blow out and simulate HE explosions better since the
inflow is reduced corresponding to incondensible detonation products. These
sprayed cavities (shots 5 and 6) scale well with the cavities generated by
small HE charges of comparable yield (the second data source in Table 5).
These latter data in turn show that the cavity and column radii increase

28

about 50 percent when the atmospheric pressure is reduced until it is smaller than the hydrostatic pressure corresponding to the cavity radius (1.5 and 6 in. of oil, respectively, for the high vacuum tests). This pressure ratio corresponds to the first parenthesized term in Eq. (8). Note that the small charge data at reduced pressure then scale well both with the NRDL for 1-lb and the Mono Lake data for 10^4-lb HE charges where the former pressure ratio was about 33/5.5 and 33/65 respectively (with each pressure in feet of water). Thus the Froude scaling rule ($R_{col} \sim W^{1/4}$) is accurate to within 12 percent spanning eight orders of magnitude in yield, even though the conditions strictly required for Froude scaling to apply were not met. For the 1-lb charges, the cavity and the column radii were affected by wall and ceiling interference for the URS wedge tank, and by column collapse for the shallowest submerged NRDL explosion.

The Mono Lake test data give only the column dimensions, since there was no underwater photography of the cavity. Thus the foregoing empirical scaling rules [Eq. (9) and (10)] are based on the column radius measured at Mono Lake and the column/cavity radius ratio ($R_{col}/R_c = 1.35$) obtained from Table 4.

Finally, CROSSROADS-Baker gives a considerably higher value of $R_{col}/W^{1/4}$ in Table 5. However, this value should be reduced before the comparison is made because Baker was not at the surface of deep water. It appears that the shallowness of the water $d_w/R_c = 180/780 = 0.23$ causes a slight reduction in the cavity and column radii (based on the wedge tank data in Ref. 4 and on Mono Lake test data for HE charges). On the other hand, the exploding wire data in Tables 1 and 3 indicate an increase in cavity radius as the water is made shallow. It will be assumed here that the Baker column diameter was unchanged by the presence of the bottom. However, the depth of burst to cavity radius ratio was $90 \times 1.35/780 = 0.16$, and the oil tank data shown in Fig. 11 of Ref. 1 indicate that the cavity radius would have been reduced by a factor of about 1.5 if Baker had been fired at the surface and if the nuclear-TNT equivalence did not change. This factor corresponds to a low ratio of atmospheric to cavity hydrostatic pressure ratio ($1.5/6.0 = 0.25$), whereas the ratio for Baker was even lower (approximately $33 \times 1.35/780 = 0.057$), so that

29

ever a higher factor might be expected. Note that just the opposite effect occurs at high values of the pressure ratio, corresponding to small charges fired under normal atmospheric pressure, i.e., the cavity radius decreases with increasing charge depth as one might expect intuitively. Reduction of the measured value of $R_{col}/W^{1/4}$ for Baker by the factor 1.5 makes the value equal to 6.3, which scales well with all the other "adjusted" data in Table 5.

It is interesting to compare the measured data in Table 5 with the Mono Lake surface burst in a different way, by starting with the test conditions and cavity radius which correspond with correct simulation and Froude scaling. The following sketch shows approximately the atmospheric pressure required to simulate the Mono Lake shot (with Baker represented as a surface HE burst for the time being). It can be seen that the pressure ranges from 8 atm for Baker to 0.01 atm for the vacuum tank charges. Since the hardest vacuum for the URS oil tank tests was 0.003 atm, the simulated yield fell between that for Mono Lake and Baker. The predicted column and cavity radii are indicated in Sketch D as scaled from Mono Lake by $W^{1/4}$ or Froude scaling. Let us compare these scaled values with the measured data from Table 5. The measured radii for the wire tests are smaller than their scaled values because the atmospheric pressure was much higher than the scaled value. The value of R_c for the URS oil tank tests scales accurately even though the vacuum (0.003 atm) was somewhat lower than the scaled value (0.01 atm). The NRDL radii for 1-lb charges are lower than predicted because the atmospheric pressure (1 atm) was higher than the scaled value (0.1 atm) and the charge was fully submerged rather than half submerged which caused the column walls to collapse inward. The wedge tank data give even smaller values of R_{col} and R_c because of the interaction of the sidewalls and ceiling with the water shock wave and water column.

The measured column radius for Baker is too large, but an adjustment should be made since the actual depth of burst was 90 ft rather than zero. This correction can be made from the upper curve in Fig. 11 of Ref. 1 since the vacuum pressure (0.003 atm) is near the correct scaled value for Baker (0.0012 atm). The curve shows that the cavity radius increases by a factor
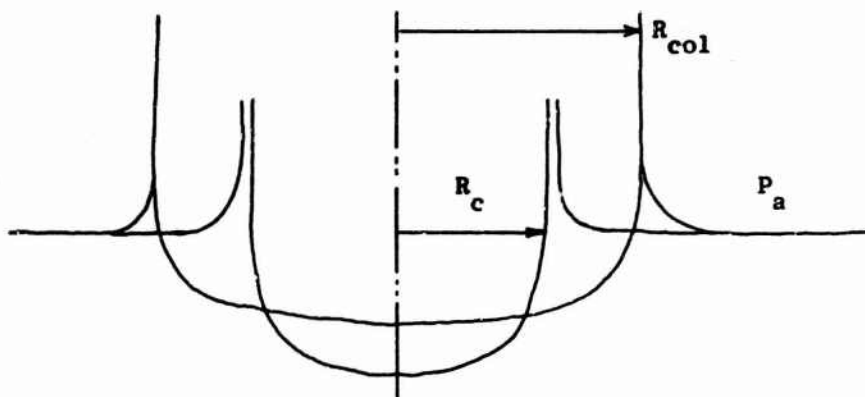
TEST	YIELD (lb)	P_a (atm) Eq. (8)	R_{col} (ft) Eq. (9)	Meas	R_c (ft) Eq. (10)	Meas
EPCO Wire	10^{-4}	0.01	0.65	0.33	0.48	0.25
URS Small HE	10^{-4}	0.01	0.65	-	0.48	0.50
NRDL	1	0.1	6.5	6.0	4.8	4.0
URS Wedge Tank	1	0.1	6.5	4.7	4.8	3.5
Mono Lake	10^4	1	65 (meas)	65	48 (65/1.35)	-
Baker	$1/2 \times 10^8$	8.4	545	780	400	-

Sketch D - Values for Froude Scaling of the Mono Lake Surface Burst

31

of about 1.5 when the depth of burst increases from zero to 0.16 R_c (as for Baker). With this correction the measured column radius for Baker is decreased to a value of 520 ft (corresponding to a surface burst) which agrees well with the scaled value of 545 ft. The submerged bubble radius from Eq. (3) is 860 ft, which is only 10 percent higher than the measured column radius for Baker.

5.1.4 Energy Partitioning

It is concluded that all the foregoing data agree closely with the empirical scaling rules given by Eqs. (9) and (10) when reasonable corrections are made to allow for variations in the test conditions. The portion of the charge yield which is put into the cavity as stored gravitational energy (for an HE explosion at the surface of deep water) can be calculated as follows.

From Eq. (9) the cavity radius is

$$R_c = 4.80W^{1/4}$$

Then from Eq. (7) the cavity energy (with $D_c = R_c$) is

$$E_c = N\pi\rho g \, R_c^{\;4} \text{ with } 1/6 < N < 1/3$$

so that

$$\frac{E_c}{W} = N\pi\rho g(4.8)^4$$

and with Eq. (2) we get

$$\frac{E_c}{E_o} = \frac{N\pi(62.5)(530)}{1.43 \times 10^6} = 0.0727N \begin{array}{c} < 0.024 \\ > 0.012 \end{array}$$

32

Thus only about 2 percent of the charge yield is stored as gravitational energy in the expanded cavity for a surface burst, whereas nearly 40 percent is stored in the expanded bubble from a submerged burst [as calculated from Eq. (3) with $E_c = (4/3) \pi A^3_{max} \rho g Z$].

When the energy in the wave train is equal to that stored in the last cavity shape shown in Sketch C with $D_c = R_c$, the peak wave height from the Kranzer-Keller theory is given by

$$R\eta_m = 0.89 \ R_c^{\ 2} \tag{11}$$

according to Table 6 of Ref. 4 for deep water. The experimental value for the constant in the foregoing equation was about 0.60 for the Mono Lake shots at shallow depths (as indicated by Fig. 13, Ref. 1, when the values shown are multiplied by 1.35^2 to allow for the fact that the measured column radius was used for R_c there). The corresponding measured value for the URS wedge tank tests was about 0.50 as shown by Fig. 13, Ref. 1. For the exploding wire tests the value was about 0.11 as shown for the surface bursts in Fig. 89. Thus the portion of the cavity energy E_c which propagated outward as surface waves was about $(0.60/0.89)^2$ or 45 percent for the Mono Lake tests, 25 percent for the wedge tank tests, and 1.5 percent for the exploding wire tests. These values indicate that the frictional losses associated with the collapsing cavity were much greater for the small surface bursts than the large ones.

The following values of energy are estimated for the exploding wire tests specifically:

● Initial stored electrical energy

$$E_i = 0.5CV^2 = 0.5 \left(15 \times 10^{-6} \ \text{farads}\right)\left(15 \times 10^3 \ \text{volts}\right)^2$$
$$= 1690 \ \text{joules} = 1240 \ \text{ft-lb}$$

33

- Energy released by equivalent TNT charge from submerged bubble radius Eq. (3)

$$A_{max} = 2.07 \text{ in.} = 0.1725 \text{ ft}$$

$$W_{TNT} = Z\left(\frac{A_{max}}{12.6}\right)^3 = 33.5\left(\frac{0.1725}{12.6}\right)^3 = 0.86 \times 10 \text{ lb}^{-4}$$

$$E_O = 1.43 \times 10^6 \times 0.86 \times 10^{-4} = 123 \text{ ft-lb}$$

- Cavity energy for surface bursts [Eq. (7)]

$$R_c = 2.30 \text{ in.} = 0.192 \text{ ft}$$

$$E_c = \frac{\pi}{3} \rho g R_c^4 = \frac{\pi}{3}\left(62.5\right)\left(.192\right)^4 = 0.090 \text{ ft-lb}$$

- Energy in wave train for surface bursts [Eq. (11)]

$$E_w = E_c\left(\frac{R\eta_m}{0.89R_c^2}\right)^2 = 0.09\left(\frac{0.11}{0.89}\right)^2$$

$$= 0.09 \times 0.154 = 0.0139 \text{ ft-lb}$$

Thus it is estimated that only 0.0011 percent of the stored electrical energy propagated away from the surface bursts in the wave trains.

5.2   UPPER CRITICAL DEPTH AND DATA SCATTER

5.2.1   Variations in Cavities

For those tests where the cavity walls did <u>not</u> collapse inward (hence, those without either necking down of the cavity or jet impingement on the

34

bottom of the cavity) the expansion and collapse of the cavity was a reasonably orderly and simple process. These non-collapsing shots included all the surface bursts at both values of atmospheric pressure, and all but the deepest shots at reduced pressure (22, 26, and 26R). Nevertheless, the cavities and waves produced by these non-collapsing shots vary greatly. For example, in Tables 1 and 2, compare shots 1 and 5 at zero depth of burst, and shots 20 and 25 at 0.08 in. depth. Some of this unrepeatability is clearly due to variation in the effective yield of the exploding wires since there was a $\pm$ 10 percent variation in the bubble size even for the deeply submerged bursts (Ref. 1). However, most of the unreproducibility for the near surface shots was not due to this cause, but rather to the fact that there were two distinctly different types of water columns produced by these shots, including the repeat shots at the same depth. The two different types of columns are clearly evident when the cavity is about half expanded. To illustrate these two types of columns, the early expansion of shots 1, 5, 20, and 25 are shown in Figs. 27 through 30.

Shots 1 and 25 produced cavities that flared open at the top during their expansion so that the fully expanded cavity is surrounded by a thin lip of water. The thin lip ends in a ragged edge which never rises above the field of view of the schlieren beam. No water or hot gas flowing out of the top of the flared cavity is visible in the schlieren pictures. On the other hand, shots 5 and 20 produced cavities which appear to be topped by a plume of spray which travels upward much faster than the lipped columns. The plume later turns into a cloud which rises out of the field of view well before the cavity is fully expanded. Although the consistency of the material in the plume and cloud is not known (i.e., how much is vapor and how much is liquid), it appears that its rapid upward projection causes a larger impulse to be applied to the water, and hence a larger cavity and wave train.

For the submerged wires, it appears that the water above the explosion is ruptured and flared open in one case, but is shattered and sprayed upward in the other case. The water shock wave reflecting off the surface as a tension wave apparently can rupture the water either by flaring it open or by breaking it into small pieces to form a spray. Examination of the

35

photographs of the cavities show that the last 12 of the first 16 shots at
normal pressure all projected a spray or cloud upward over the expanding
cavities; the first 4 shots produced flared cavities. For all the submerged
shots, the cavity walls subsequently collapsed inward and impinged on the
bottom of the cavity. Two of the surface bursts (5R and 6R) gave cavity walls
which tapered inward but did not impinge on the bottom.

At reduced ambient pressure the shots which produced the largest cavities
consistently produced a spray (shots 18, 18R, 19, 19R, 20, 24, and 25R)
whereas most of the others produced a flared open cavity (shots 17, 21, 21R,
23, and 25). For the deepest shots 22, 26, and 26R, it is not clear which
type of cavity was produced because of the subsequent inward collapse of the
walls.

It is clear that the spray producing shots subsequently resulted in
larger cavities and waves, and this effect will be described further because
it appears to be the physical basis for both the upper critical depth
effect and the poor repeatability of explosions at shallow depths of burst
which has been observed consistently during previous HE tests (indicated,
for example, by the dashed lines in Fig. 14 of Ref. 1.

All of the surface bursts for which the cavity flared open produced
nearly the same expanded cavity size regardless of the ambient pressure level.
That is, for shots 1 through 4, 17, and 23 in Table 1, the cavity diameter
varies only from 4.55 to 4.75 in., which is less than the $\pm$ 10 percent
variation in the submerged bubble diameter. The only two surface bursts in
the present test series which sprayed open were shots 5 and 6 where the probe
was placed horizontally and the wire was oriented vertically. These shots
gave distinctly larger cavities. Repeats of these shots also sprayed open
but then gave tapered columns and smaller cavities.

It is not clear how the spray was formed by these surface bursts, but
its formation does not correlate with the wire orientation, since the three
surface bursts in the previous test series (shots 12, 21, and 32 in Table 2
of Ref. 1) also projected spray (as shown by the high-speed films), and the

36

cavities were larger even though the probe was oriented in its normal position (vertically upright with the wire lying on the water surface). Although values of D_{max} for these shots range between 3.19 and 3.37 in., as listed in Table 2 of Ref. 1, these values were obtained from the last frame of the high-speed films before the cavities were fully expanded. The corresponding values for the new tests range between 2.25 to 2.30 in. for the flared cavities (1, 17, and 23) and between 3.00 and 3.60 in. for the sprayed cavities (shots 5 and 6). Thus it is concluded that the previous surface bursts produced large sprayed cavities (consistent with shots 5 and 6) even though the probe orientation corresponded with shots 1, 17, and 23 which gave small flared cavities. This difference illustrates the fact that for shallow explosions the cavity size correlates more with the production of a flared or sprayed cavity than with the orientation or depth of the wire, but there is a statistical probability for each type of cavity which depends on depth of burst, ambient pressure, probe orientation, etc.

5.2.2 Upper Critical Depth

It can be seen in Figs. 87 and 88 that the variation of cavity size and peak wave height with depth of burst is much more orderly, consistent, and repeatable at normal atmospheric pressure than when the pressure was reduced. This is because of all the shots (with the normal probe position) produced spray except for the surface bursts in Fig. 87, whereas in Fig. 88 some of the repeat shots produced flared cavities and some produced spray as described previously.

The existence of the upper critical depth peaks in Figs. 87 and 88 is thus associated with the probability of water being sprayed upward rather than flared open, and this probability is apparently highest (but not 100 percent) at the upper critical depth.

However, there appears to be another distinction between the sprayed and flared cavities which explains why the larger (sprayed) cavities were somewhat more efficient wave generators than the smaller (flared) cavities. This is

37

apparent from the larger values of $R\eta_m/R_c^2$ for shots 5 and 6 in Table 1 and for the other sprayed cavities at reduced pressure in Fig. 89.

To illustrate this distinction the shapes of the successive water mounds and cavities are shown in Figs. 31 through 34 for two repeat surface shots (1 and 5) and for two repeat shots at reduced pressure (20 and 25). These mounds and cavities show the maximum displacement of the water as it oscillates. It can be seen that cavities which sprayed upward (shots 5 and 20) not only produced larger fully expanded cavities, but also the subsequent water mounds were disporportionately larger still.

It is believed that the reason for this is that the sprayed clouds prevented the flow of surrounding air into the fully expanded cavities, whereas the ambient air rapidly filled the fully expanded cavities which flared open at the top. Hence a partial vacuum was held longer over the fully expanded sprayed cavities which caused them to rise into much higher mounds than the flared cavities.

In Figs. 87 and 88 there is a sharp reduction in cavity radius as the depth of burst is reduced to zero, and this reduction might be attributed either to the upper critical depth effect, or to the loss of energy by radiation to the atmosphere from a highly concentrated burst at the water surface. However, it appears that the decrease is actually a statistical effect caused by the formation of two types of cavities (sprayed or flared) and that either of these two types can be formed by bursts at any shallow depth (at least when the atmospheric pressure is reduced). The calculations in Subsection 4.1 indicated that the blow-in associated with the flared cavities will decrease with increasing yield (under normal atmospheric pressure) since the pressure within the larger cavities will not drop so far below the atmospheric level. The low atmospheric pressure required to significantly reduce the blow-in for small bursts cannot be achieved with water (since it flashes to steam at about 0.05 atm) although water is required (rather than oil) to generate condensible steam detonation gas by exploding wires. Two alternative ways to generate small yield surface burst with steam, but without blow-in, might be to use steam producing charges (lithanol) in

38

an oil tank under high vacuum (although such small charges are difficult to detonate), or to use exploding wires in a centrifuged water tank such as the NOL facility (although coriolis forces will distort the water column).

5.3 SIMULATION OF LARGE HE AND NUCLEAR TESTS IN SHALLOW WATER

5.3.1 Cavities

Mono Lake (Shot 8). During the 1965 Mono Lake tests, shot 8 was fired at a depth of 51 ft, the total water depth was 130 ft. The shot produced a plume (or mound) of water over 300 ft high with a maximum diameter of about 160 ft (at a height of 80 ft) according to Ref. 6. The bubble radius A_{max} calculated from Eq. (3) is 61 ft. Four wires were exploded to approximate the conditions for this shot, two repeat tests at normal atmospheric pressure (33 and 34) and two at 1/2 atm (41 and 42). The water depth and depth of burst were scaled in proportion to A_{max} which was taken equal to 4.10 in. for the wire under normal pressure (as estimated from the results in Ref. 1) and 5.16 in. under vacuum [in accordance with Eq. (31)]. The bubbles produced by the four shots were between 12 and 23 percent larger than predicted, but the pictures of the bubble and plume in Figs. 38 and 44 show at least quali- tatively the initial water motion for the Mono Lake shot. It can be seen that the bubble migrates downward to the bottom as the plume expands so that the waves are generated by the collapse of an initially elevated mound of water rather than a surface cavity. The size of the mound relative to the bubble increased when the atmospheric pressure was dropped to 1/2 atm during the wire tests, and increased even further for the Mono Lake test since the atmospheric pressure was even smaller (relative to the hydrostatic head of the bubble radius).

The peak wave heights generated by the full-scale and laboratory tests appear to scale well based on the maximum bubble radius A_{max} since

$$\frac{R\eta_m}{A_{max}^2} = 0.13 \text{ for Mono Lake shot 8}$$

$$= 0.15 \text{ and } 0.11 \text{ for shots 41 and 42}$$

39

Considerably larger values were given by the two tests at normal pressure (0.23 and 0.24 for tests 33 and 34 in Table 3) so that these bubbles were more efficient wave generators. This apparently occurred because the higher atmospheric pressure confined the water plume to a narrow mound (Fig. 38), whereas the partial vacuum caused the plume to be more irregular with the protrusion of spike jets of water as indicated in Fig. 44.

CROSSROADS-Baker. Tests 29, 30, 37, and 38 and their repeats were designed to simulate CROSSROADS-Baker, a 23.5 kt burst at mid-depth in 180 ft of water. The measured maximum column diameter was about 1560 ft as assumed in Ref. 4, where the calculated and measured wave trains are given along with the original data sources. Thus the actual value of D_{max}/d_w was 8.7, whereas the values obtained for the tests ranged between 12.9 and 24.2 as shown in Table 3. Thus the water depth and gage ranges for the tests were considerably smaller in proportion to the column diameter than for the actual burst because the column diameters were much larger than predicted. This increase in column diameter with reduced water depth does not agree with the results obtained previously in the URS wedge tank or at Mono Lake (where there was almost no change in column diameter as the water depth was decreased as described in Ref. 4). The closest scaled test was 38R for which the wire yield was abnormally low, but this test gave peak wave heights which were too small ($\pm$ 0.01 in.) to be measured accurately, as shown in Fig. 83. The column walls tapered inward for this test more than the others, even those at normal atmospheric pressure. The scaled wave heights for Baker given in Table 2 of Ref. 4 were considerably larger than the test values in Table 3, probably because of the overly shallow water during the tests. However, the wave gage records have the same general shape as those measured at CROSSROADS-Baker as shown by comparison of Figs. 79 and 82 with Figs. 14 of Ref. 8.

HARDTACK-Umbrella. The same difficulties encountered with Baker occurred for the tests designed to simulate HARDTACK-Umbrella. The actual column diameter to water depth ratio was 9.3 from Ref. 4, whereas the tests (31, 32, 39, and 40) gave values ranging from 12.2 to about 21.3. Again the tests most closely simulating Umbrella (39R and 40) gave very small waves.

CASTLE-Flathead. The tests designed to simulate CASTLE-Flathead (27, 28, 35, and 36) gave very large ratios of column diameter to water depth (ranging between 91 and 107). These values are much higher than the estimated full-scale value of 17.7 both because the column diameters for the tests was underestimated and because the diameter for Flathead was overestimated. The estimates were off because in both cases the column radius was estimated to be equal to the bubble radius A_{max} as for the previous tests. In deep water this approximation is accurate until the depth of burst becomes smaller than $A_{max}/4$ as shown in Fig. 11 of Ref. 1. The approximation is also reasonably accurate for both Baker and Umbrella even though the water depth was much less than the column diameter. However, for large bursts at very shallow depths, such as for Flathead, the column radius R_c is much smaller than A_{max} (even though small explosions give just the opposite effect as shown in Fig. 11 of Ref. 1. Hence for near surface bursts (where $d \ll A_{max}/4$) the scaling rule given by Eq. (9) should be used to estimate the column radius rather than the approximation that was used ($R_{col} = A_{max}$ which applies only when $d \geq A_{max}/4$). This scaling rule applied to Flathead gives the predicted full-scale value $R_{col}/d_w = 17.7$. This ratio should be reduced to allow for nuclear radiation losses to the atmosphere at very shallow depth so that the final predicted ratio for Flathead is not much greater than for Baker (8.7) or Umbrella (9.3). In other words, the scaled water depth was nearly the same for all three tests.

All of the tests to simulate Flathead gave wave gage records which were almost imperceptibly small and they are not reported here. However, the data in Table 3 show that for bursts in very shallow water ($D_{max}/d_w > 10$) the column diameter D_{max} does not depend upon the water depth, depth of burst, or atmospheric pressure (at least within the experimental scatter for tests 27 through 32 and 35 through 40). The Flathead tests (27, 28, 35, and 36) all gave very thin column walls which tapered slightly either inward or outward when the atmospheric pressure was either normal or half-normal (as shown in the figures giving the cavity shapes for these shots).

The Baker tests gave column walls which tapered inward more than the fore-going tests at normal pressure, and which were nearly parallel at 1/2 atm (except for test 38R for which the low yield produced a small collapsed column).

The Umbrella tests gave column walls which collapsed inward at normal pressure, but were nearly parallel at 1/2 atm (except for tests 39R and 40 for which the low yield produced small collapsed columns).

Tests 35 through 40 in shallow water at 1/2 atm indicate that the column wall collapsed inward when the yield was insufficient to produce a column diameter to water depth ratio greater than about 15. Hence it appears that the column walls collapsed inward more readily than for small HE charges, as reported in Ref. 7. This probably was caused by the condensible gas (steam) generated by the bridge wires rather than the HE detonation products.

5.3.2 Wave Trains

The wave trains were calculated for tests 5R, 18R, and 19R in deep water and for shot 38 in shallow water. The computer code from Ref. 4 based on the Kranzer-Keller theory for dispersive wave trains was used. The calculated wave peaks are shown in Figs. 51, 67, 69, and 82 for comparison with the measured wave gage records. All of the calculated wave peaks shown were reduced by the factor K = 10 and the initial time adjustment for the calculations are shown in the figures. The assumed initial cavity shape is the last one shown in Sketch C except that the bottom of the cavity was truncated in shallow water. It can be seen that the three wave trains measured in deep water correlate reasonably well with the wave peaks calculated in the first lobe of the theoretical wave train (after the calculated peaks are shifted by a constant time increment and reduced in height by a constant factor). The agreement could be improved somewhat if the larger column diameter were used for the initial cavity diameter rather than the "fully expanded" cavity diameter. This would make the calculated wave lengths and periods somewhat longer.

The calculated wave train in shallow water does not agree nearly so well with the measured data. It can be seen in Fig. 82 that the measured waves

have periods much longer than calculated and even longer than the lobes in the
calculated wave envelope (which lie between the nodes indicated in Fig. 82).
It appears that many of the theoretical waves disappeared or combined to form
fewer waves.

The main reason for the poor agreement in Fig. 82 is that the gage range
(20 in.) is not much larger than the column radius (4.6 in.). At such short
range the full-scale wave trains did not agree with those calculated (Ref. 4)
even though the agreement was fairly close at longer range. The main diffi-
culty it short range is that there are very few waves in each lobe of the wave
envelope. In the present case (Fig. 82) there are no waves in the first lobe,
one in the second, and one in the third. There is poor agreement beyond the
first lobe of the calculated envelope even for the wave trains over deep water
(Ref. 4), and with so few waves in the lobes the "method of stationary phase"
used to calculate the waves becomes inaccurate.

Another difficulty is that the calculated wavelengths are reduced since
they lie further back in the wave envelope. Thus the period of the calculated
peak wave between the second and third nodes in Fig. 82 is about 0.26 sec, and
the wavelength is about 4.3 in. Thus the calculated waves are longer than
capillary waves, even in shallow water, but the nodes cause short sharp peaks
to appear in the calculated wave trains and these tend to be smoothed out by
surface tension. This affect is not included in the theory of course. The
same smoothing effect was observed in the comparison of the calculated and
measured full-scale wave trains in Ref. 4 to a much smaller extent, and the
effect was ascribed to hydrodynamic instability (also neglected in the theory).

43

Section 6
RESULTS, CONCLUSIONS, AND RECOMMENDATIONS

The main results of the foregoing exploding wire tests and their analysis are:

1. The cavities generated at the surface of the deep water scale well with those generated by small and large HE explosions and by nuclear explosions when all the data are adjusted to the normalized condition of an HE explosion at the surface of deep water. The gravitational energy in the normalized cavities is about 2 percent of the explosive yield.

2. The wires exploded just beneath the water surface under normal atmospheric pressure produced collapsing column walls with jet impingement on the bottom of the cavities just as observed for 1-lb HE charges. However, there was no jet impingement for surface bursts (for which there are no 1-lb data), or for shallow depths of burst when the atmospheric pressure was reduced to half the normal value.

3. The atmospheric pressure must be reduced somewhat more to prevent the column walls from tapering inward for exploding wires than for HE explosions. Apparently this is because the steam produced inside the columns by the wire explosions condenses and reduces the pressure lower than for the HE detonation products.

4. There was a distinct increase in the column diameter as the water depth was reduced even though this was not the case for HE explosions. This caused all of the scaled dimensions for the shallow water tests to be too small in proportion with the column diameter.

5. The distinct upper critical depth effect observed for the exploding wire tests was caused by the fact that two types of cavities were produced, those that flared open and those that sprayed upward. The sprayed cavities were distinctly larger and hence produced larger waves with slightly greater efficiency since the spray appeared to prevent the inflow of ambient air into the cavity. Therefore, a vacuum was held longer over the larger cavities causing them to rise into much larger mounds of water than for the flared cavities. Both types of cavities were produced at the same depth of burst when the atmospheric pressure was reduced which caused large variations in the data.

6. The maximum column radius was about 35 percent larger than the radius of the cavity when it was fully expanded to maximum depth. This

45

factor gives the cavity radius needed to calculate the wave trains from the column radius observed for large explosions near the surface of deep water.

7. The wave trains calculated from the cavities produced by explosions near the surface of deep water correlate well with the measured wave gage records. However, only about 1.3 percent of the cavity energy propagated away as surface waves so that all the calculated wave heights must be reduced by a factor of about 10. The frictional losses associated with these collapsing cavities were much greater than for larger cavities. This was not the case for more deeply submerged explosions since the bubbles and peak wave height scaled geometrically with those produced for shot 8 of the Mono Lake 1965 test series. The frictional losses were also much higher for the wave trains produced in shallow water corresponding with CROSSROADS-Baker, although the scaled water depth was too shallow.

8. The tests which simulated the deepest Mono Lake shot (8) produced bubbles which first generated a mound of water and then migrated to the bottom.

It is concluded from the foregoing results that the cavities and wave trains produced by the exploding wires with an equivalent yield of about 10^{-4} lbs of TNT can be scaled up to correlate with those produced by large nuclear explosions (over 10^{8} lbs), if the atmospheric pressure and water depth are adjusted so that the geometric shape of the expanded cavity and column is similar to the full-scale shape, and if a higher frictional loss coefficient is used for the smaller cavities.

It is recommended that the tests described here be extended to include:

1. Repetition of those in shallow water to adjust the water depth, atmospheric pressure, and wave gage ranges to more accurately simulate the full-scale tests.

2. Completion of a parametric variation of water depth, depth of burst, and atmospheric pressure; and comparison of the data with that reported by Kaplan and Hudson for small HE charges tested at reduced atmospheric pressure.

3. Simulation of some additional nuclear tests under conditions of special interest, and simulation of multiple and successive bursts.

Section 7

TABLES AND ILLUSTRATIONS

Table 1

DATA FOR TESTS IN DEEP WATER WITH NORMAL ATMOSPHERIC PRESSURE

TEST	d	D_{max} (in.)	η_{m1} (in.)	η_{m2} (in.)	$\dfrac{R_1 \eta_{m1}}{R_c^2}$	$\dfrac{R_2 \eta_{m2}}{R_c^2}$
1	0	4.62	0.060	0.022	0.101	0.074
2	0	4.75	0.050	0.036	0.080	0.116
3	0	4.62	0.055	0.022	0.092	0.074
4	0	4.55	0.030	0.019	0.052	0.066
5	0	7.40	0.120	0.100	0.078	0.130
5R	0	5.85	0.060	0.040	0.040	0.053
6	0	5.92	0.050	0.044	0.051	0.090
6R	0	5.20	0.040	0.030	0.053	0.080
7	0.04	6.37	0.087	0.064	0.077	0.113
8	0.05	6.37	0.105	0.072	0.093	0.127
9	0.06	5.80	0.093	0.058	0.100	0.124
10	0.07	5.87	0.072	0.060	0.072	0.125
11	0.08	5.15	0.060	0.044	0.081	0.120
12	0.10	4.76	0.075	0.040	0.119	0.127
13	0.20	4.90	0.050	0.032	0.075	0.096
14	0.04	6.65	0.073	0.064	0.059	0.104
15	0.06	5.85	0.080	0.056	0.085	0.127
16	0.08	5.80	0.050	0.026	0.053	0.056

NOTE: Wire probe up for all tests except for:

Tests 3 and 4, probe down

Tests 5, 5R, and 6, probe horizontal with wire vertical

Tests 6R, probe horizontal with wire horizontal

R_1 = 9 in., R_2 = 18 in., $d_w \simeq 36$ in.

48

Table 2

DATA FOR TESTS IN DEEP WATER WITH HALF NORMAL ATMOSPHERIC PRESSURE

TEST	d	D_{max} (in.)	η_{m1} (in.)	η_{m2} (in.)	$\dfrac{R_1 \eta_{m1}}{R_c^2}$	$\dfrac{R_2 \eta_{m2}}{R_c^2}$
17	0	4.60	0.045	0.032	0.076	0.109
17R	0	-	0.075	0.045	-	-
18	0.06	6.35	0.112	0.080	0.100	0.143
18R	0.06	5.80	0.105	0.065	0.112	0.139
19	0.07	-	0.100	0.085	-	-
19R	0.07	5.40	0.110	0.075	0.136	0.185
20	0.08	8.10	>0.13	0.130	>0.07	0.142
21	0.10	4.90	0.067	0.37	0.101	0.111
21R	0.10	4.62	-	-	-	-
22	0.20	7.80	>0.120	0.110	>0.071	0.130
23	0	4.62	0.055	0.032	0.093	0.109
24	0.06	5.80	0.072	0.050	0.077	0.107
25	0.08	5.10	0.070	0.040	0.097	0.111
25R	0.08	>9.5	>0.125	>0.125	-	-
26	0.20	5.80	0.070	0.043	0.075	0.092
26R	0.20	3.30	0.037	0.022	0.048	0.123

NOTE: Dash indicates data missing

$p_a = 1/2$ atm, $R_1 = 9$ in., $R_2 = 18$ in., $d_w \simeq 36$ in.

Table 3

DATA FOR TESTS IN SHALLOW WATER

TEST	P_a (atm)	d_w (in.)	d (in.)	D_{max} (in.)	D_{max}/d_w	η_{m1}	η_{m2} (in.)	$\dfrac{R_1 \eta_{m1}}{R_c^2}$	$\dfrac{R_2 \eta_{m2}}{R_c^2}$
27	1	0.073	0	7.50	103.0	-	-	-	-
28	1	0.073	0	7.85	107.0	-	-	-	-
29	1	0.43	0.22	10.40	24.2	0.037	0.022	0.014	0.016
30	1	0.43	0.22	9.85	22.9	0.035	0.022	0.014	0.009
30R	1	0.43	0.22	10.10	23.5	0.038	0.022	0.005	0.017
31	1	0.53	0.53	8.10	15.3	-	-	-	-
32	1	0.53	0.53	7.50	14.1	-	-	-	-
33	1	4.37	1.71	5.06	1.16	-	0.075	-	0.234
34	1	0.245	1.71	4.60	1.05	0.105	0.065	0.197	0.245
35	1/2	0.092	0	8.40	91.0	-	-	-	-
36	1/2	0.092	0	10.40	103.0	-	-	-	-
37	1/2	0.54	0.28	>11.5	>21.3	0.077	0.038	-	-
38	1/2	0.54	0.28	9.25	17.2	0.050	0.027	0.023	0.025
38R	1/2	0.54	0.28	7.00	12.9	0.013	0.007	0.011	0.011
39	1/2	0.67	0.67	≈11.5	≈21.3	0.055	0.032	-	-
39R	1/2	0.67	0.67	6.40	11.8	0.008	0.004	0.008	0.008
40	1/2	0.67	0.67	6.60	12.2	0.023	0.008	0.021	0.015
41	1/2	5.50	2.15	5.78	1.05	0.065	0.065	0.077	0.154
42	1/2	5.50	1.15	6.35	1.15	0.067	0.057	0.066	0.113
43	1	36	4.0	4.62	-	0.020	0.015	-	-

NOTE: Dash indicates data missing

Normal atmospheric pressure except for Tests 35 through 42 at 1/2 atm

$R_1 = 10$ in., $R_2 = 20$ in., $\eta = H/2$ except for Shot 43

Table 4

COLUMN TO CAVITY DIAMETER RATIO FOR DEEP WATER TESTS

SHOT	d (in.)	P_a (atm)	D_{max}	D_{col}	D_{col}/D_{max}
1 flare	0	1	4.62	6.40	1.39
2 flare	0	1	4.75	6.40	1.35
6 spray	0	1	5.92	7.80	1.32
17 flare	0	1/2	4.60	6.25	1.36
21 flare	0.10	1/2	4.90	6.90	1.41
23 flare	0	1/2	4.60	6.07	1.32
25 flare	0.08	1/2	5.10	6.80	1.33
				average	1.36

Table 5

SCALED CAVITY AND COLUMN RADII FOR NEAR SURFACE BURSTS

W (lb)	W^1/4	d (ft)	d_w (ft)	MEASURED R_col (ft)	MEASURED R_c (ft)	$\frac{R_{col}}{W^{1/4}}$	$\frac{R_c}{W^{1/4}}$	$\frac{R_{col}}{R_c}$	DATA SOURCE
0.84×10^{-4}	0.096	0	3	0.27	0.19	2.8	2.0	1.4	EPCO WIRE, Table 1 Shot 1 - flare
		0	3	0.33	0.25	3.4	2.6	1.3	Shot 6 - spray
		0	3	-	0.31	-	3.2	-	Shot 5 - spray
1.19×10^{-4}	0.104	0	2	-	0.33	4.3	3.2	-	URS VACUUM TANK, Ref. 3 and Fig. 11, Ref. 1 1 atm
		0	2	-	0.50	6.5	4.8	-	0.003 atm
1.0	1.00	0	8	4.7	3.5	4.7	3.5	1.3	URS WEDGE TANK, Fig. 4, Ref. 4 0.003 atm
1.0	1.00	1.8	24	6.0	4.0	6.0	4.0	1.5	NRDL- HYDRA, Fig. 4.1, Ref. 5
0.95×10^{4}	9.90	0	130	65	-	6.5	-	-	MONO LAKE (1), Fig. 9, Ref. 6
0.47×10^{8}	82.8	90	180	780	-	9.4	-	-	BAKER, Ref. 8
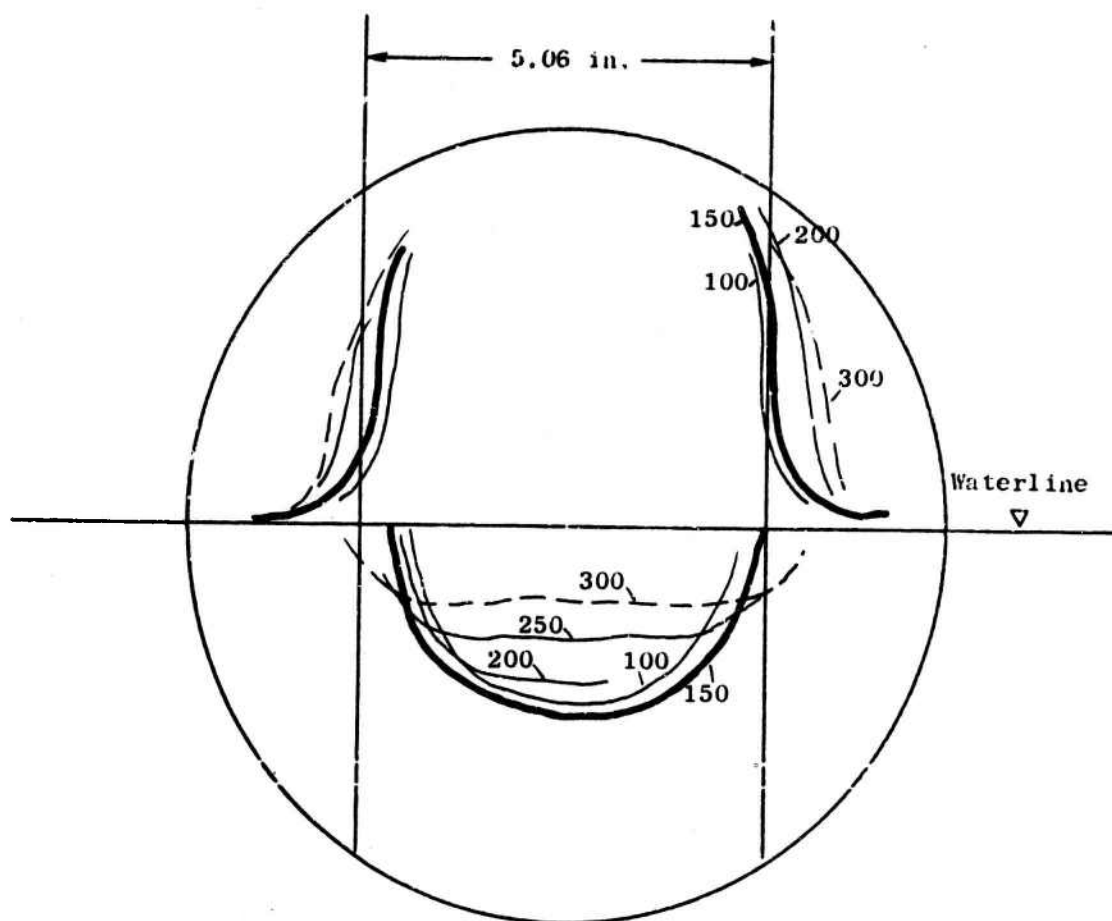
Frame numbers indicated, framing rate = 2500/sec

$$D_{max} = 4.62$$

$$d = 0$$

Shot 1

Fig. 1. Expansion of Cavity and Water Column
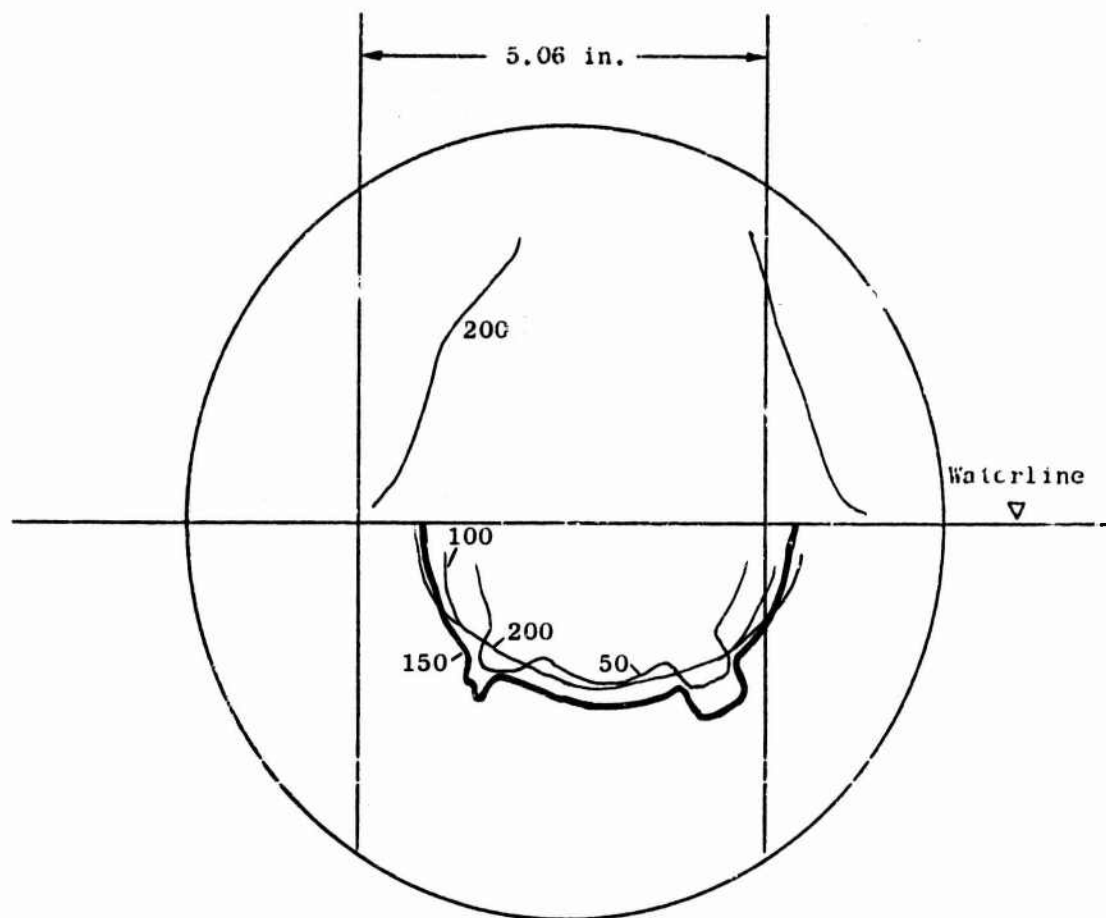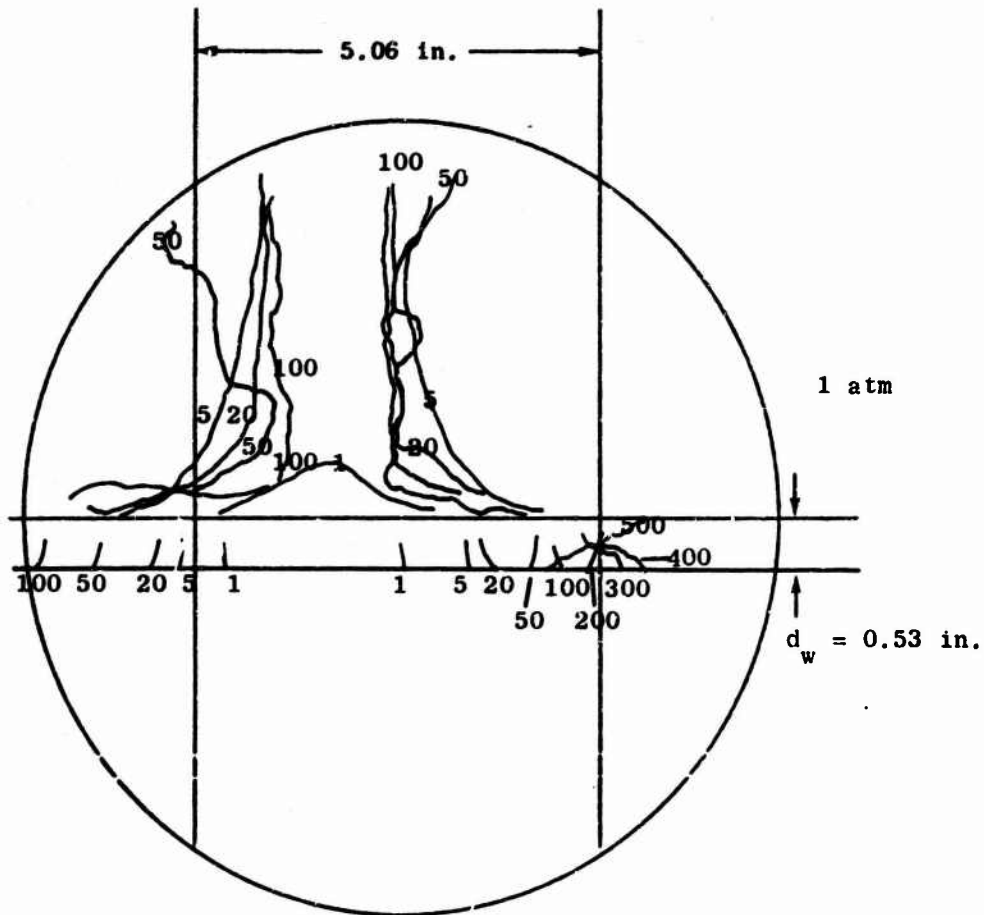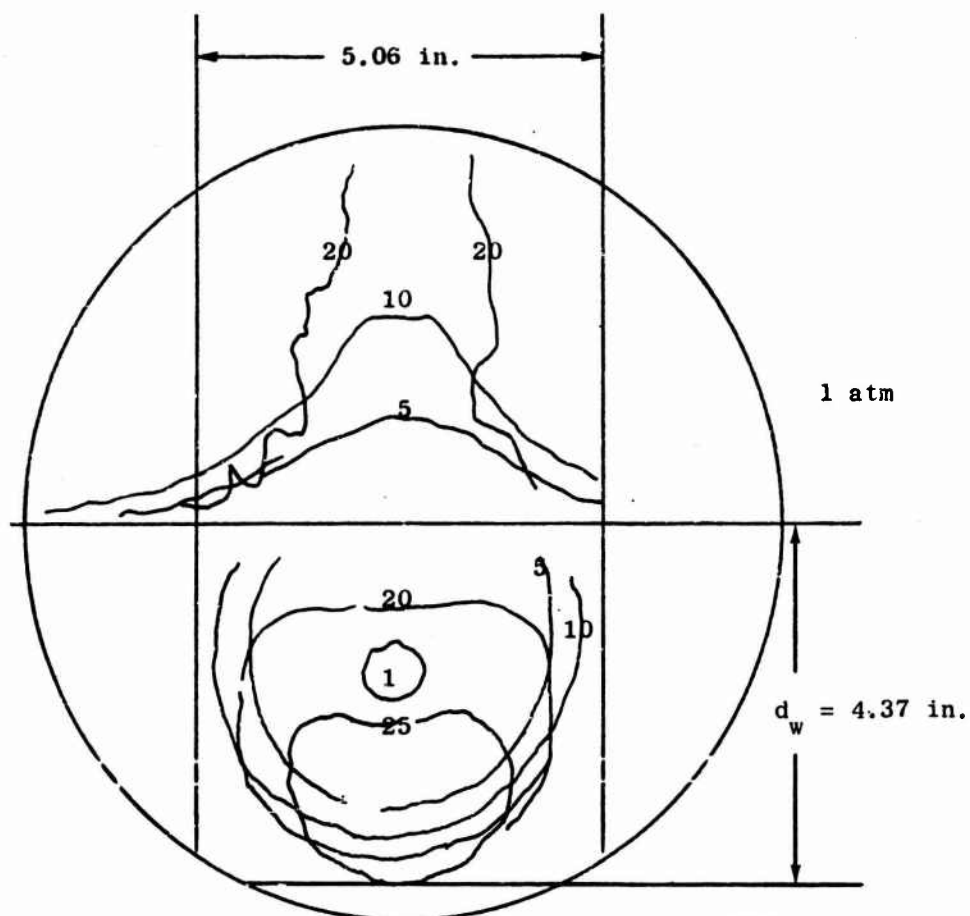
Frame numbers indicated, framing rate = 2500/sec

$$D_{max} = 4.62$$
$$d = 0$$
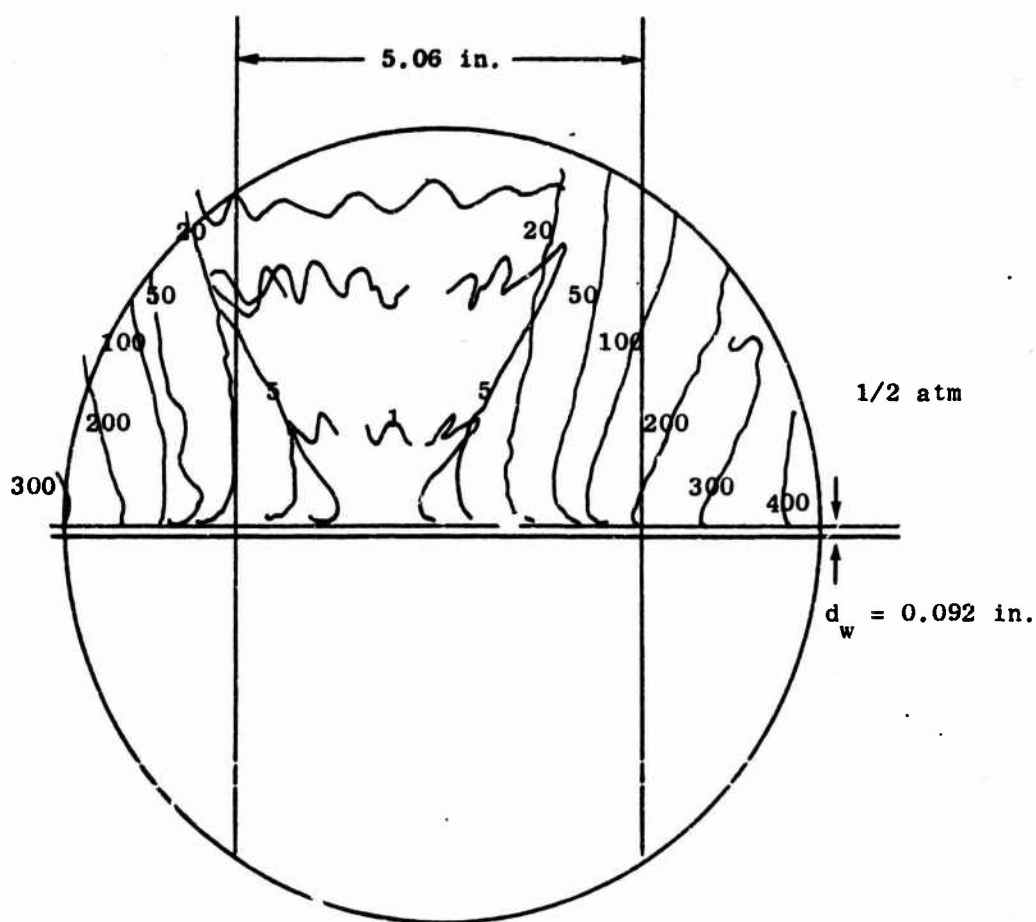Shot 3

Fig. 3.   Expansion of Cavity and Water Column

Frame numbers indicated, framing rate = 2500/sec

$$D_{max} = 4.62$$
$$d = 0$$
Shot 3
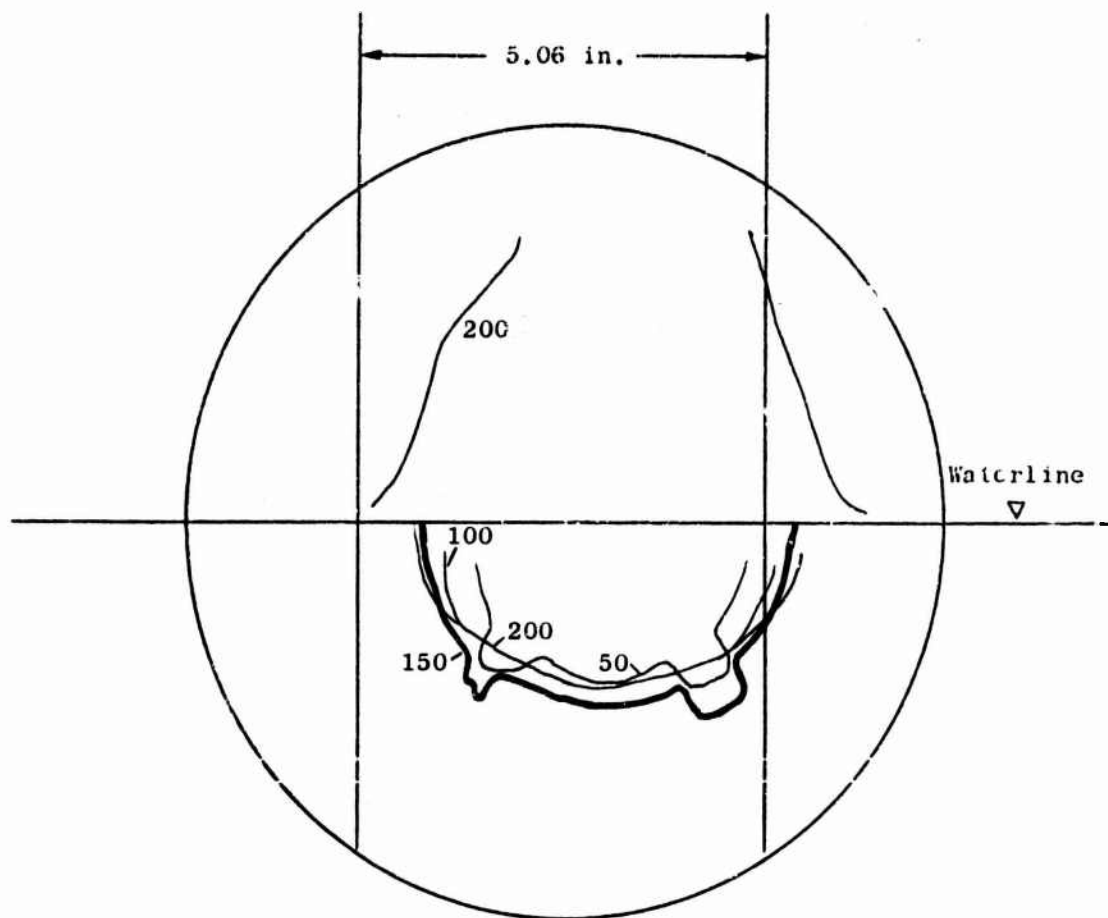
Fig. 3. Expansion of Cavity and Water Column
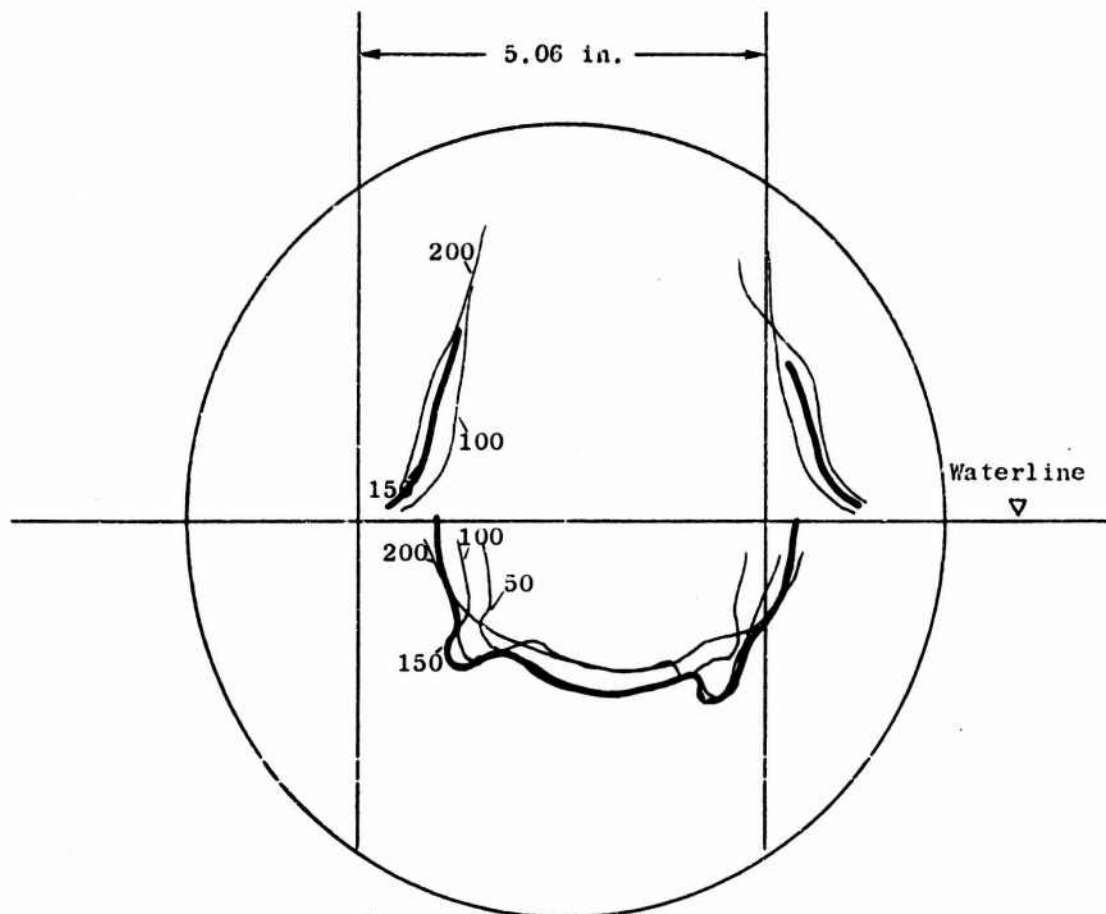
Frame numbers indicated, framing rate = 2500/sec

$$D_{max} = 4.55$$
$$d = 0$$
Shot 4

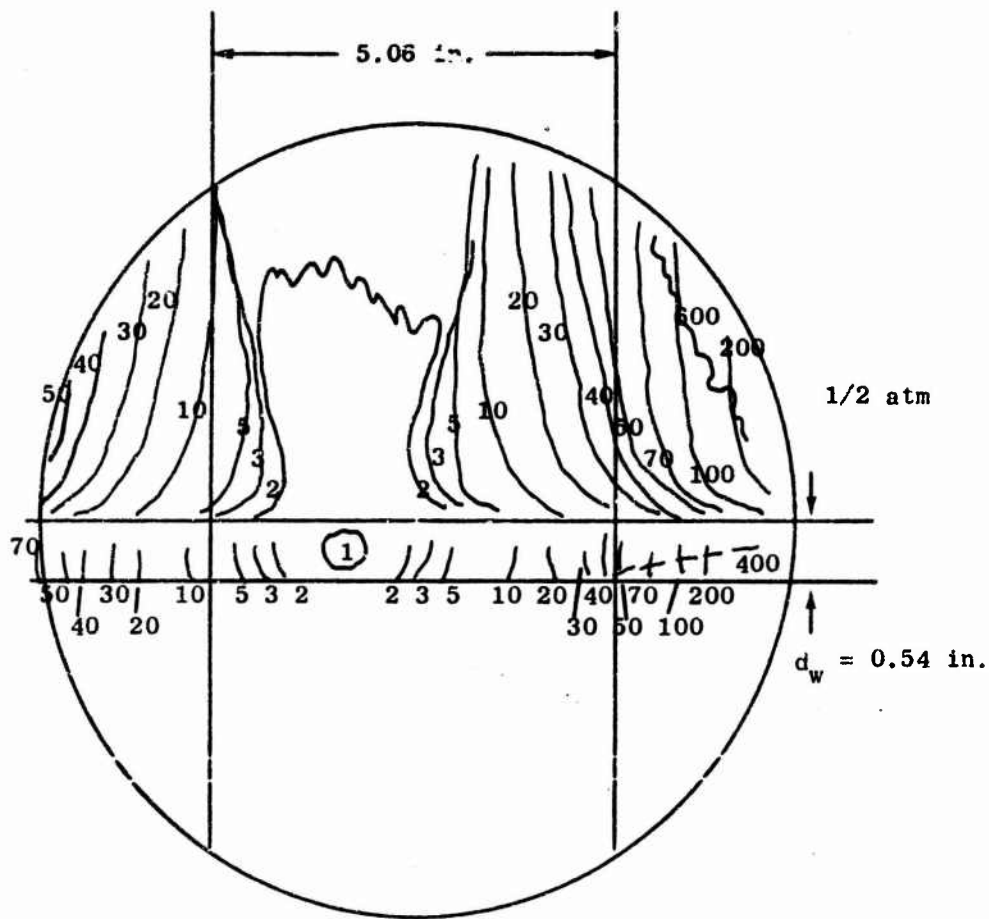Fig. 4. Expansion of Cavity and Water Column

56

$D_{max} = 5.85$

$d = 0$

Shot 5R

$D_{max} = 7.40$

$d = 0$

Shot 5
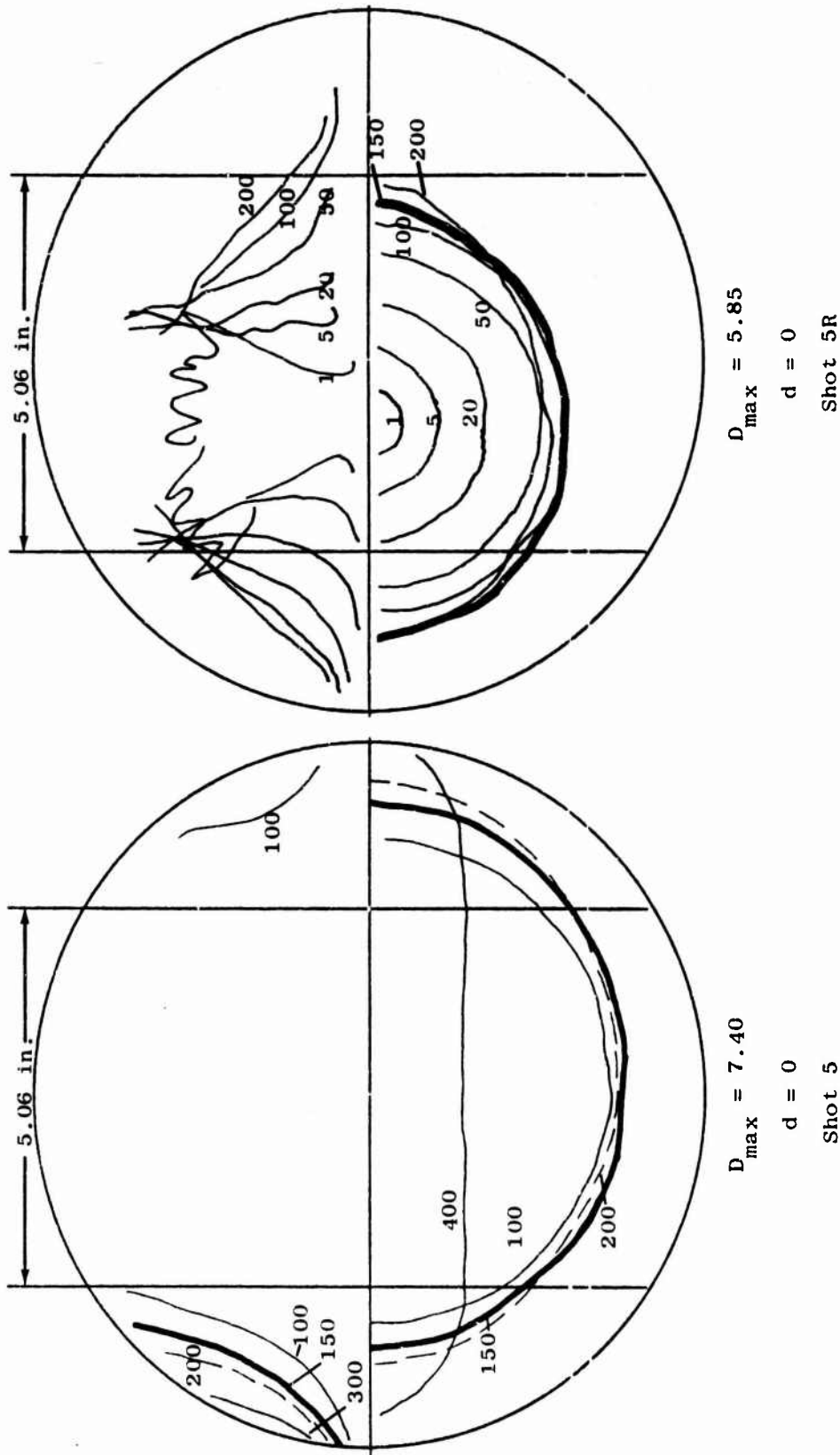
Frame numbers indicated, framing rate = 2500/sec

Fig. 5. Expansion of Cavity and Water Column

57
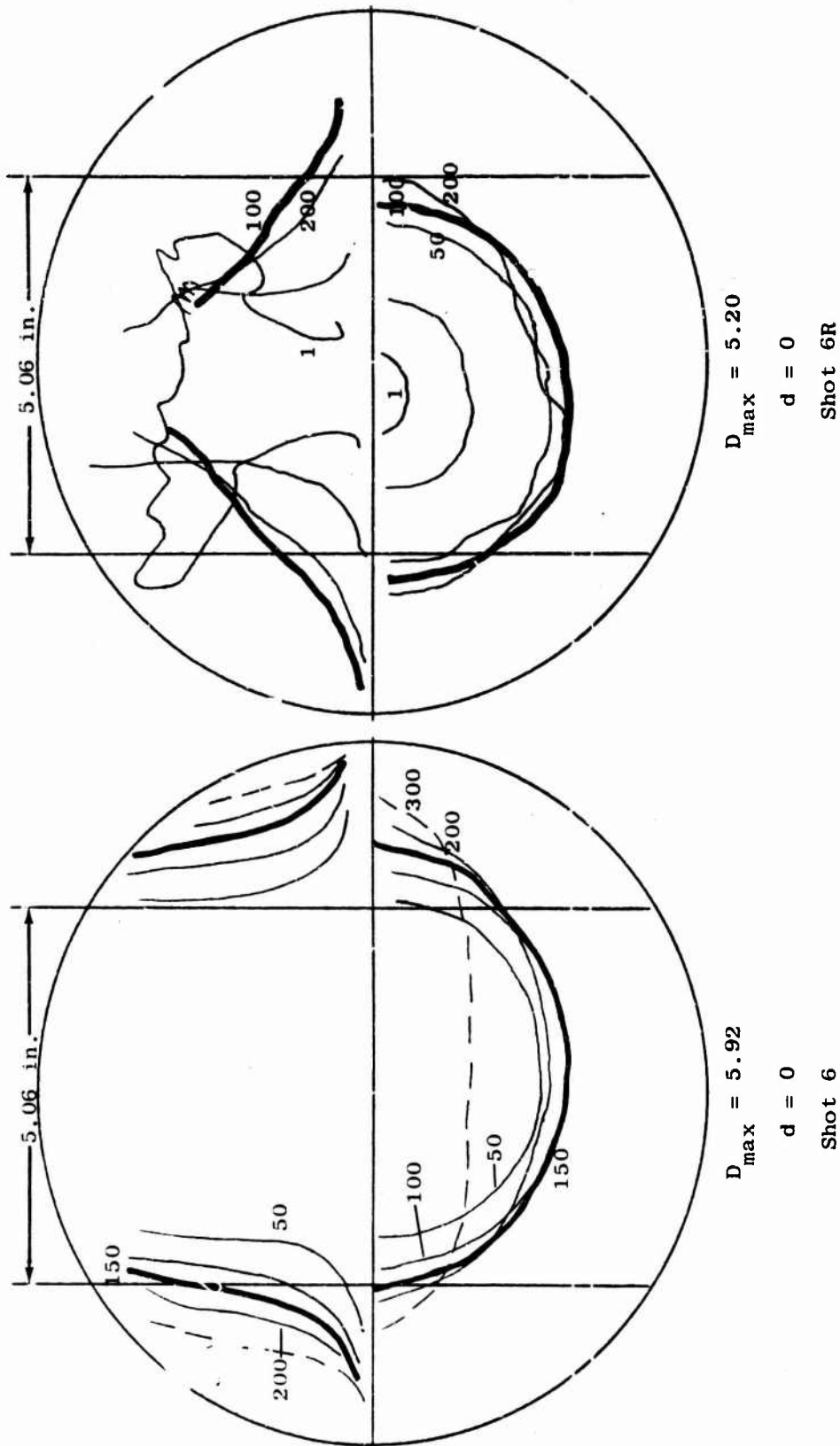
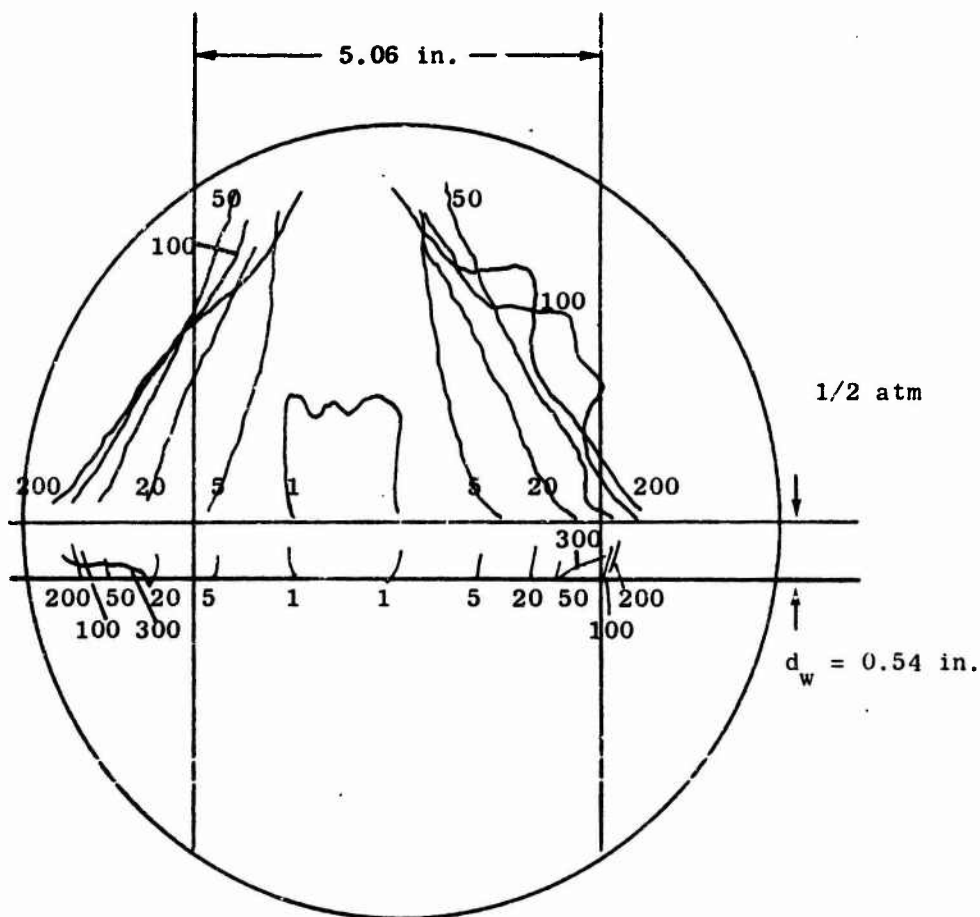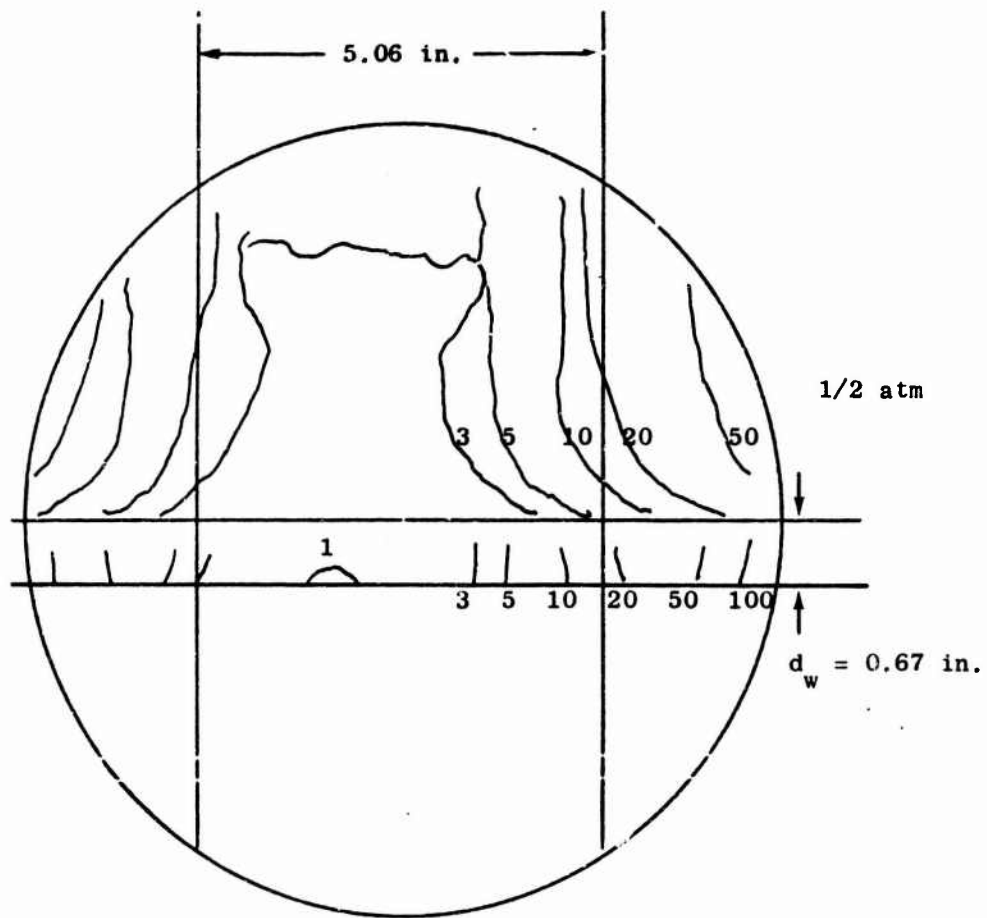Frame numbers indicated, framing rate = 2500/sec

Fig. 6. Expansion of Cavity and Water Column
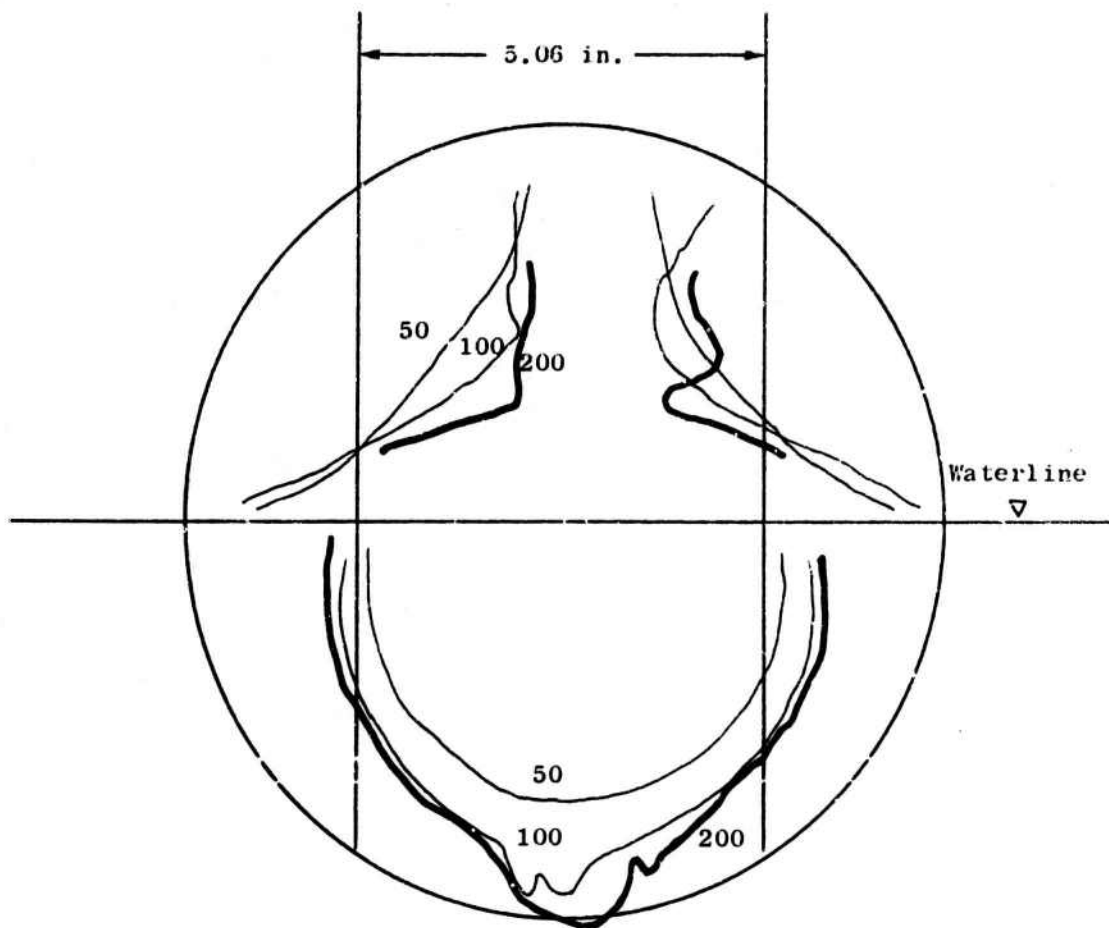
Frame numbers indicated, framing rate = 2500/sec

$$D_{max} = 6.37$$

$$d = 0.04$$

Shot 7

Fig. 7. Expansion of Cavity and Water Column
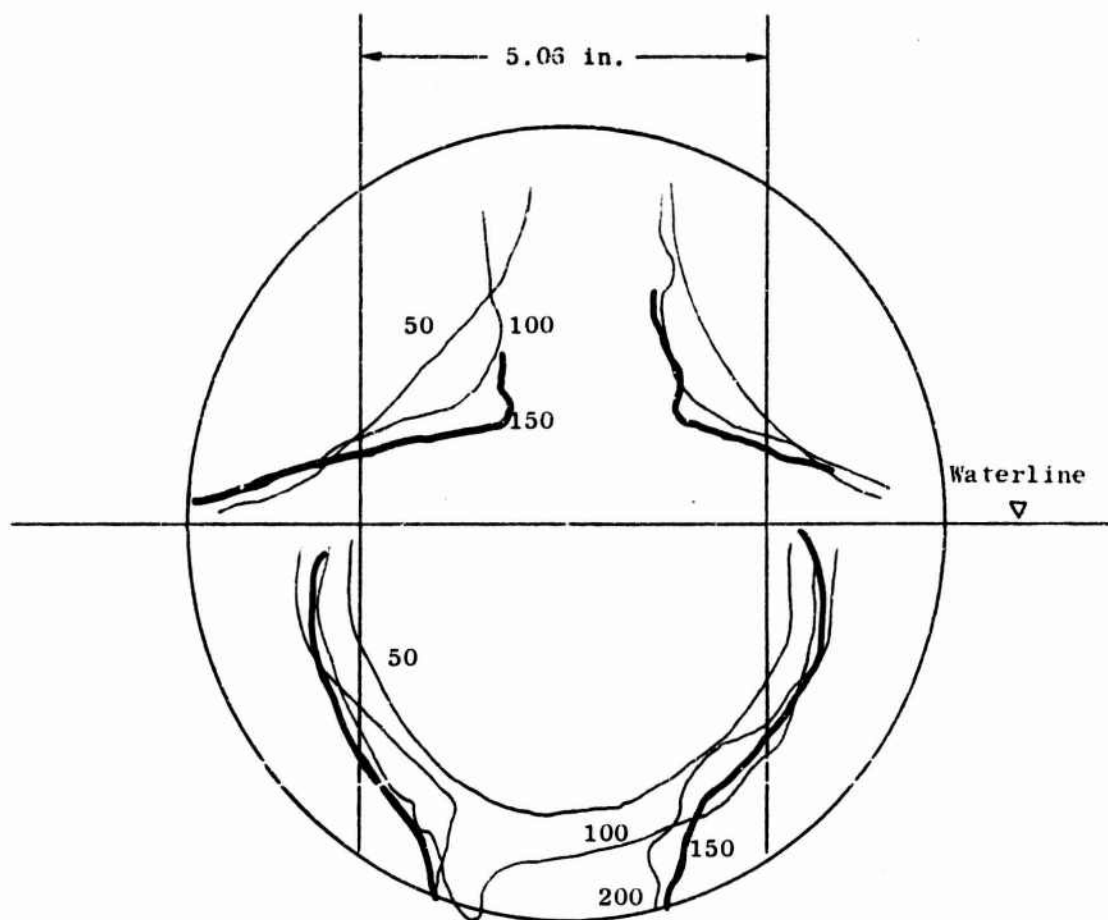
Frame numbers indicated, framing rate = 2500/sec

$$D_{max} = 6.37$$

$$d = 0.05$$

Shot 8

Fig. 8.   Expansion of Cavity and Water Column
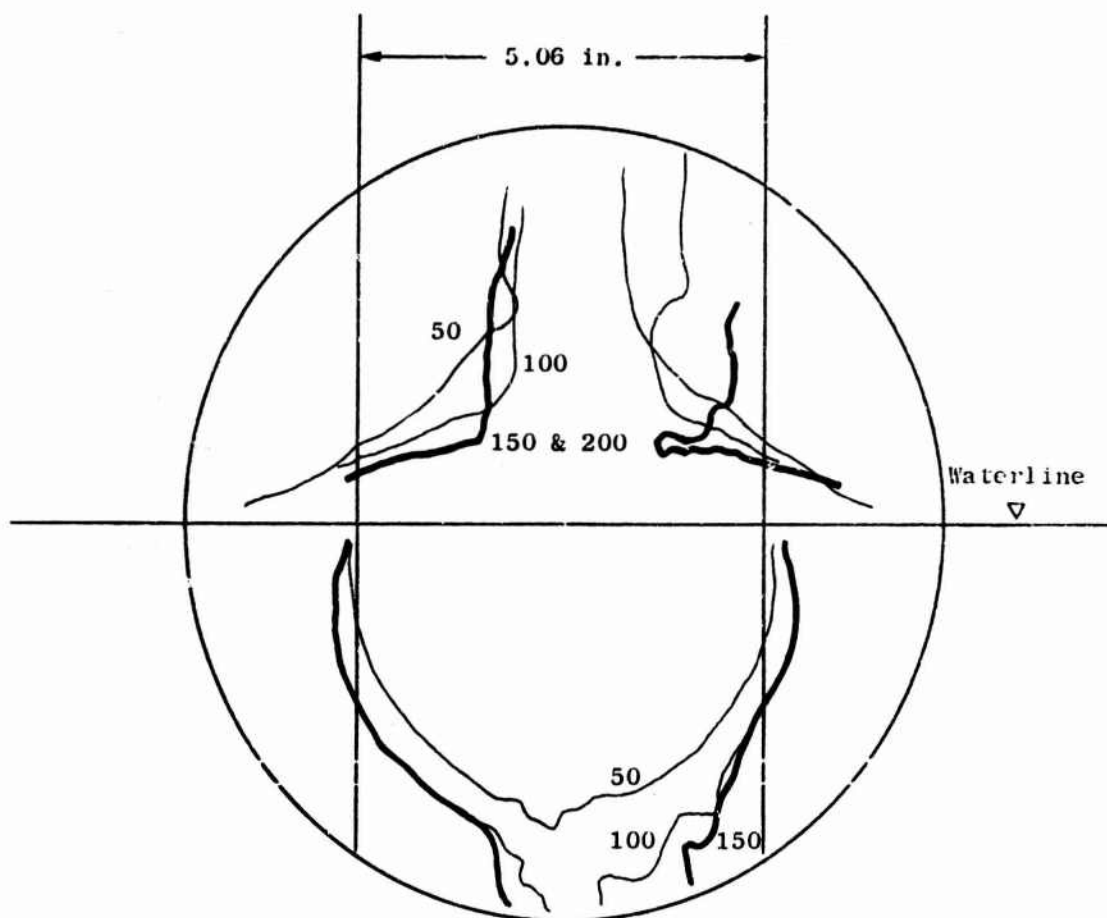
Frame numbers indicated, framing rate = 2500/sec

$$D_{max} = 5.80$$
$$d = 0.06$$
Shot 9

Fig. 9.   Expansion of Cavity and Water Column
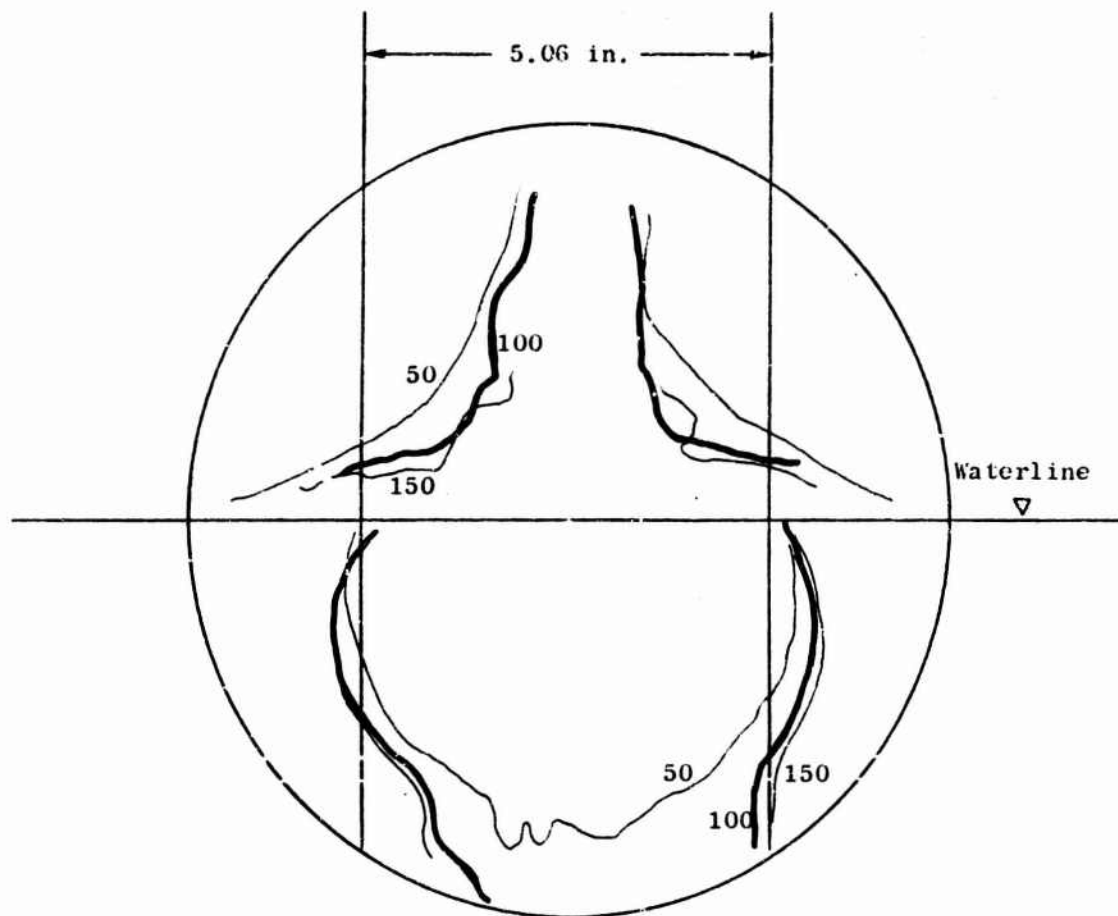
Frame numbers indicated, framing rate = 2500/sec

$$D_{max} = 5.87$$

$$d = 0.07$$

Shot 10

Fig. 10.   Expansion of Cavity and Water Column
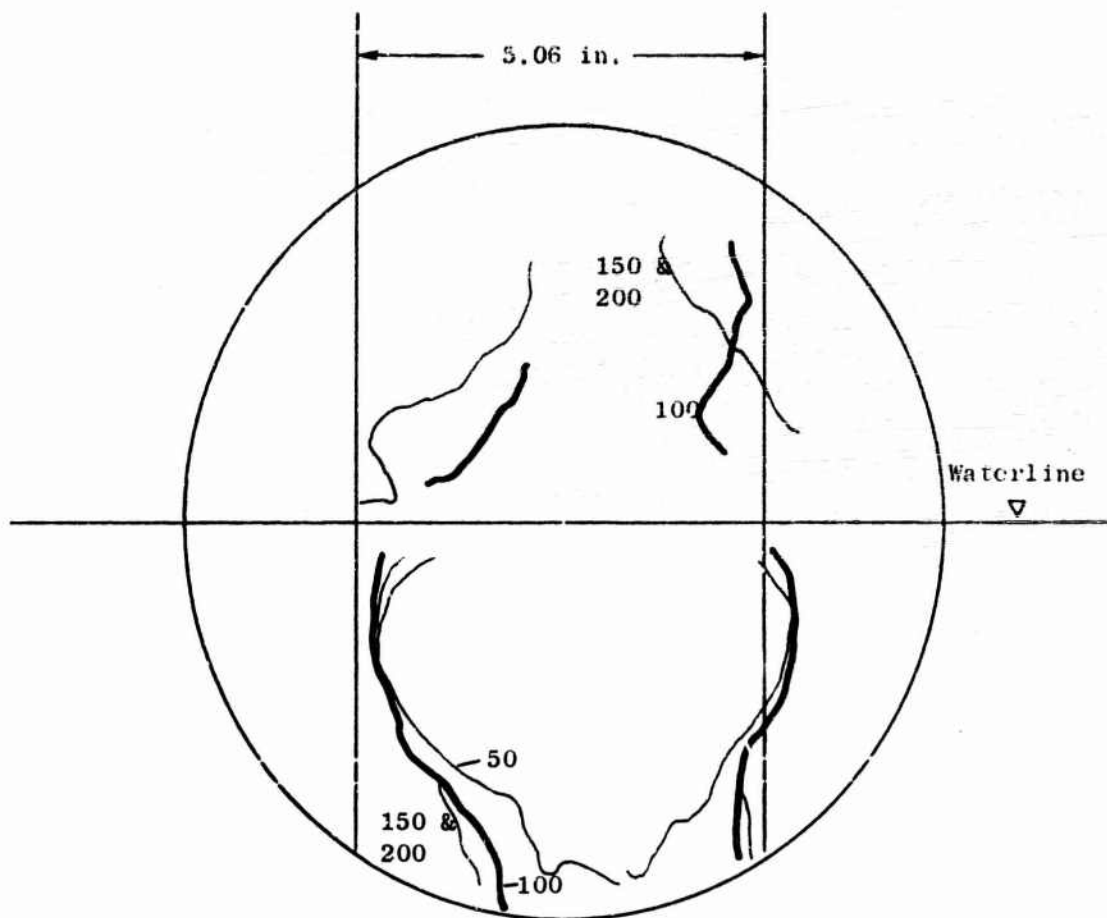
Frame numbers indicated, framing rate = 2500/sec

$$D_{max} = 5.15$$
$$d = 0.08$$
$$\text{Shot} \quad 11$$

Fig. 11. Expansion of Cavity and Water Column

63
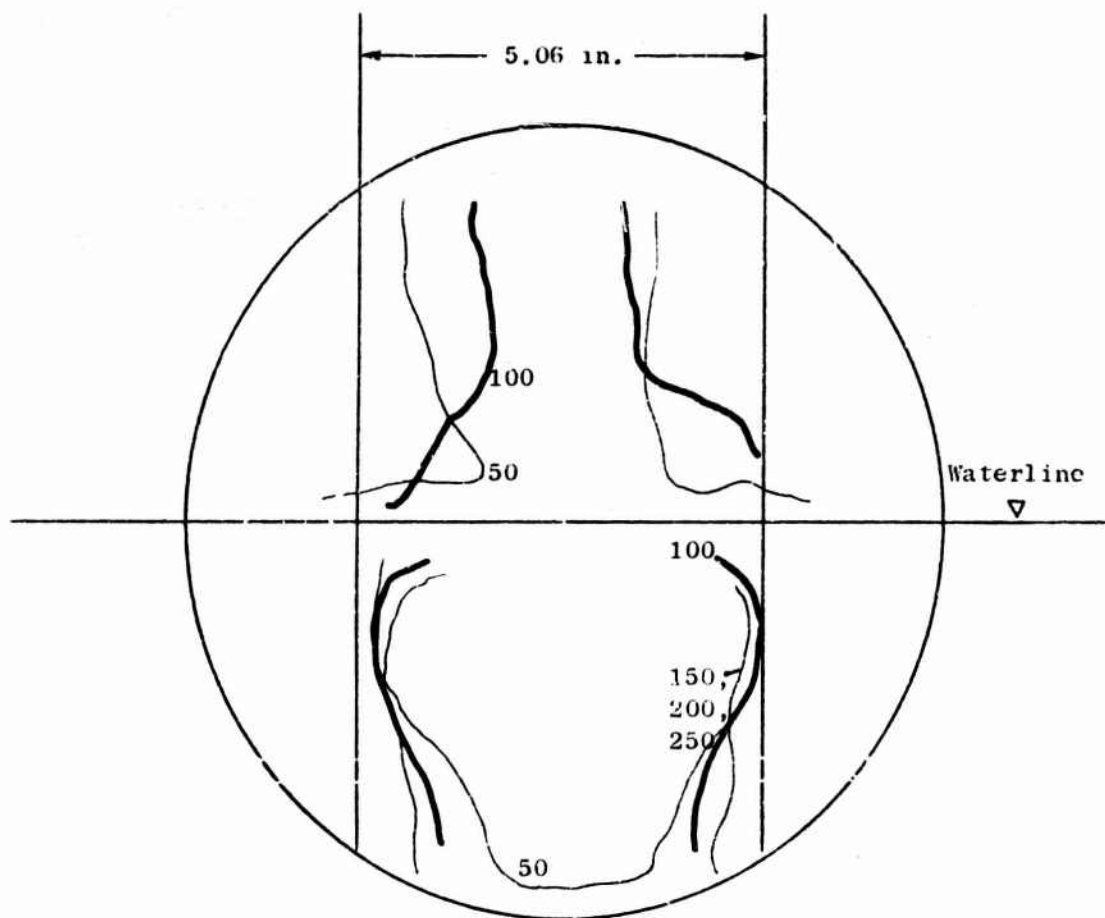
Frame numbers indicated, framing rate = 2500/sec

$$D_{max} = 4.76$$

$$d = 0.10$$

Shot 12

Fig. 12. Expansion of Cavity and Water Column
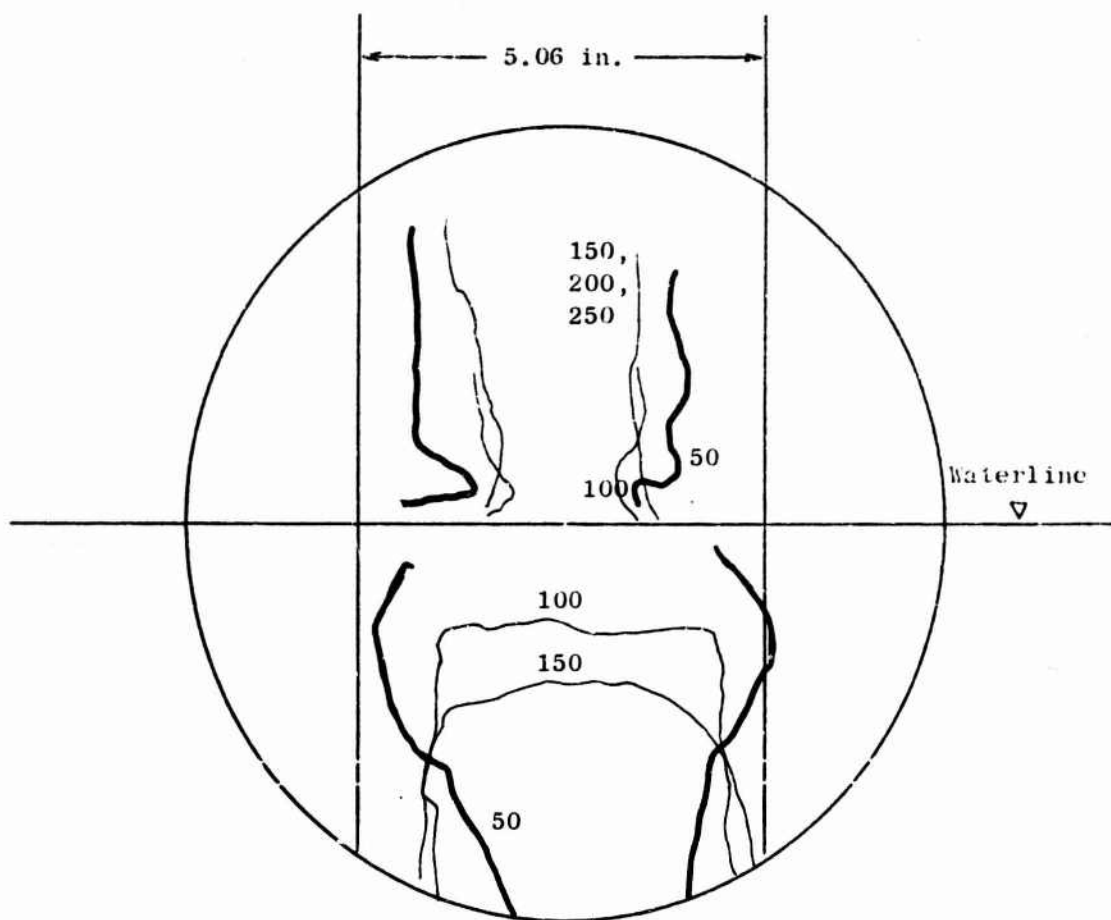
Frame numbers indicated, framing rate = 2500/sec

$$D_{max} = 4.90$$

$$d = 0.20$$

Shot 13

Fig. 13. Expansion of Cavity and Water Column
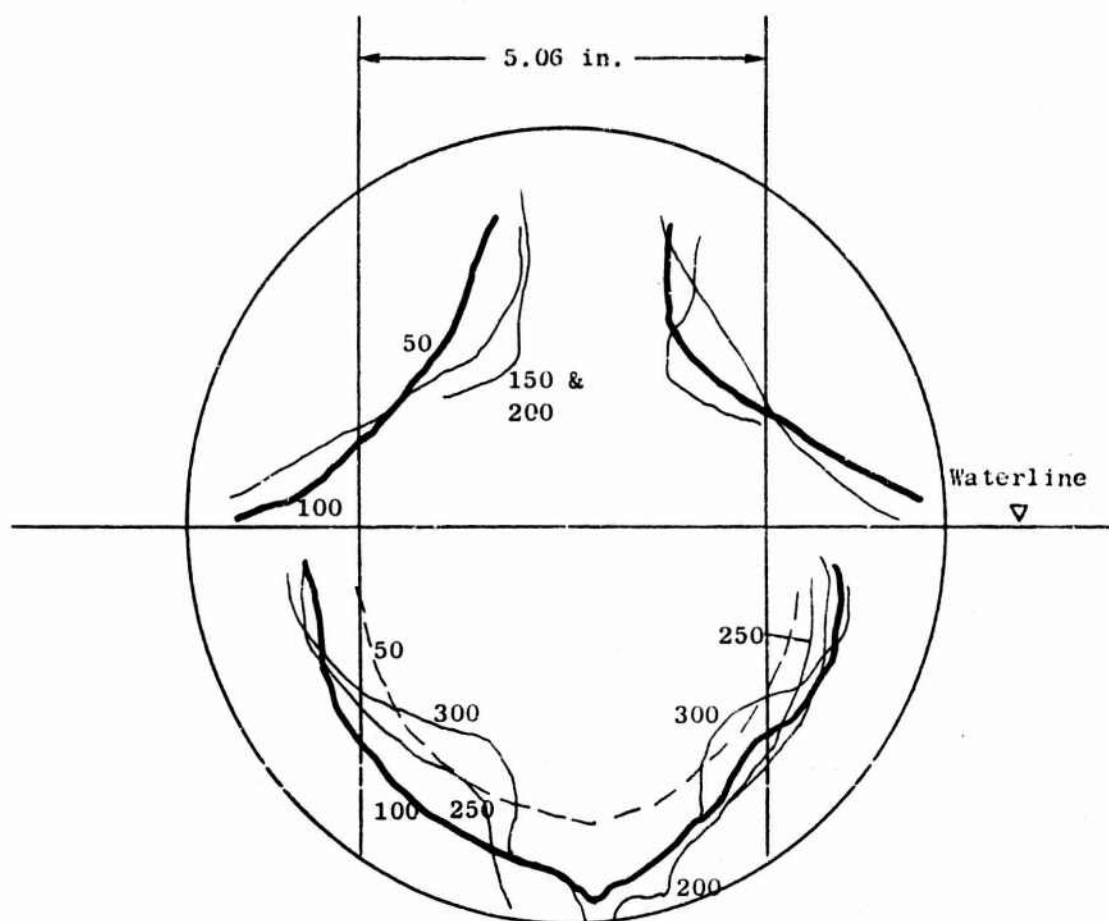
Frame numbers indicated, framing rate = 2500/sec

$$D_{max} = 6.65$$

$$d = 0.04$$

Shot 14

Fig. 14. Expansion of Cavity and Water Column
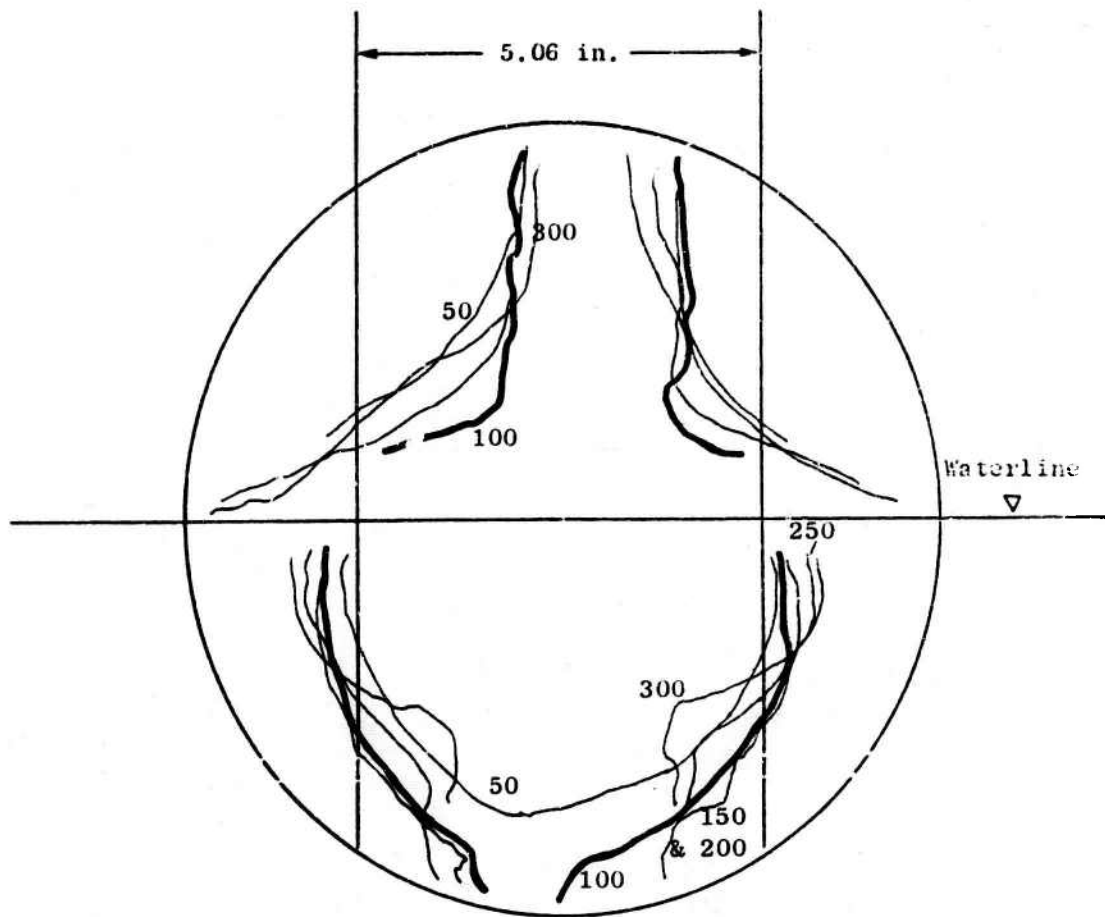
Frame numbers indicated, framing rate = 2500/sec

$$D_{max} = 5.85$$

$$d = 0.06$$

Shot 15

Fig. 15. Expansion of Cavity and Water Column

61
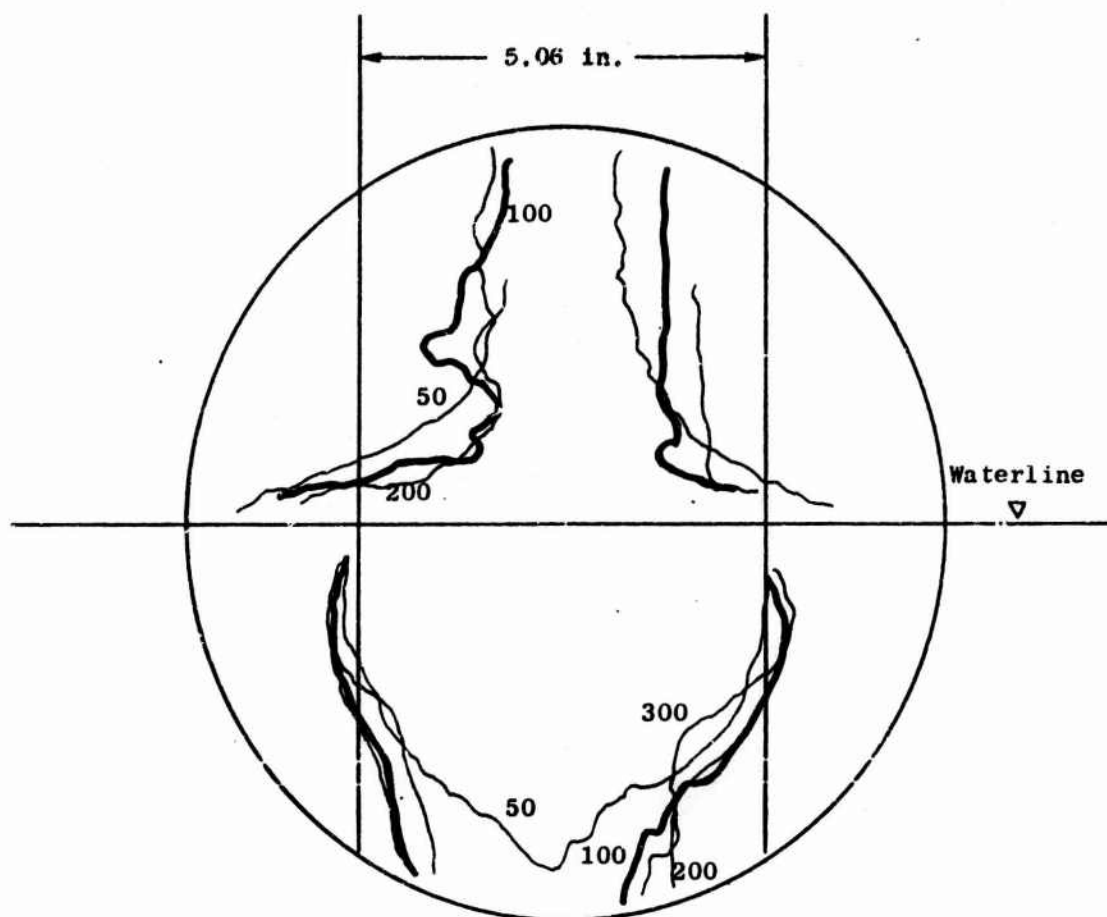
Frame numbers indicated, framing rate = 2500/sec

$$D_{max} = 5.80$$

$$d = 0.08$$

Shot 16

Fig. 16. Expansion of Cavity and Water Column

68
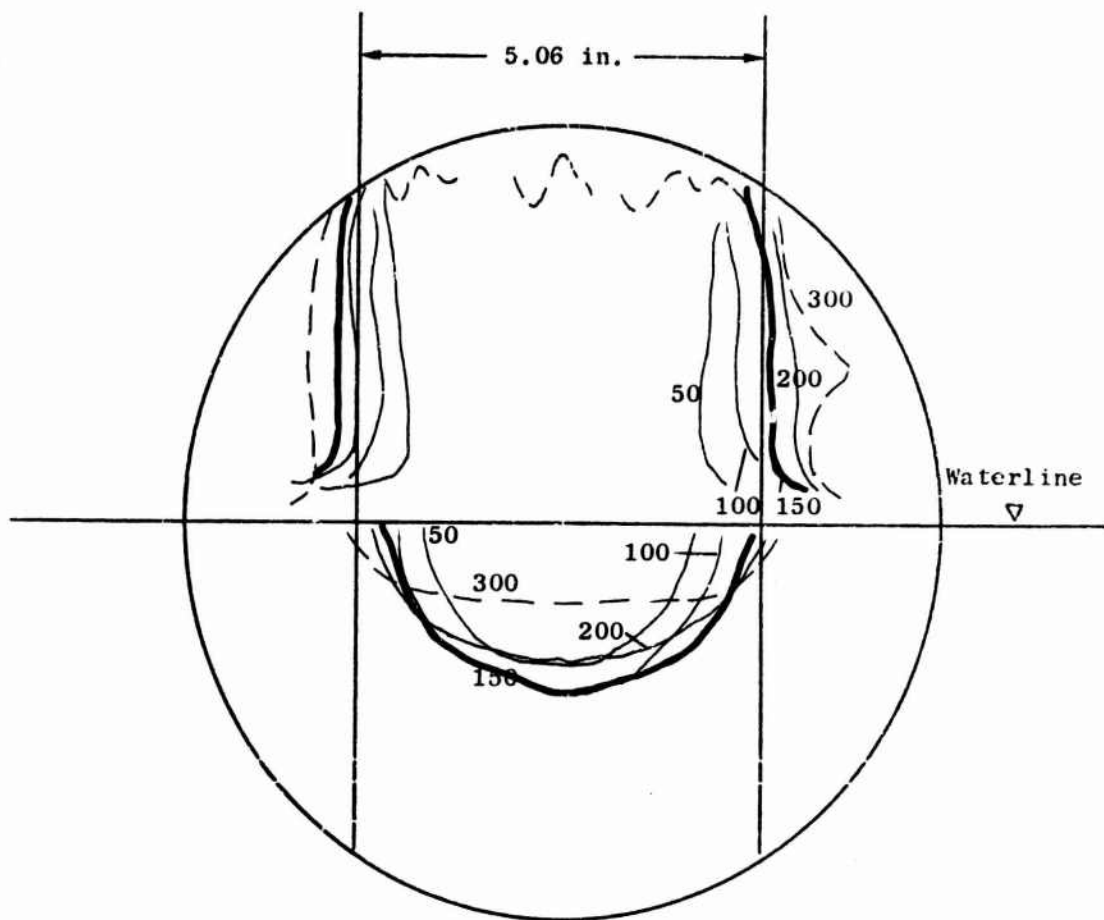
Frame numbers indicated, framing rate = 2500/sec

$$D_{max} = 4.60$$

$$d = 0$$

Shot 17

Fig. 17. Expansion of Cavity and Water Column

$D_{max} = 5.80$

$d = 0.06$

Shot 18K

$D_{max} = 6.35$

$d = 0.06$
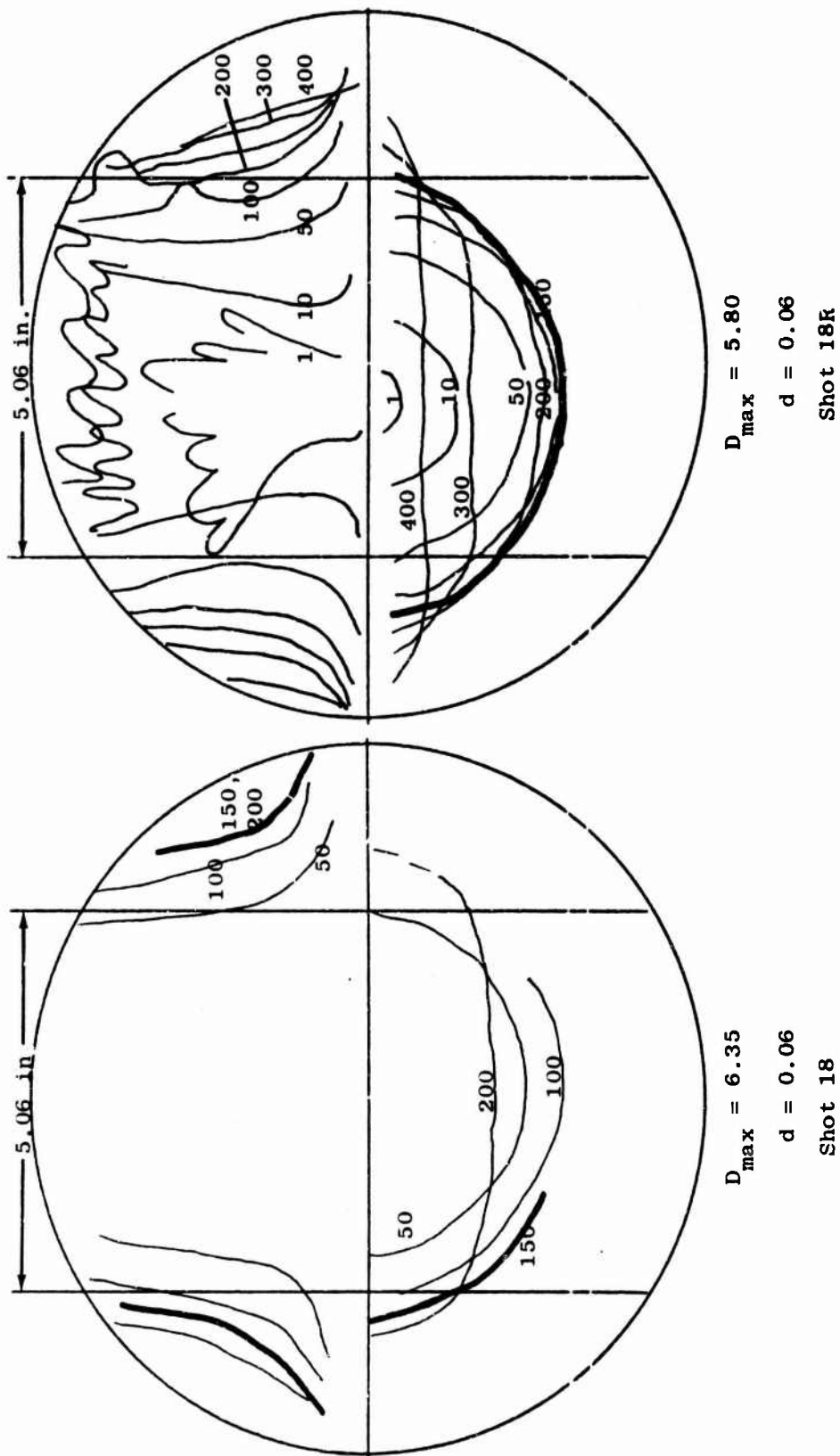
Shot 18

Frame numbers indicated, framing rate = 2500/sec

Fig. 18.   Expansion of Cavity and Water Column
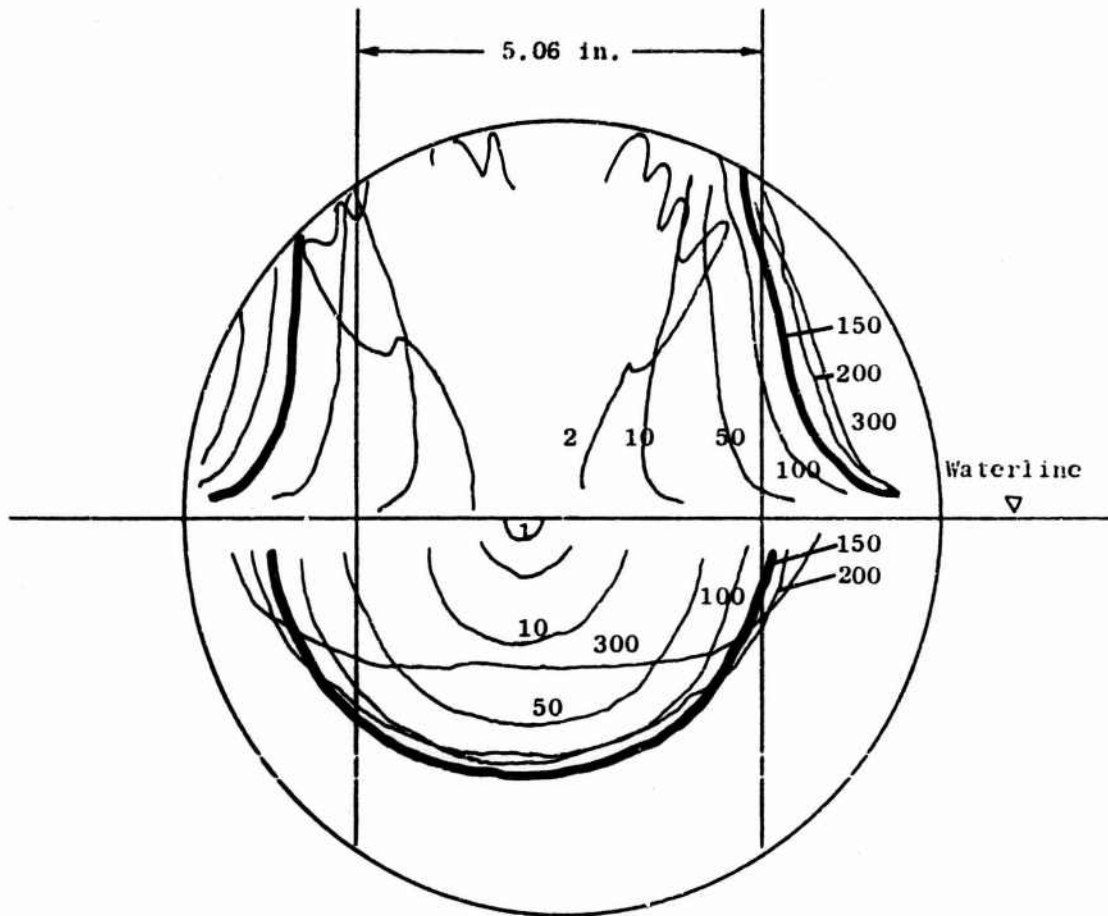
Frame numbers indicated, framing rate = 2500/sec

$$D_{max} = 5.40$$

$$d = 0.08$$

Shot 19R

Fig. 19. Expansion of Cavity and Water Column

5.06 in.

Waterline
▽
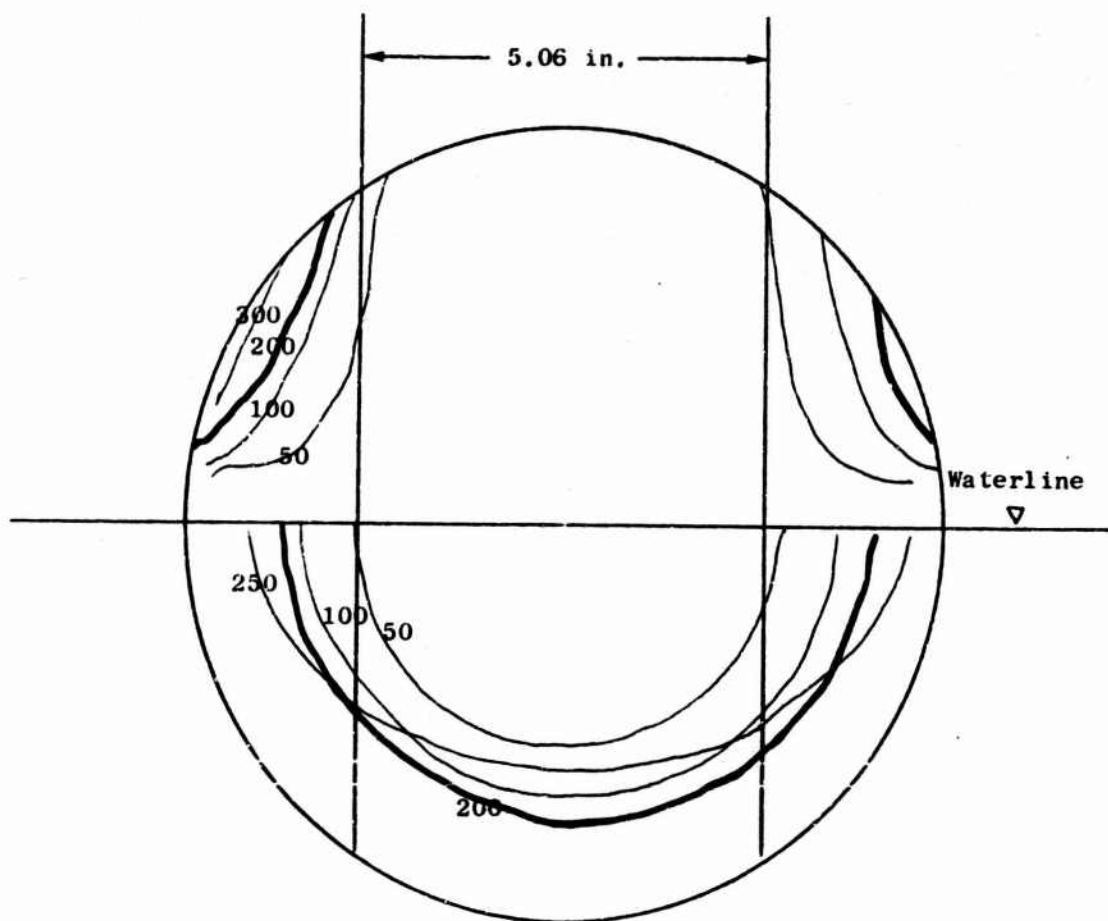
Frame numbers indicated, framing rate = 2500/sec

$$D_{max} = 8.10$$
$$d = 0.08$$
Shot 20

Fig. 20. Expansion of Cavity and Water Column

$D_{max} = 4.90$

$d = 0.10$

Shot 21

$D_{max} = 4.62$

$d = 0.10$

Shot 21R

Frame numbers indicated, framing rate = 2500/sec
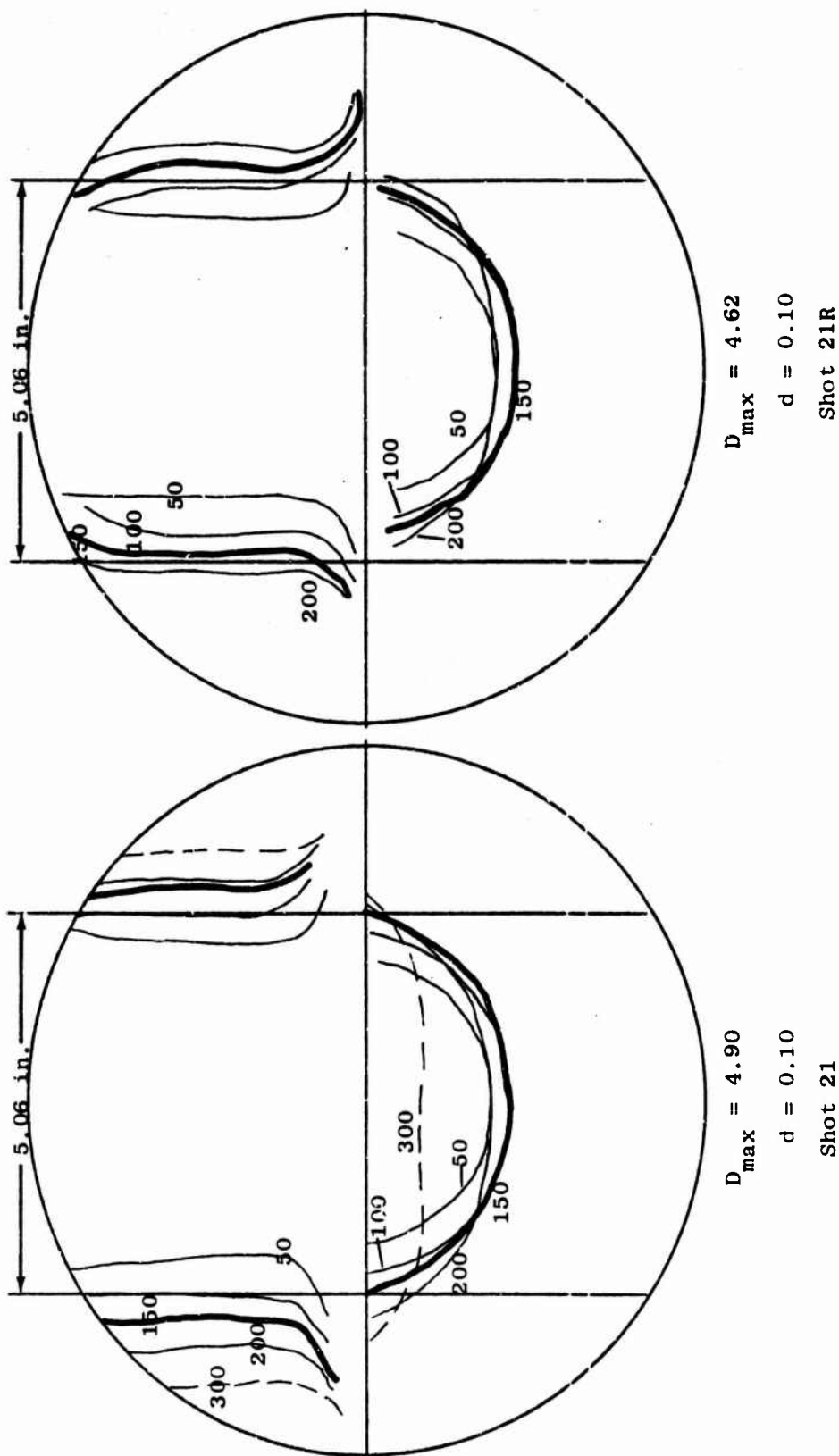
Fig. 21. Expansion of Cavity and Water Column

73
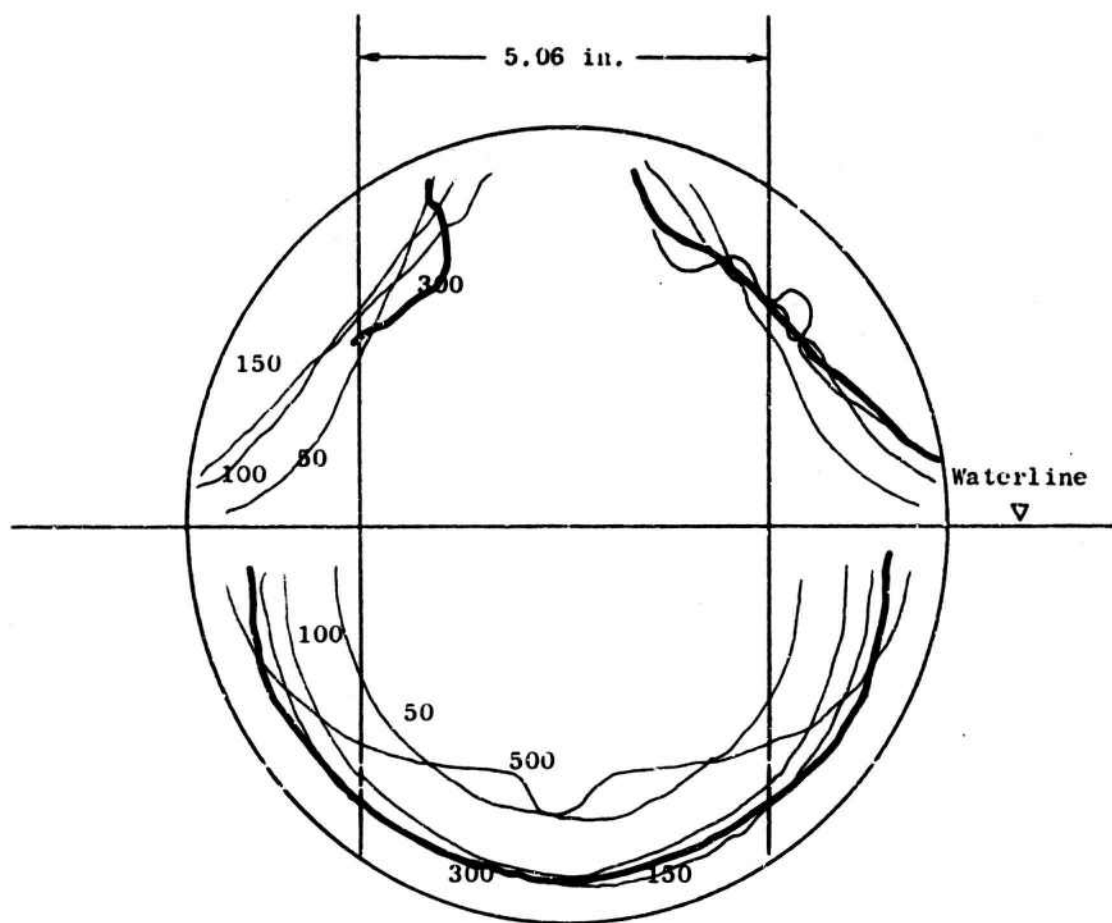
Frame numbers indicated, framing rate = 2500/sec

$$D_{max} = 7.80$$

$$d = 0.20$$

Shot 22

Fig. 22. Expansion of Cavity and Water Column
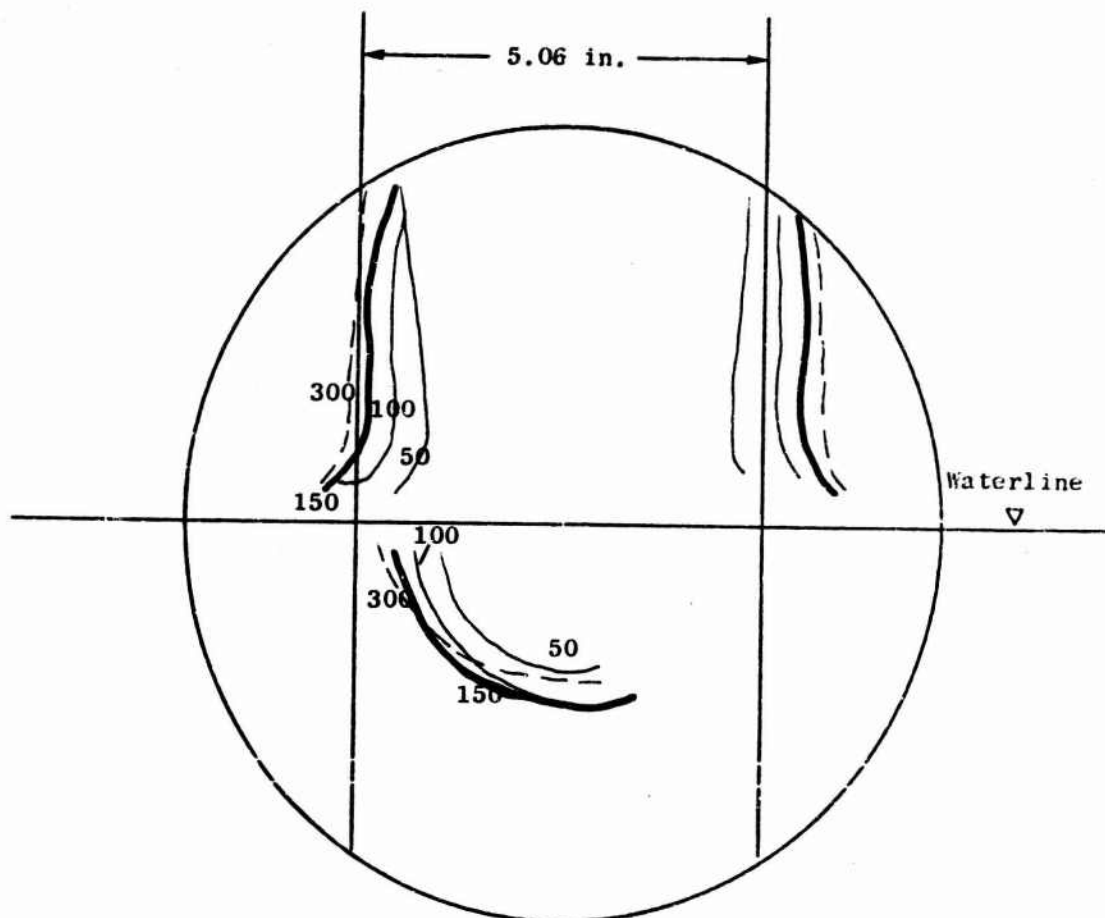
Frame numbers indicated, framing rate = 2500/sec

$$D_{max} = 4.60$$

$$d = 0$$

Shot 23

Fig. 23. Expansion of Cavity and Water Column
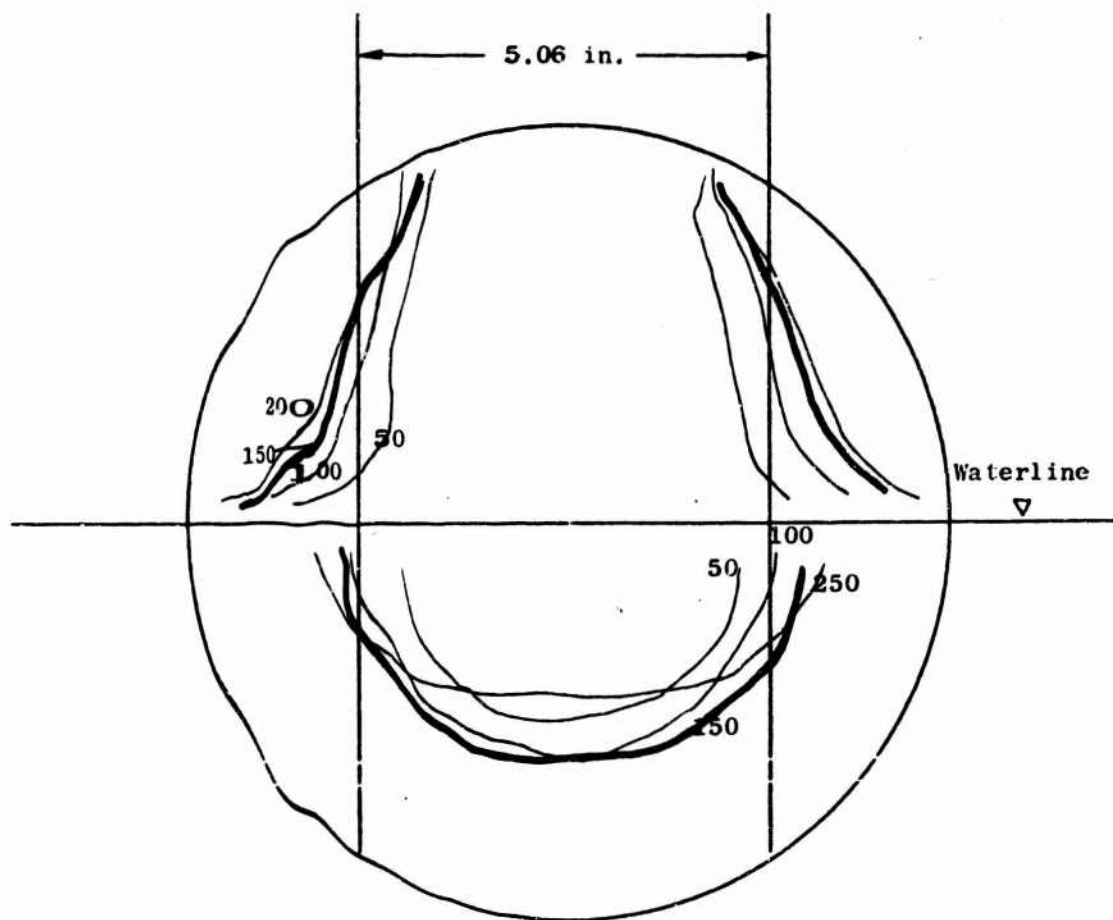
Frame numbers indicated, framing rate = 2500/sec

$$D_{max} = 5.80$$
$$d = 0.06$$
$$\text{Shot} \ 24$$

Fig. 24. Expansion of Cavity and Water Column

D$_{max}$ ≃ 9.5

d = 0.08

Shot 25R

D$_{max}$ = 5.10

d = 0.08

Shot 25
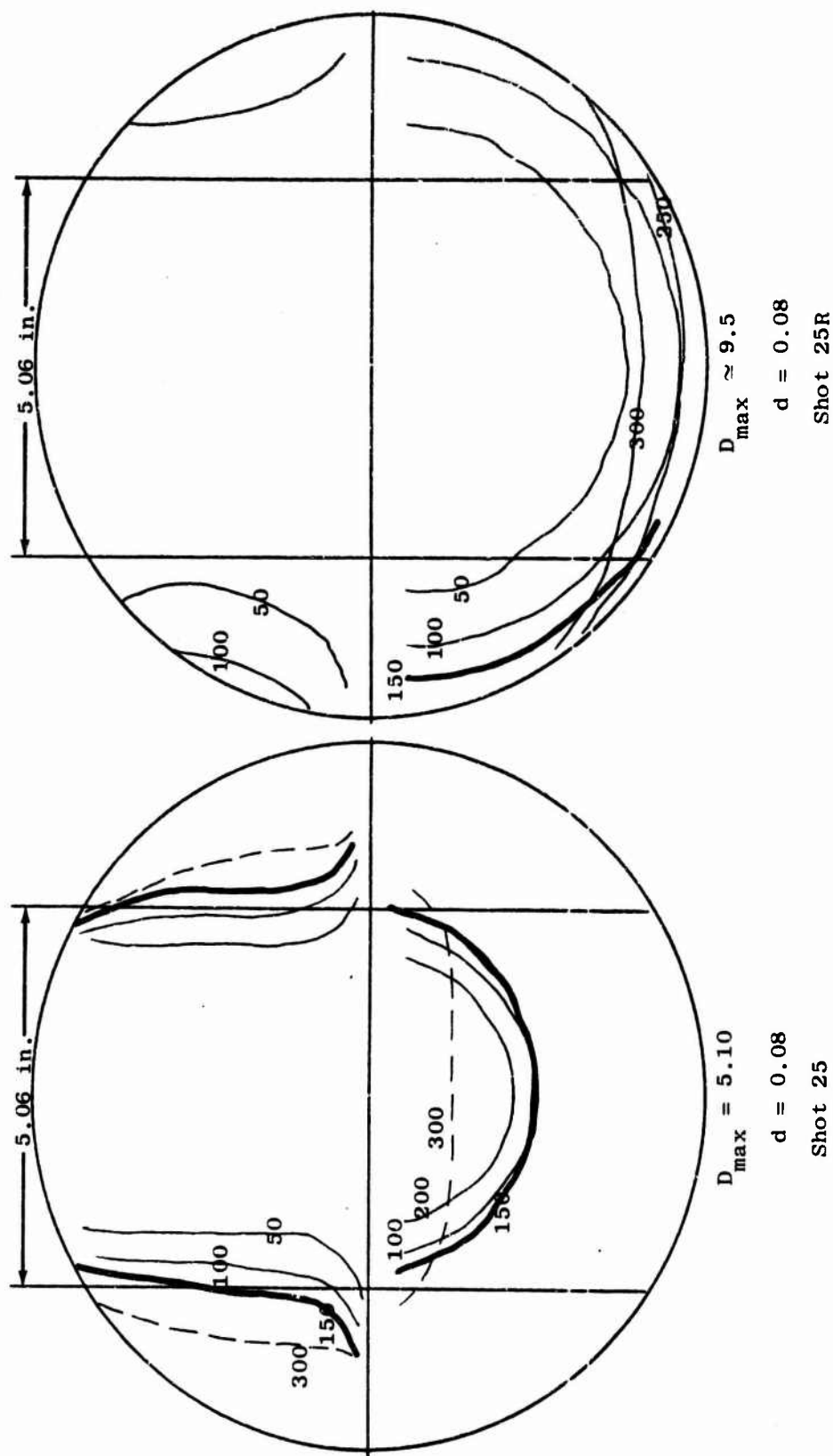
Frame numbers indicated, framing rate = 2500/sec

Fig. 25. Expansion of Cavity and Water Column

77

$D_{max} = 3.30$

$d = 0.20$

Shot 26R

5.06 in.

$D_{max} = 5.80$

$d = 0.20$

Shot 26

5.06 in.
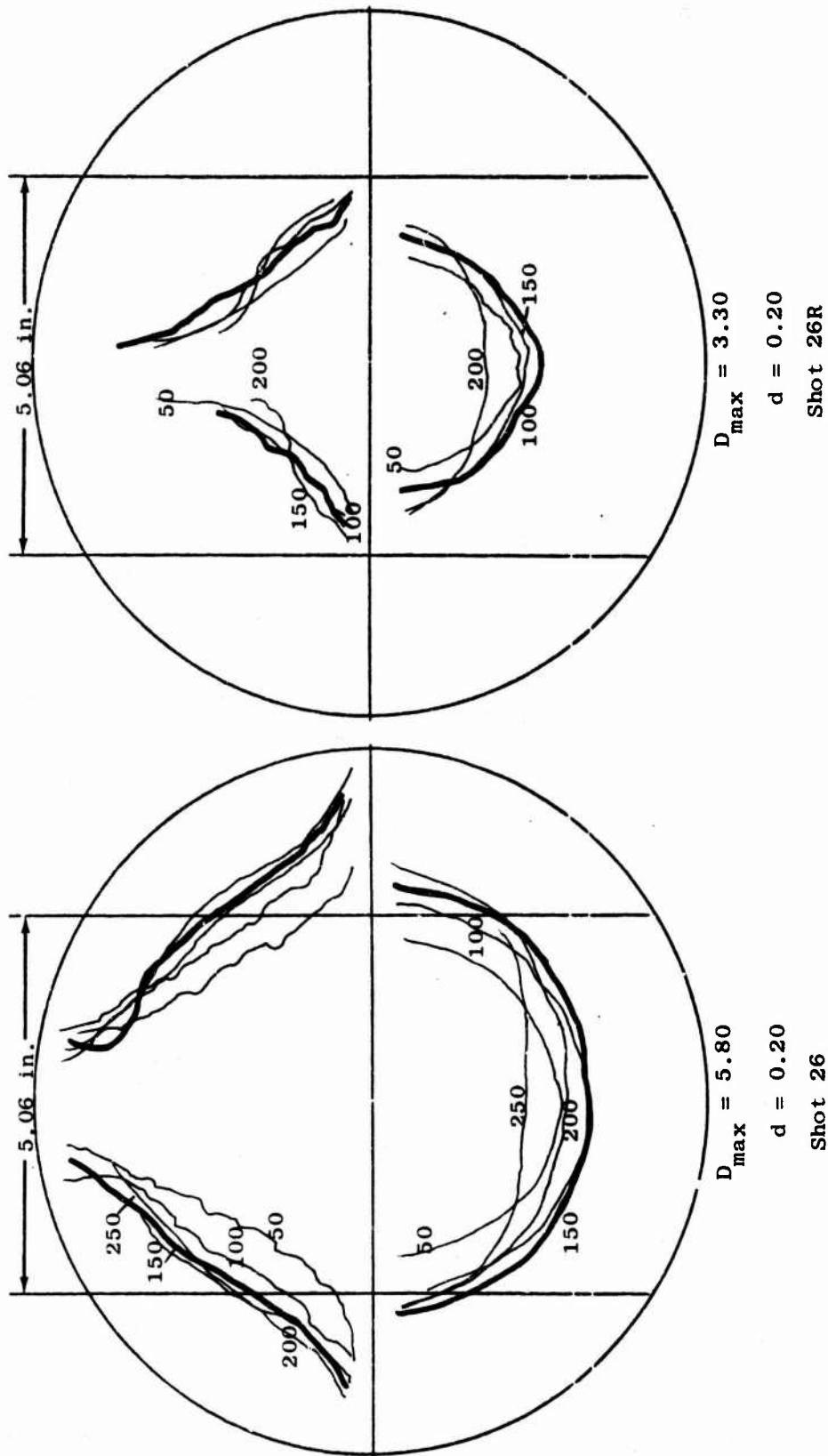
Frame numbers indicated, framing rate = 2500/sec

Fig. 26. Expansion of Cavity and Water Column

78

5.06 in.

Waterline ▽

1
5
20
50
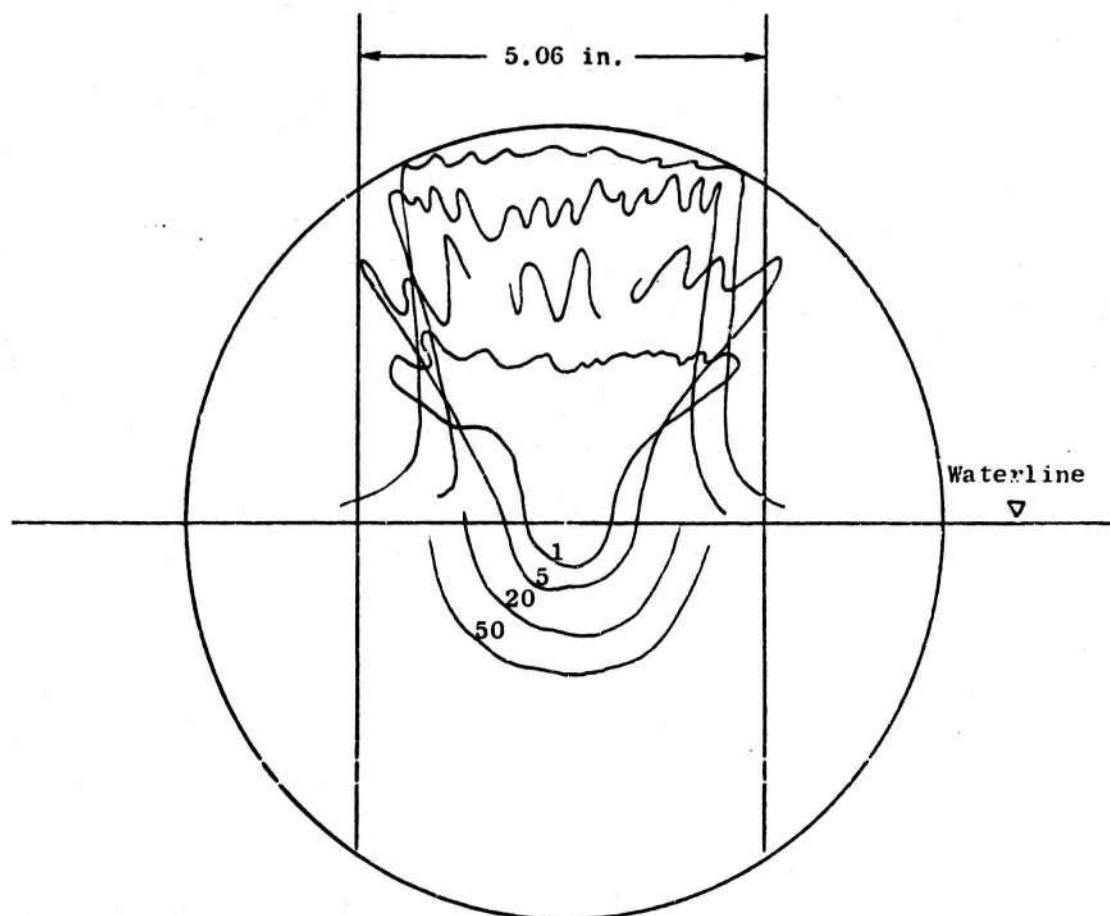
Frame numbers indicated, framing rate = 2500/sec

$$D_{max} = 4.62$$

$$d = 0$$

Shot 1 - flare

Fig. 27. Expansion of Cavity and Water Column

79
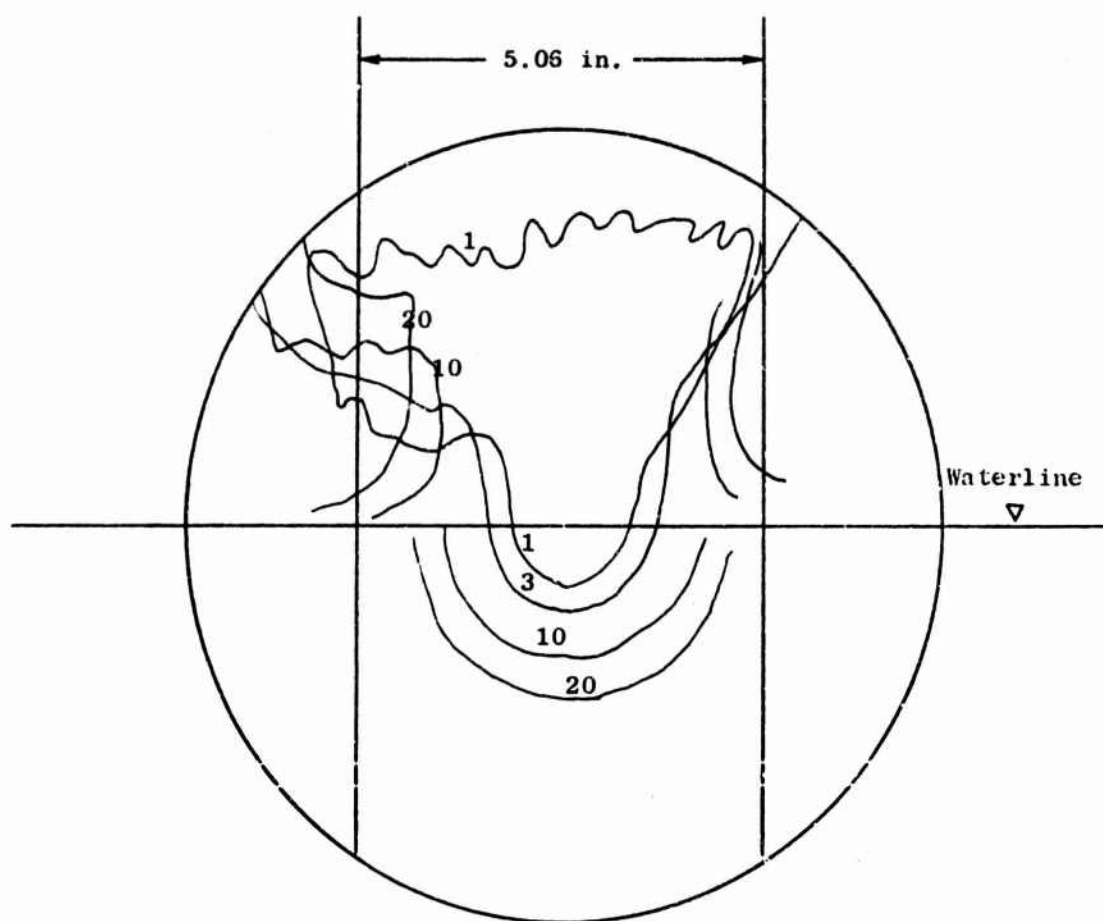
Frame numbers indicated, framing rate = 2500/sec

$$D_{max} = 7.40$$

$$d = 0$$

Shot 5 - spray

Fig. 28.   Expansion of Cavity and Water Column

80
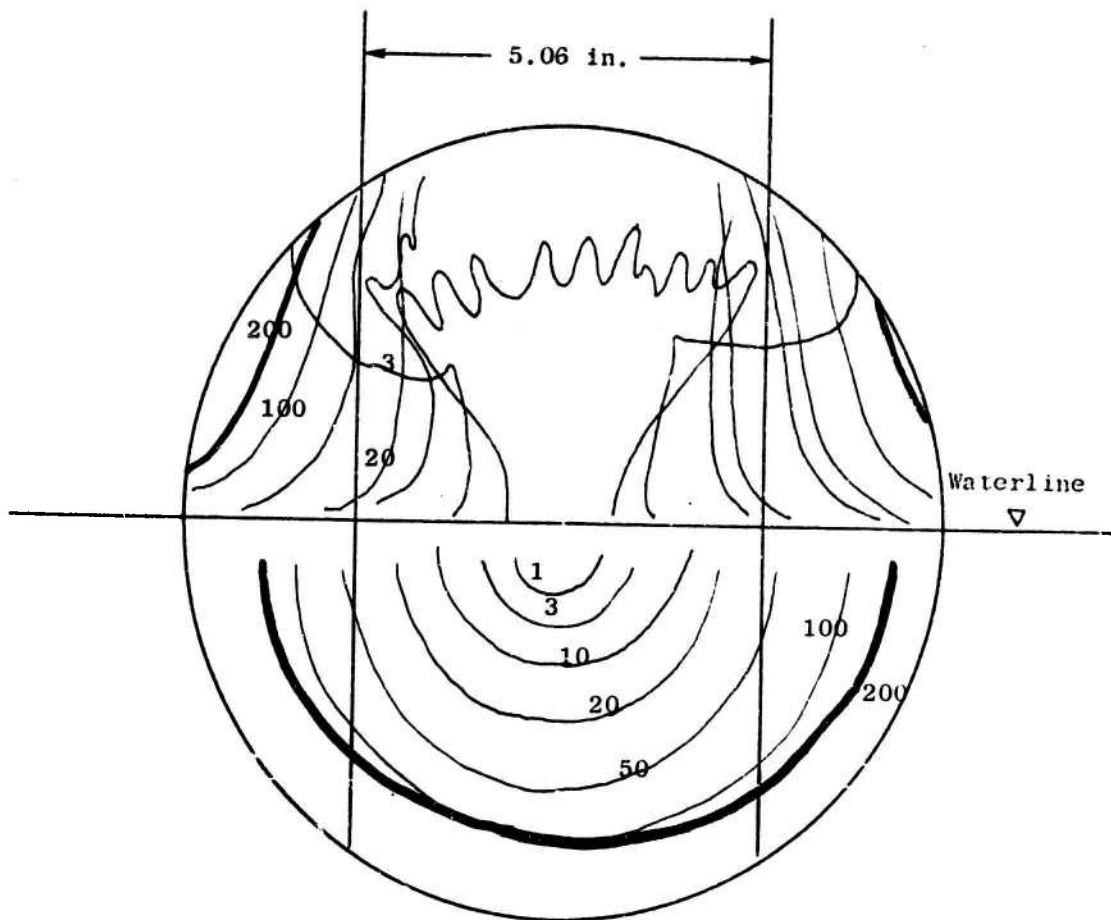
Frame numbers indicated, framing rate = 2500/sec

$$D_{max} = 8.10$$

$$d = 0.08$$

Shot 20 - spray

Fig. 29. Expansion of Cavity and Water Column

81
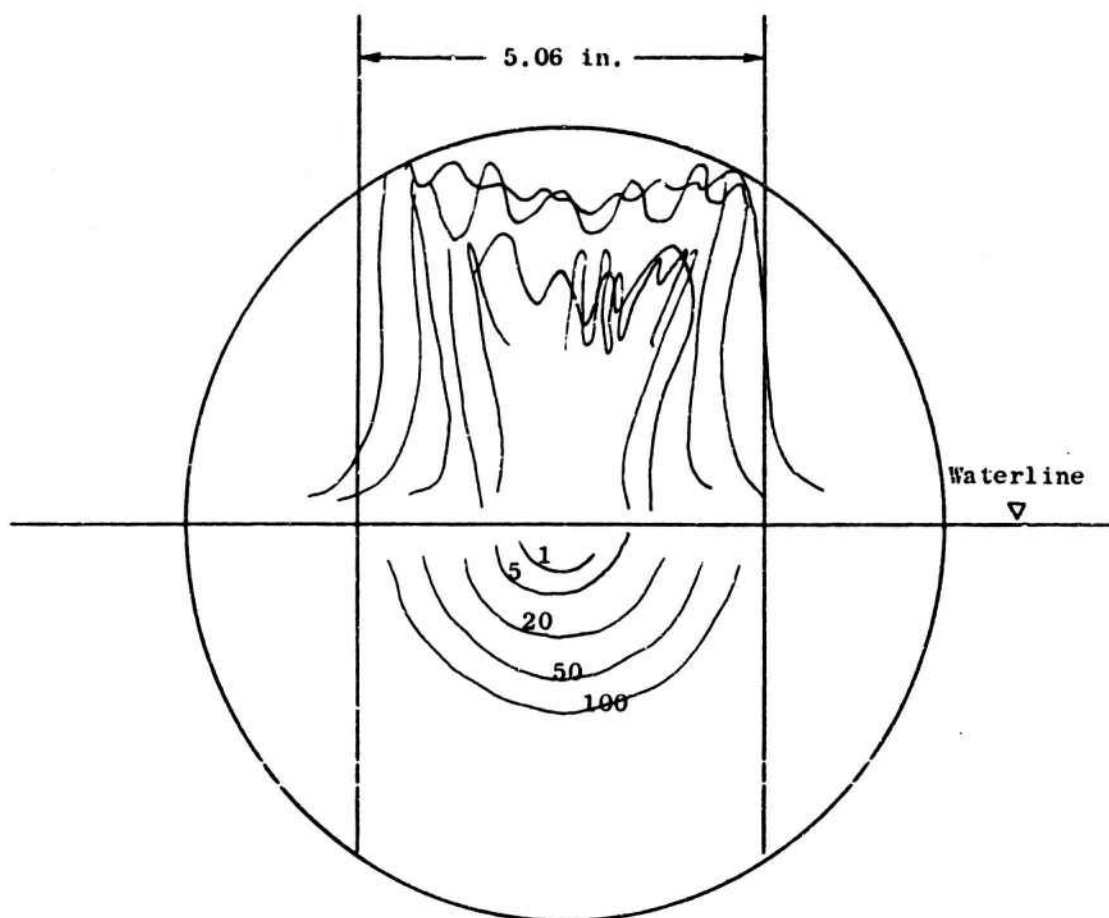
Frame numbers indicated, framing rate = 2500/sec

$$D_{max} = 5.10$$

$$d = 0.08$$

Shot 25 - flare

Fig. 30. Expansion of Cavity and Water Column

1   fully expanded cavity, frame 150, D_{max} = 4.62 in.

1B maximum column diameter, frame 300, D_{col} = 6.40 in.

2   maximum water mound

3   second cavity expansion

4   second mound

5   third cavity expansion
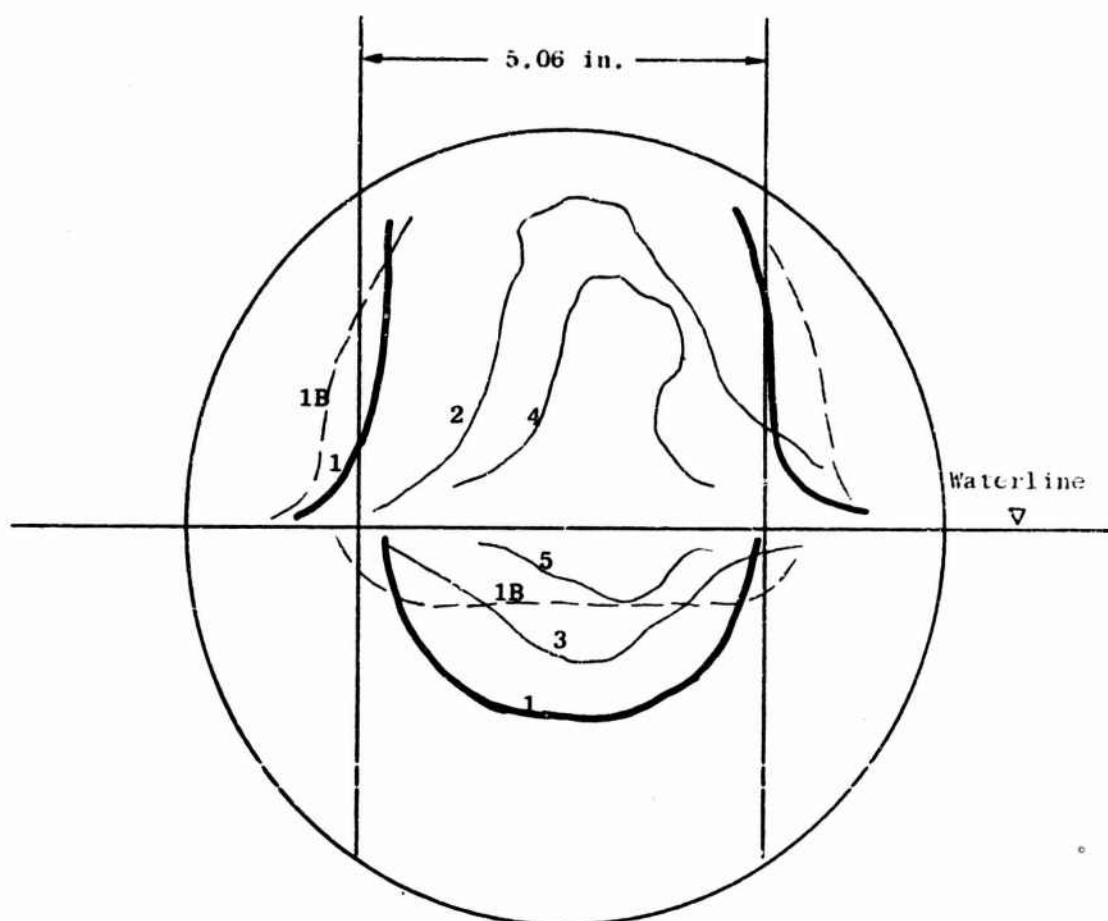
d = 0

Shot 1

Fig. 31.   Expansion of Cavity and Water Column

83

1   fully expanded cavity, frame 150, D_{max} = 7.40 in.

2   maximum water mound

3   second cavity expansion

4   second mound

5   third cavity expansion
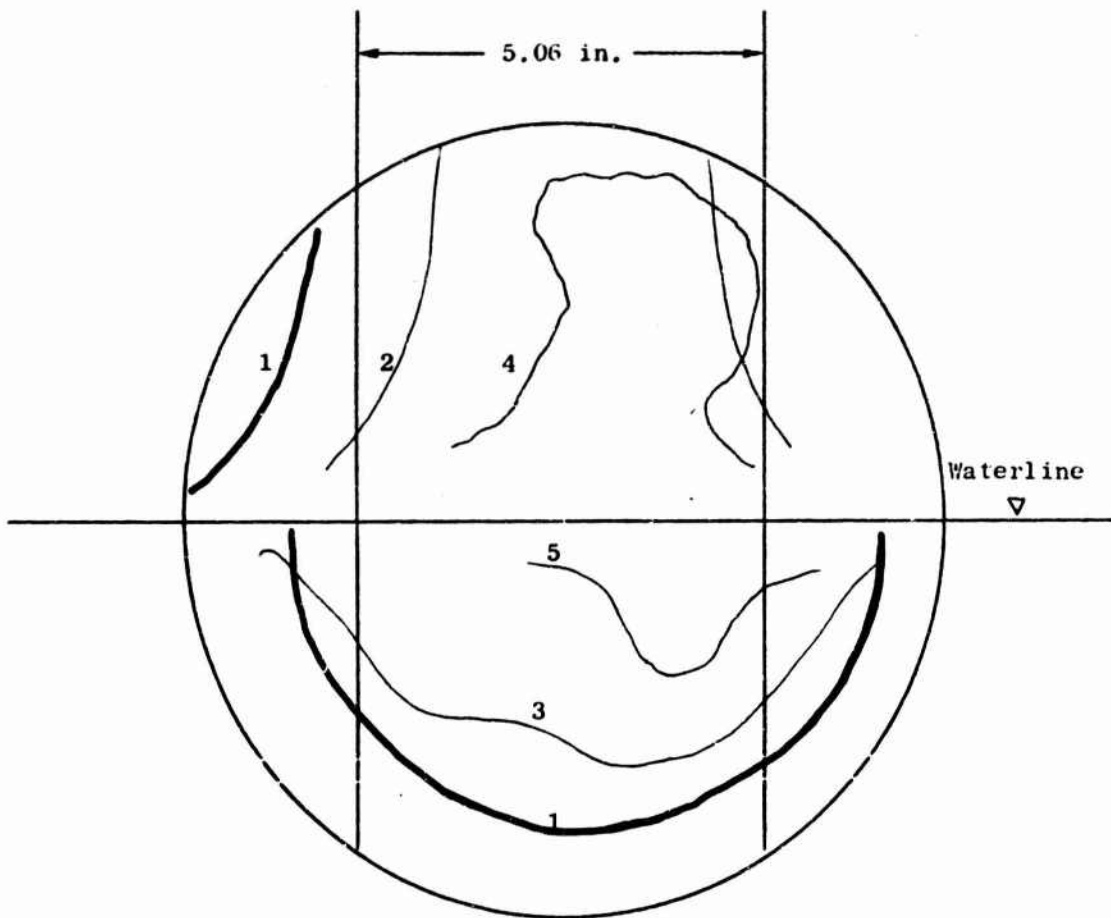
d = 0

Shot 5

Fig. 32.   Expansion of Cavity and Water Column

1   fully expanded cavity, frame 200, D_{max} = 8.10 in.

2   maximum water mound

3   second cavity expansion

4   second mound

5   third cavity expansion
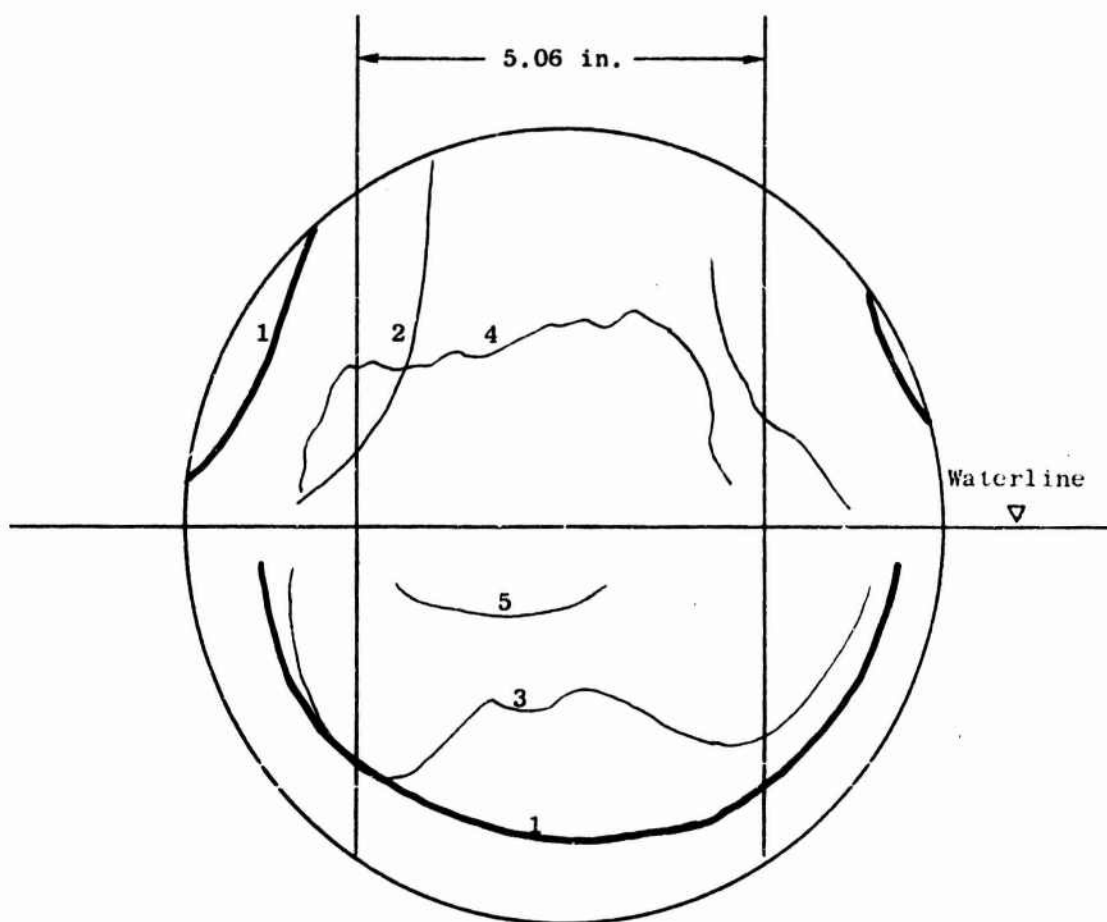
d = 0.08

Shot 20

Fig. 33.   Expansion of Cavity and Water Column

85

1   fully expanded cavity, frame 150, D_{max} = 5.10 in.

1B   maximum column diameter, frame 300, D_{col} = 6.80 in.

2   maximum water mound

3   second cavity expansion

4   second mound

5   third cavity expansion
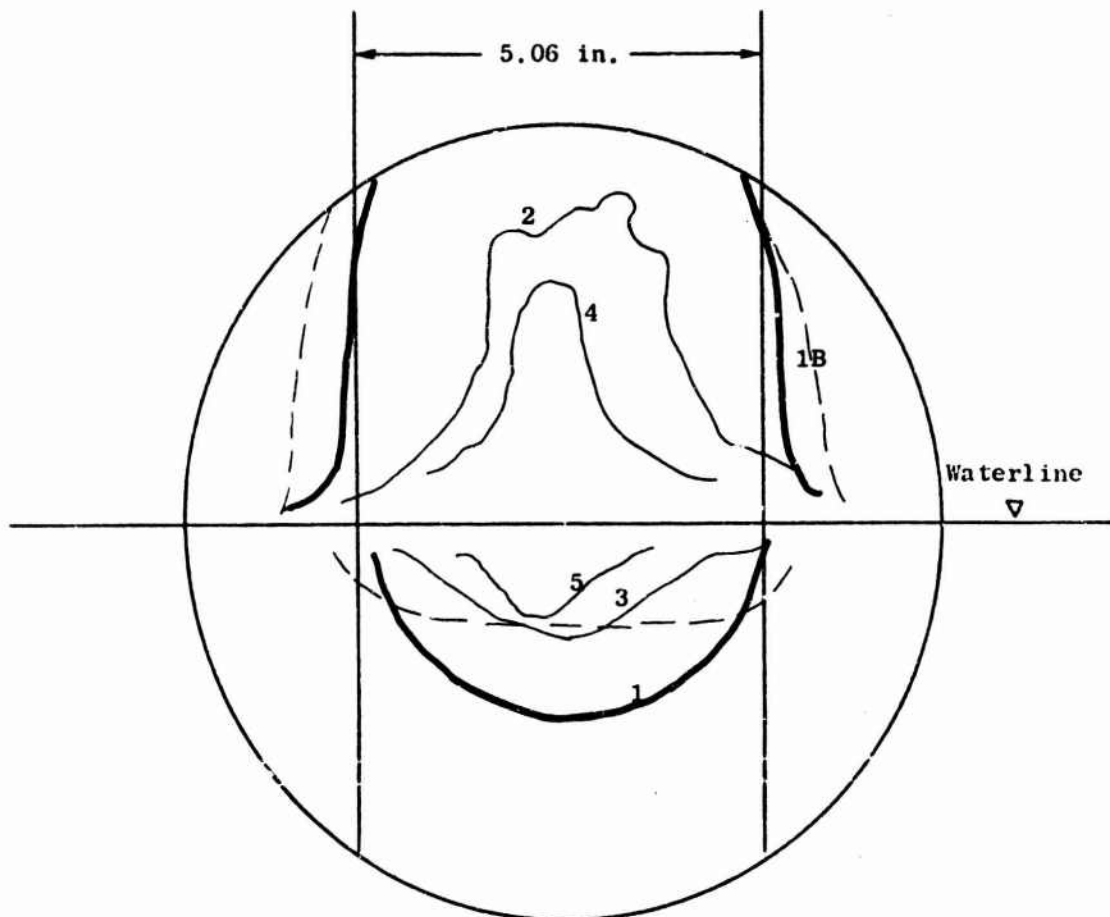
d = 0.8

Shot 25

Fig. 34.   Expansion of Cavity and Water Column
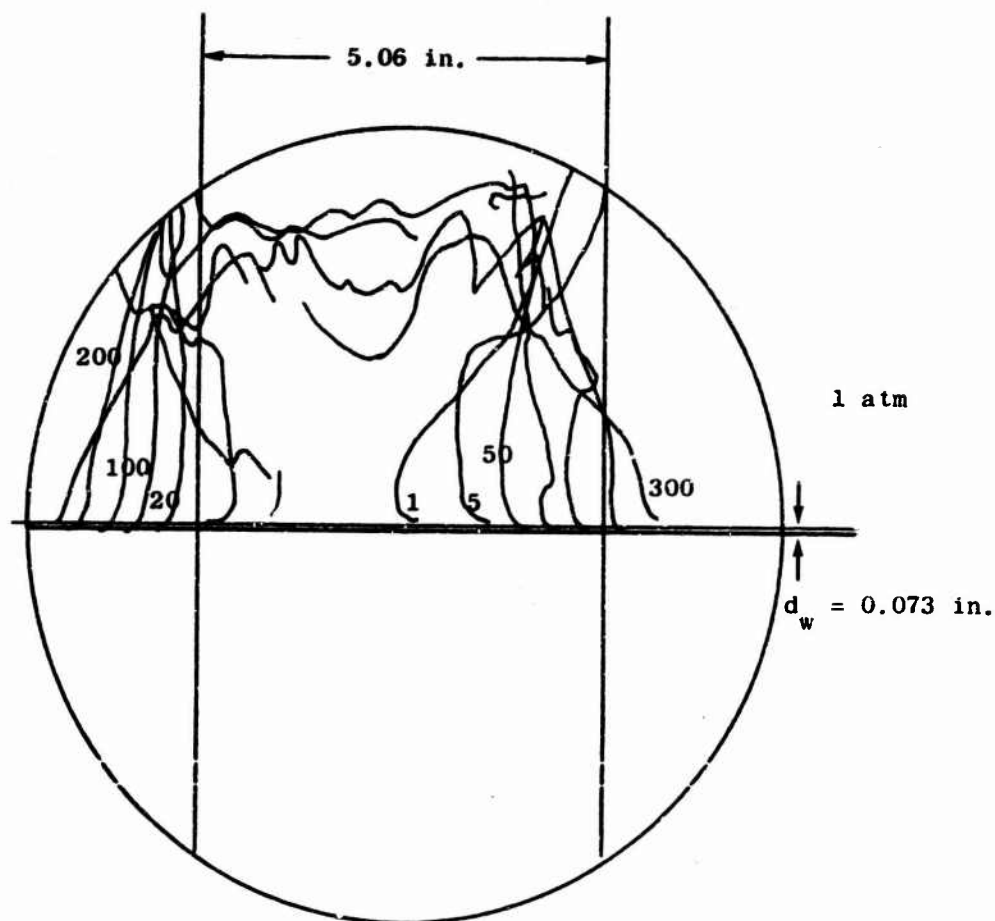
Frame numbers indicated, framing rate = 2500/sec

Flathead

$$D_{max} = 7.50 \text{ in.} = D_{col}$$

$$d = 0$$

Shot 27

Fig. 35.   Expansion of Cavity and Water Column
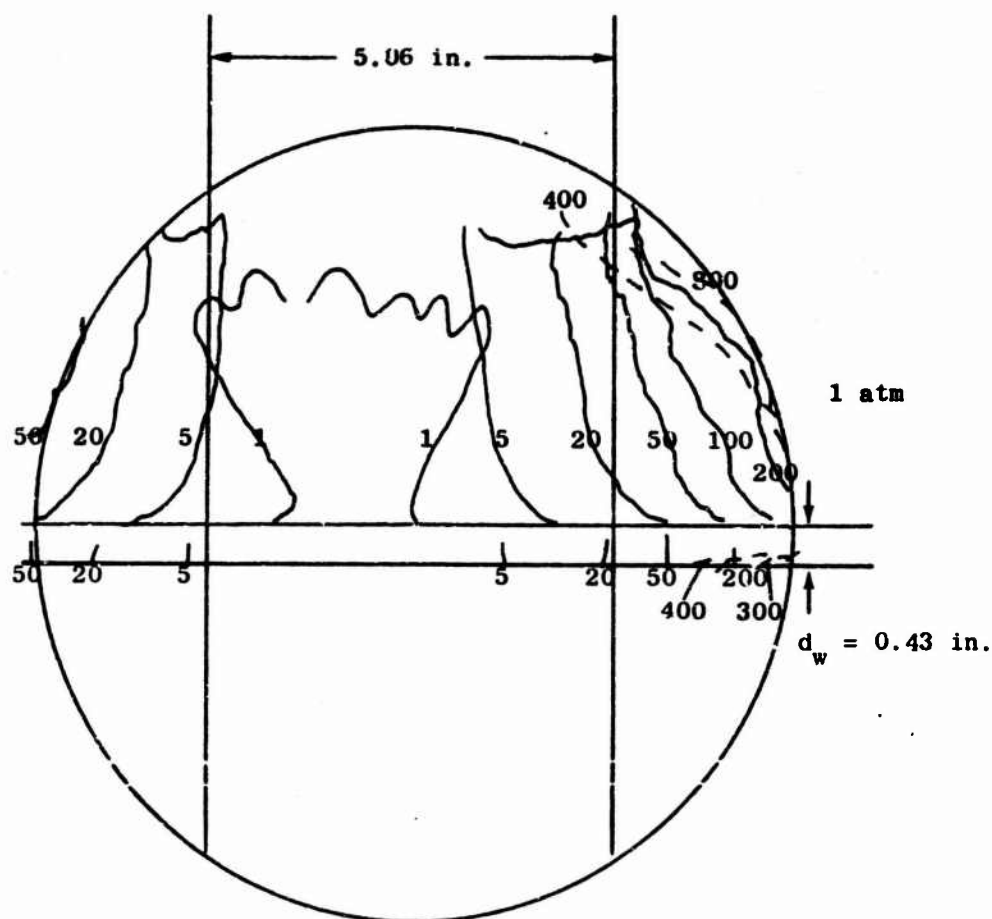
Frame numbers indicated, framing rate = 2500/sec

Baker

$$D_{max} = 9.85 \text{ in.} \simeq D_{col}$$

$$d = 0.22$$

Shot 30

Fig. 36.   Expansion of Cavity and Water Column

Frame numbers indicated, framing rate = 2500/sec

Umbrella

D_{max} = 8.10 in.

d = 0.53 in.

Shot 31

Fig. 37.   Expansion of Cavity and Water Column

Frame numbers indicated, framing rate = 2500/sec

Mono (8)

D_{max} = 4.60 in.

d = 1.71 in.

Shot 34

Fig. 38. Expansion of Cavity and Water Column

90

Flathead

$$D_{max} = 10.4 \text{ in.}$$

$$d = 0$$

Shot 36

Frame numbers indicated, framing rate = 2500/sec

Fig. 39.   Expansion of Cavity and Water Column

Baker

$$D_{max} = 9.25 \text{ in.} \simeq D_{col}$$

$$d = 0.28 \text{ in.}$$

Shot 38

Frame numbers indicated, framing rate = 2500/sec

Fig. 40. Expansion of Cavity and Water Column

Baker

$$D_{max} = 7.0 \text{ in.}$$

$$d = 0.28 \text{ in.}$$

Shot 38R

Frame numbers indicated, framing rate = 2500/sec

Fig. 41.   Expansion of Cavity and Water Column

93

Umbrella

D_{max} out of sight $\simeq 11.5$ in.

$d = 0.67$ in.

Shot 39

Frame numbers indicated, framing rate = 2500/sec

Fig. 42. Expansion of Cavity and Water Column
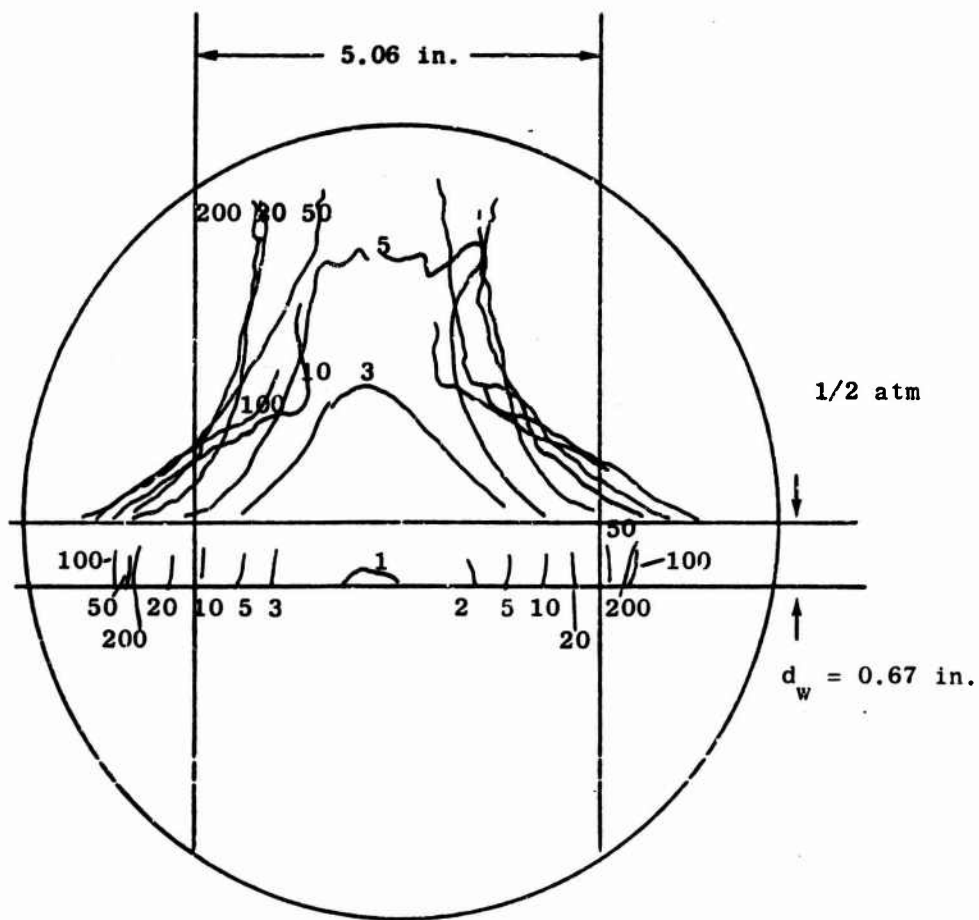
Umbrella

D_{max} = 6.65 in.

d = 0.67 in.

Shot 40

Frame numbers indicated, framing rate = 2500/sec

Fig. 43.   Expansion of Cavity and Water Column

95

5.06 in.

30
20

10

6

1/2 atm

20 10

40

30 1

6

50

d_w = 5.50 in.
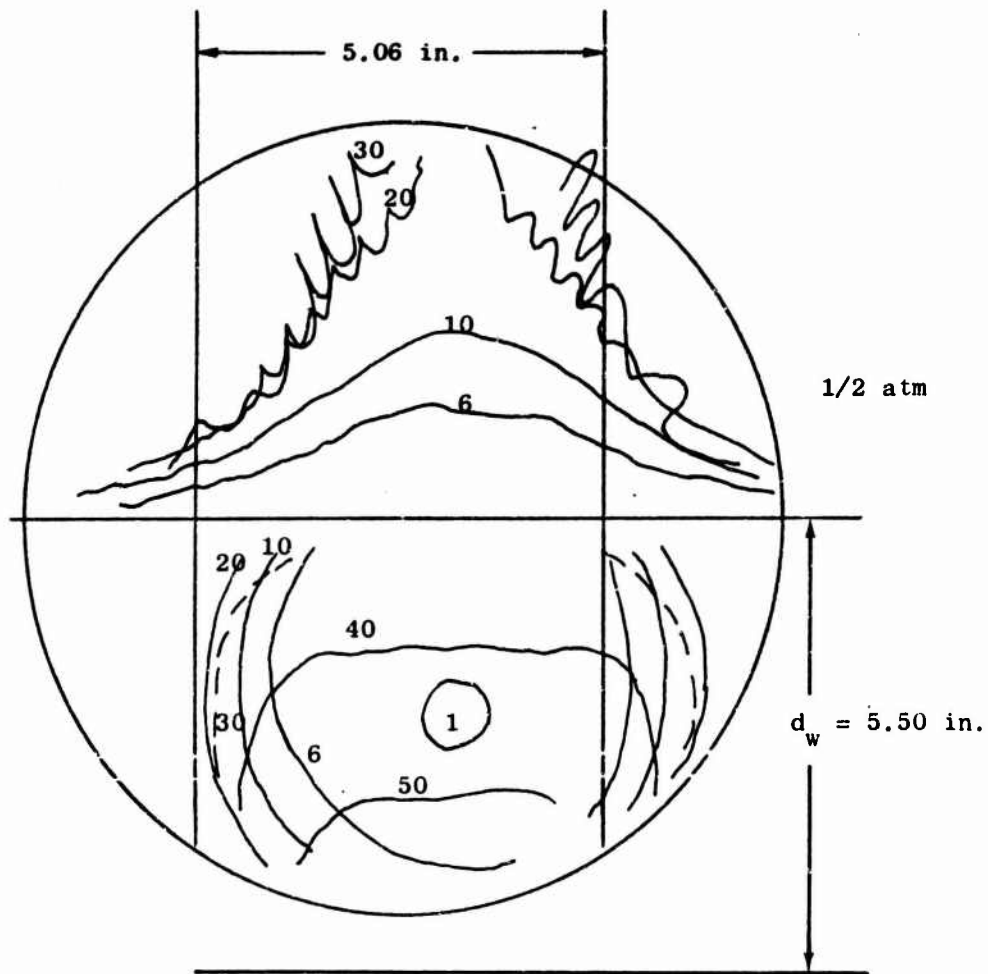
Mono (8)

D_{max} = 6.35 in.

d = 2.15 in.

Shot 42

Frame numbers indicated, framing rate = 2500/sec

Fig. 44. Expansion of Cavity and Water Column
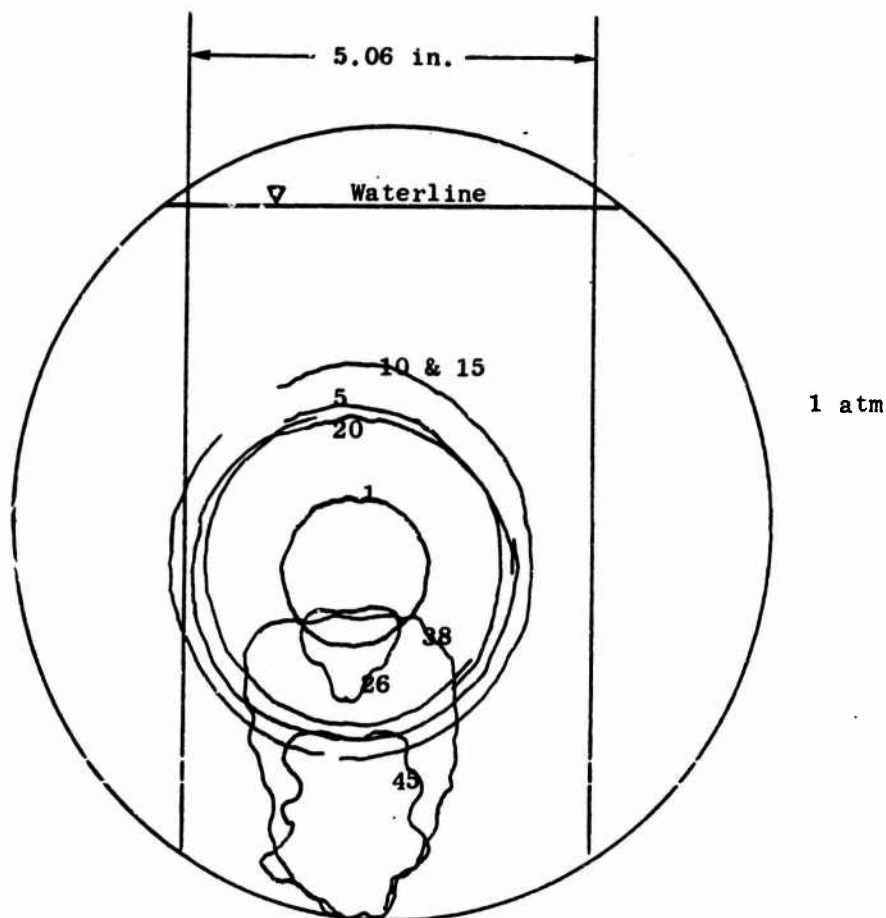
$$D_{max} = 4.62 \text{ in.}$$

$$d = 4 \text{ in.}$$

Shot 43

Frame numbers indicated, framing rate = 2500/sec

Fig. 45. Expansion of Cavity and Water Column
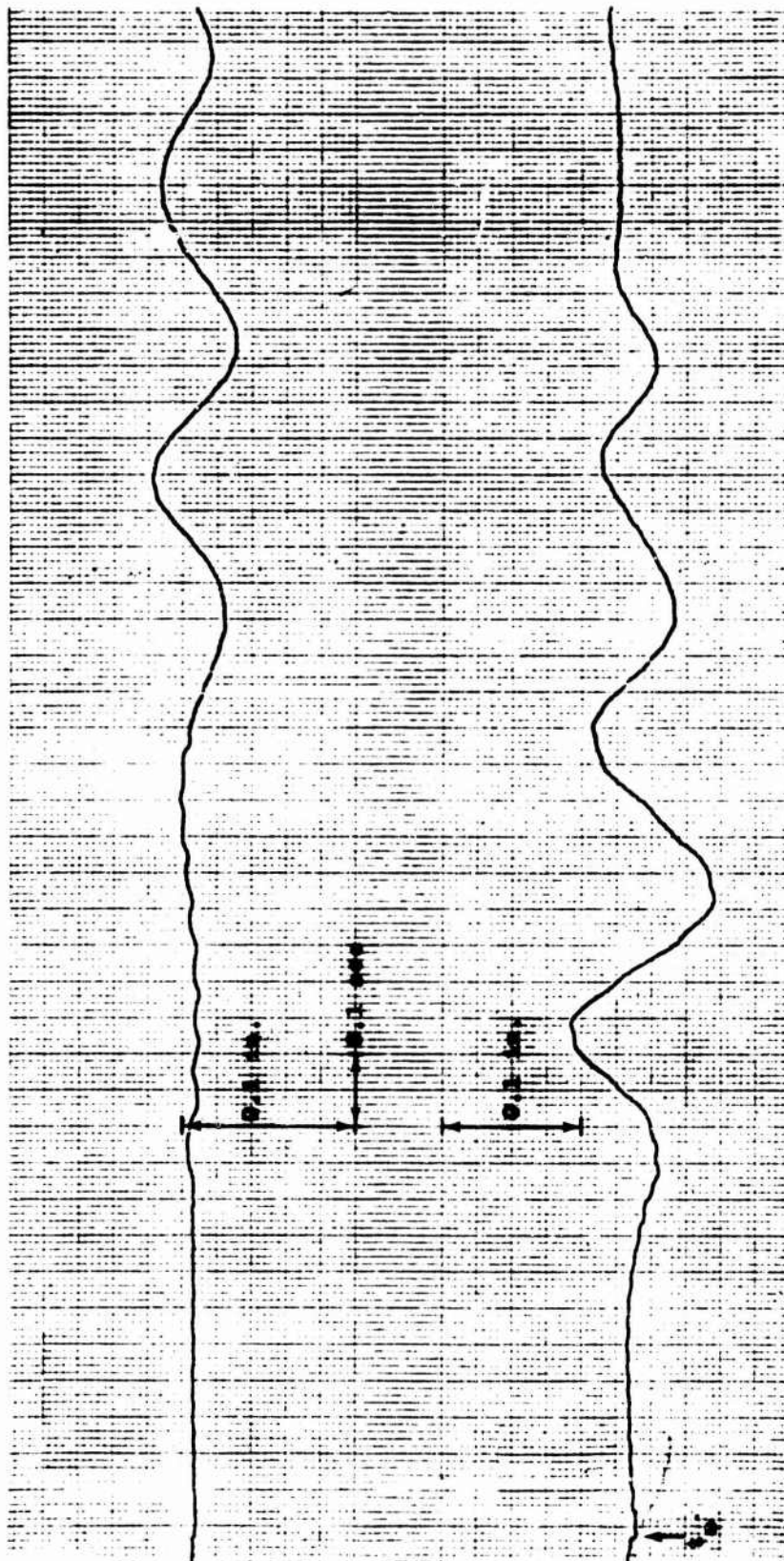
Fig. 46. Wave Gage Records, Shot 1
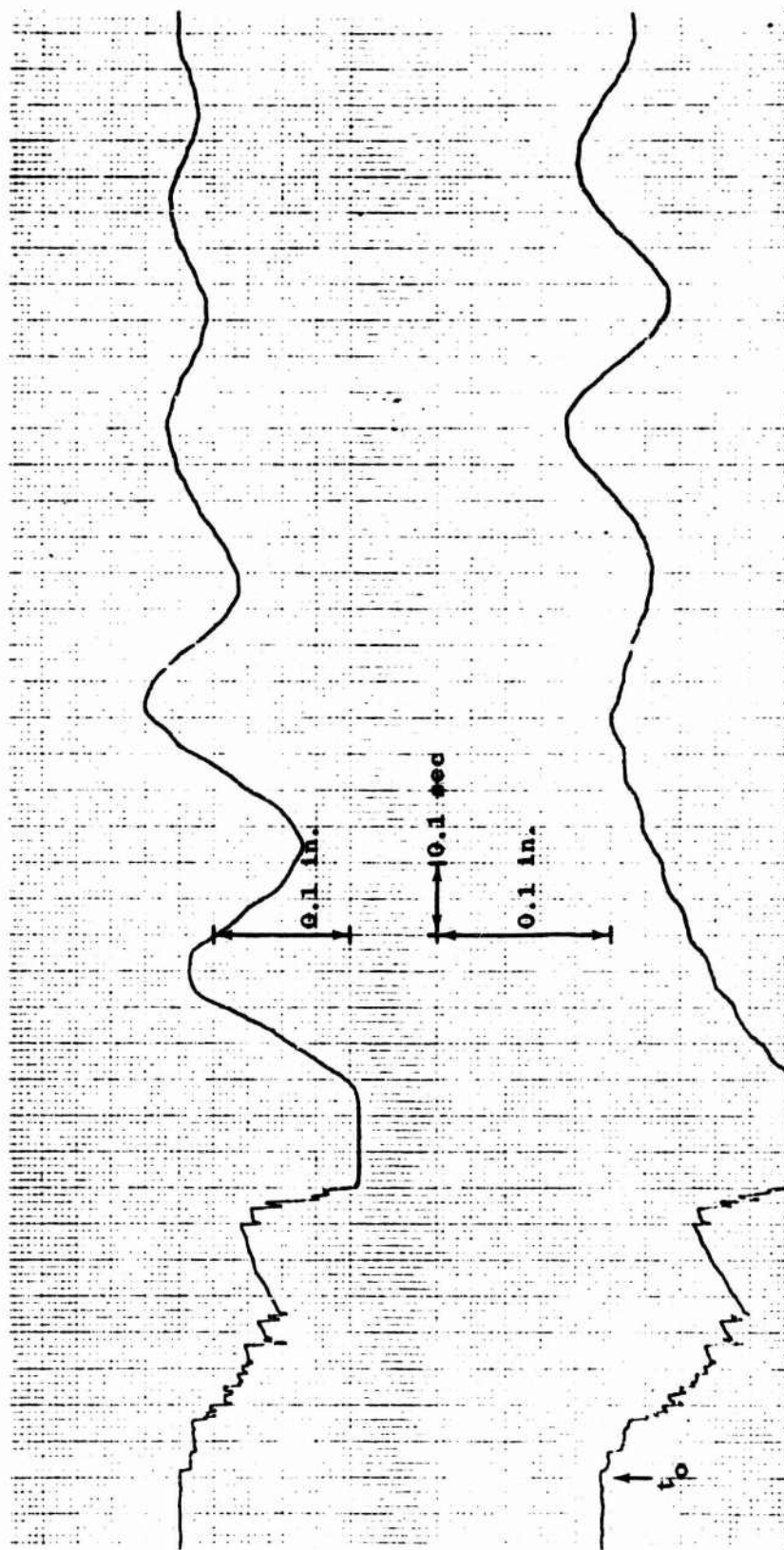
Fig. 47. Wave Gage Records, Shot 2

99
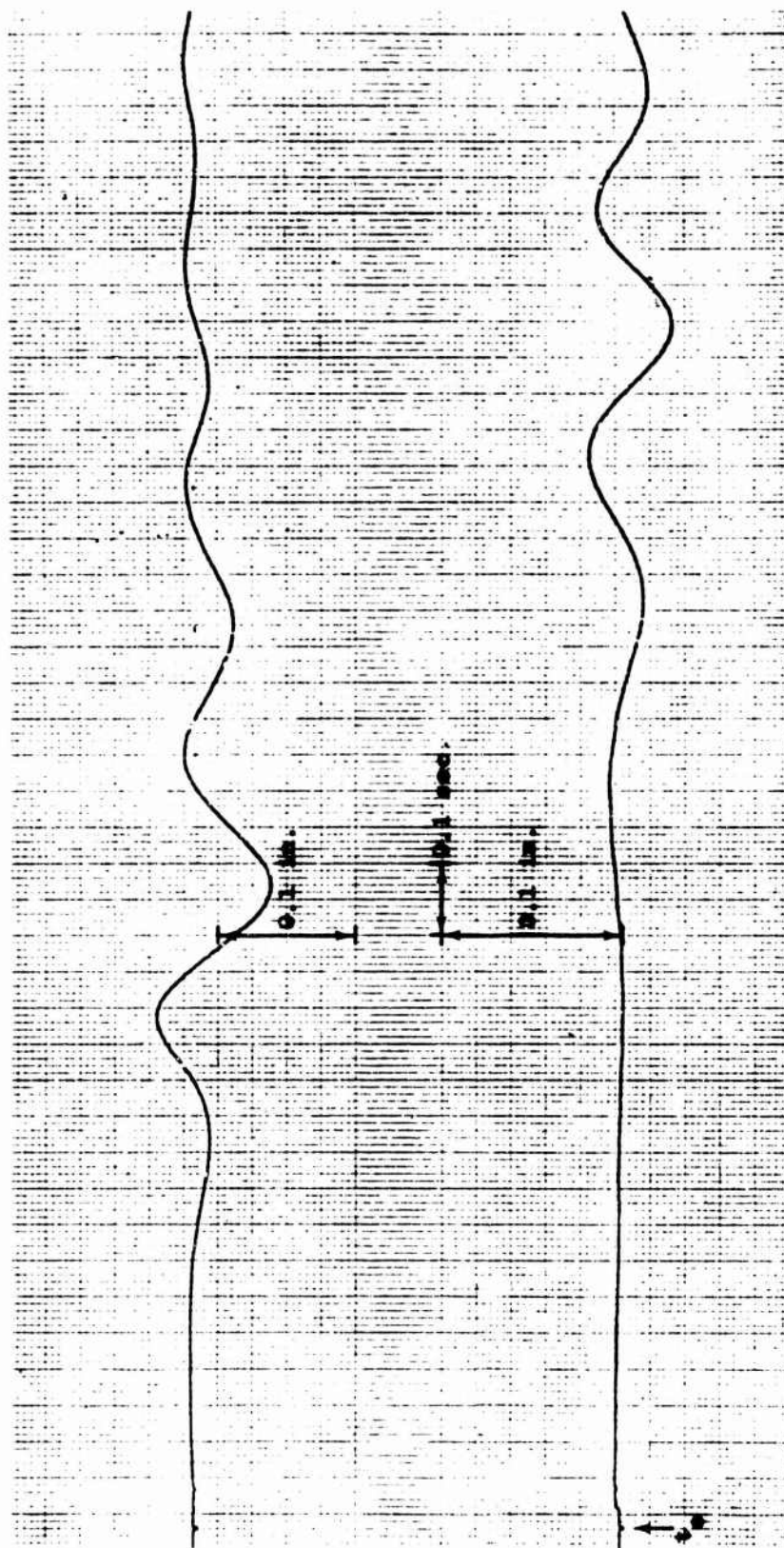
Fig. 48. Wave Gage Records, Shot 3
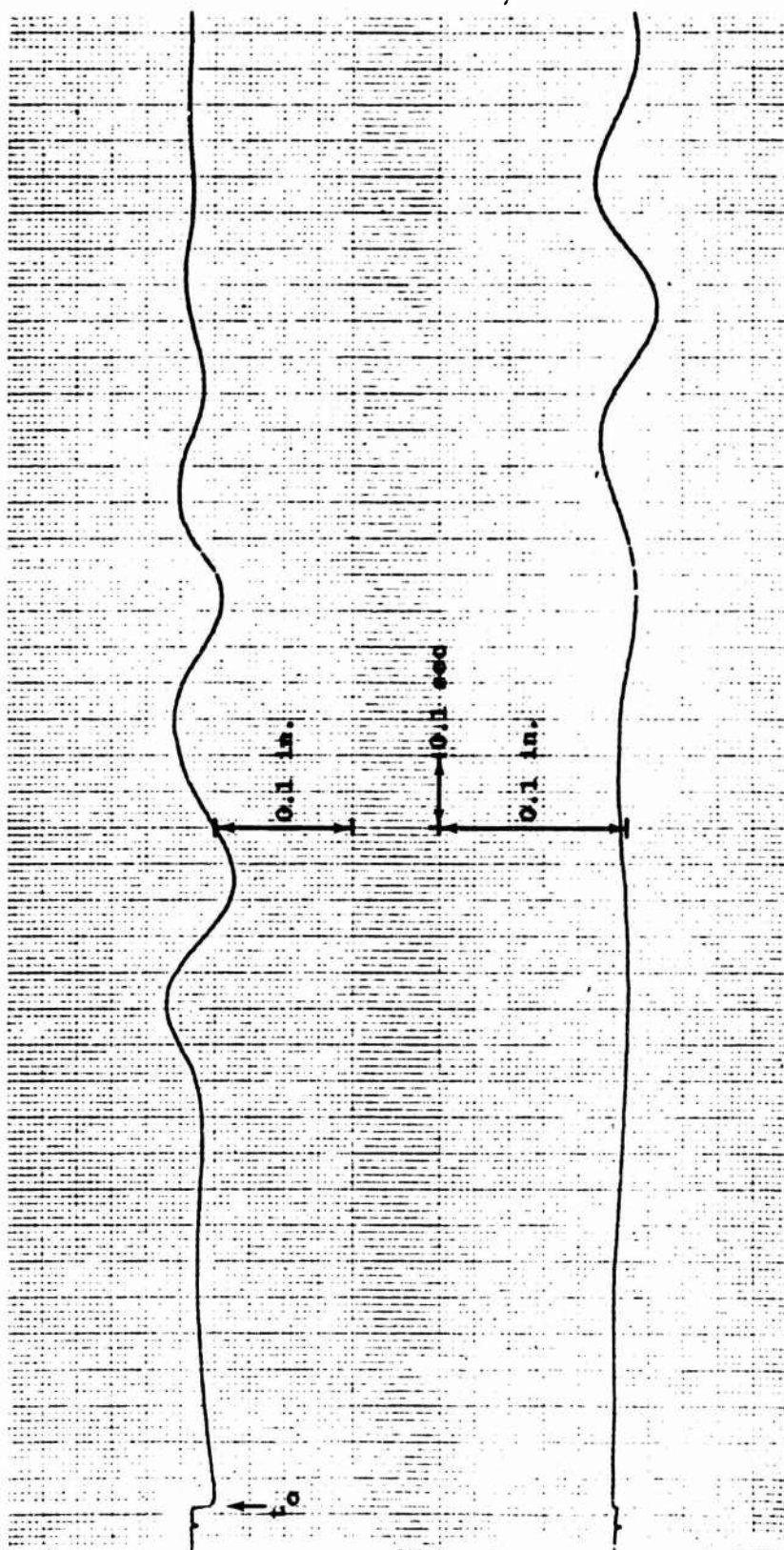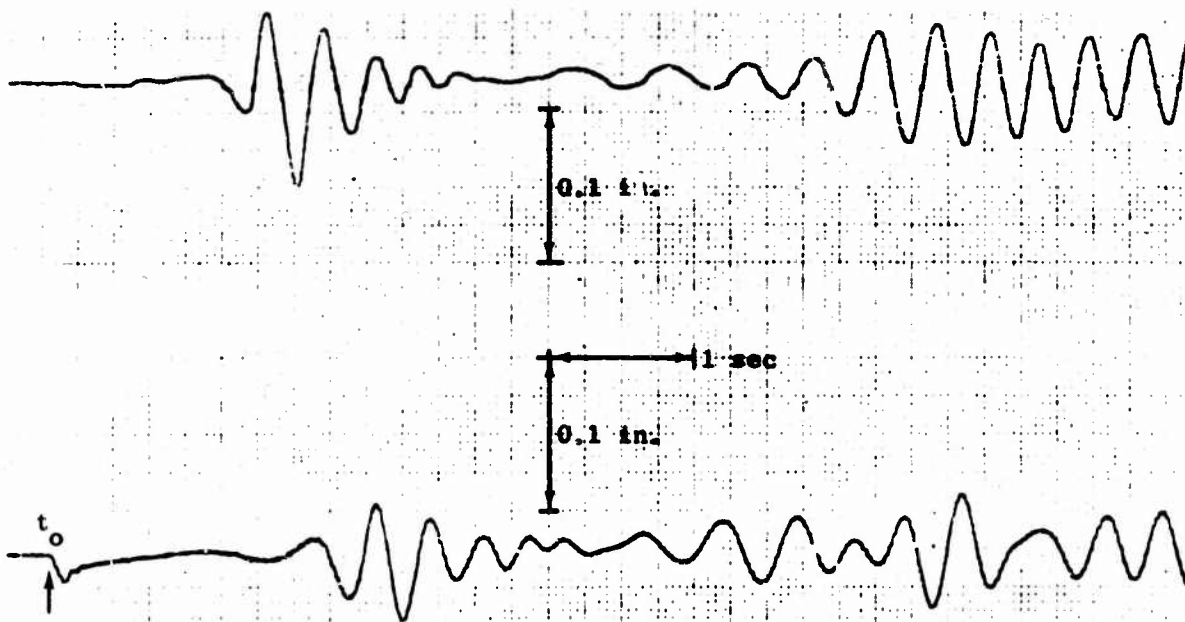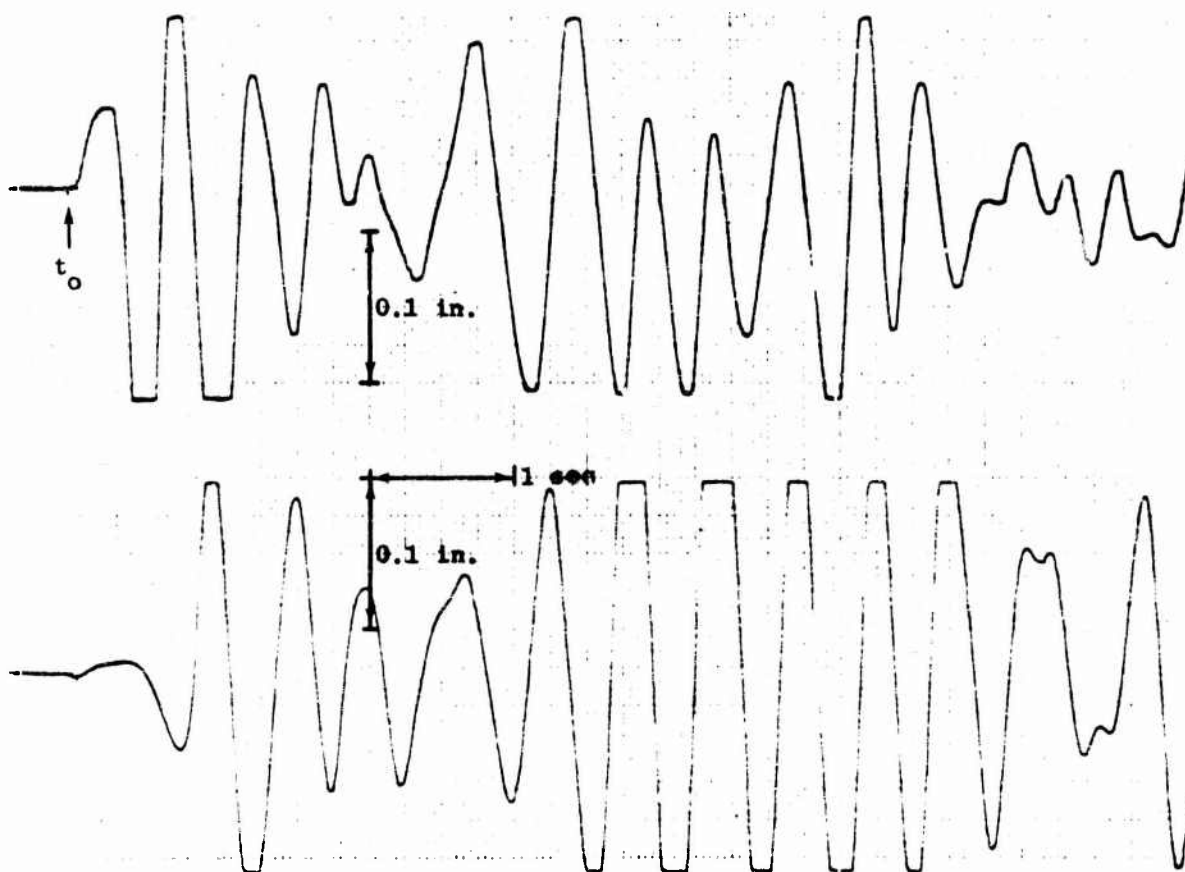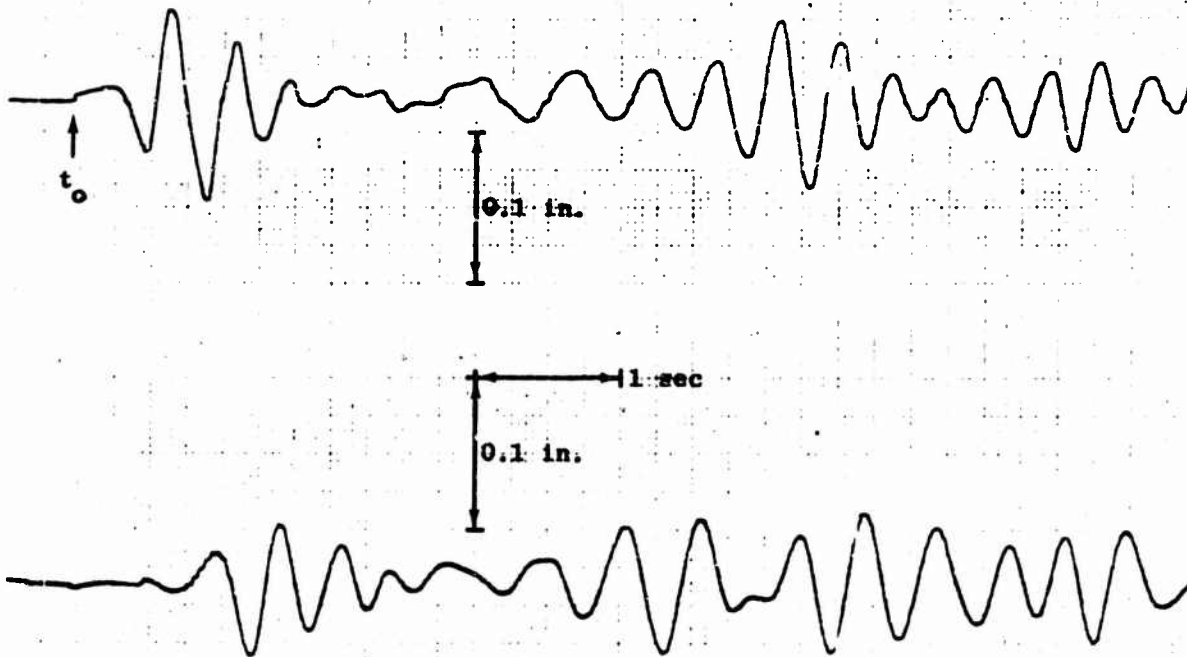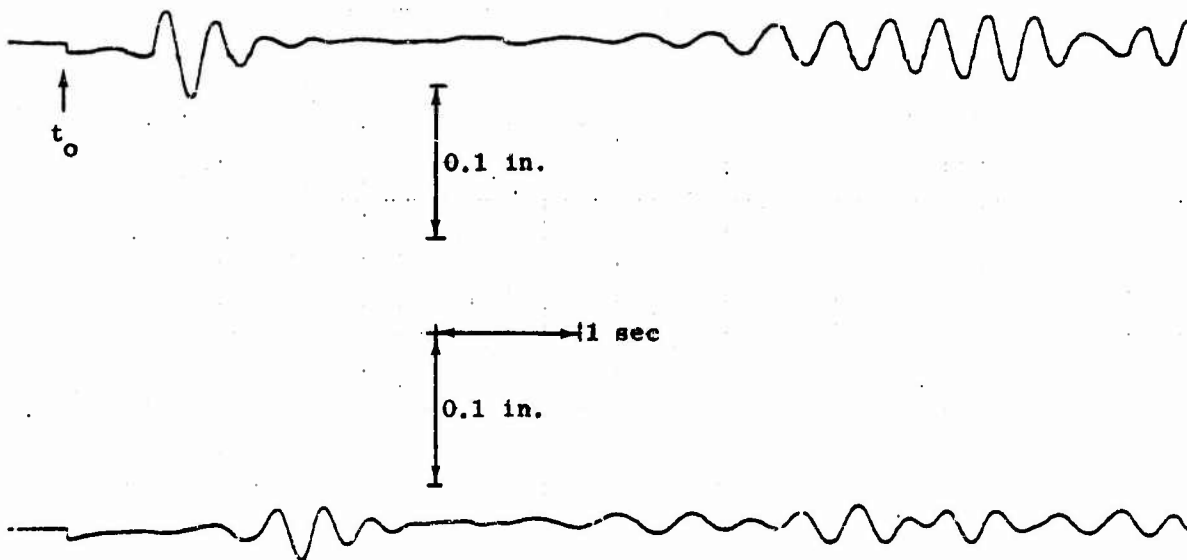
Fig. 49. Wave Gage Records, Shot 4

101
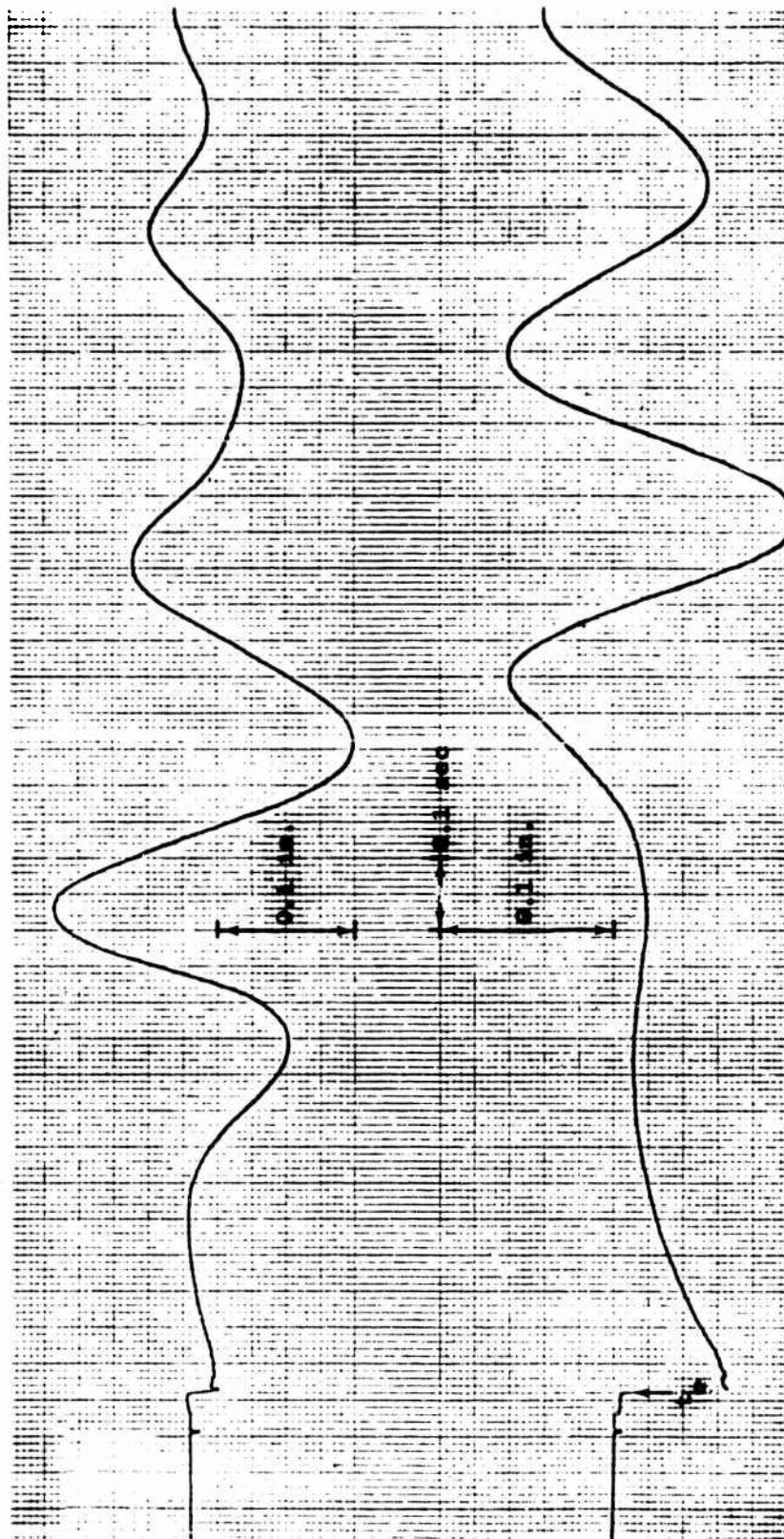
Fig. 50. Wave Gage Records, Shot 5
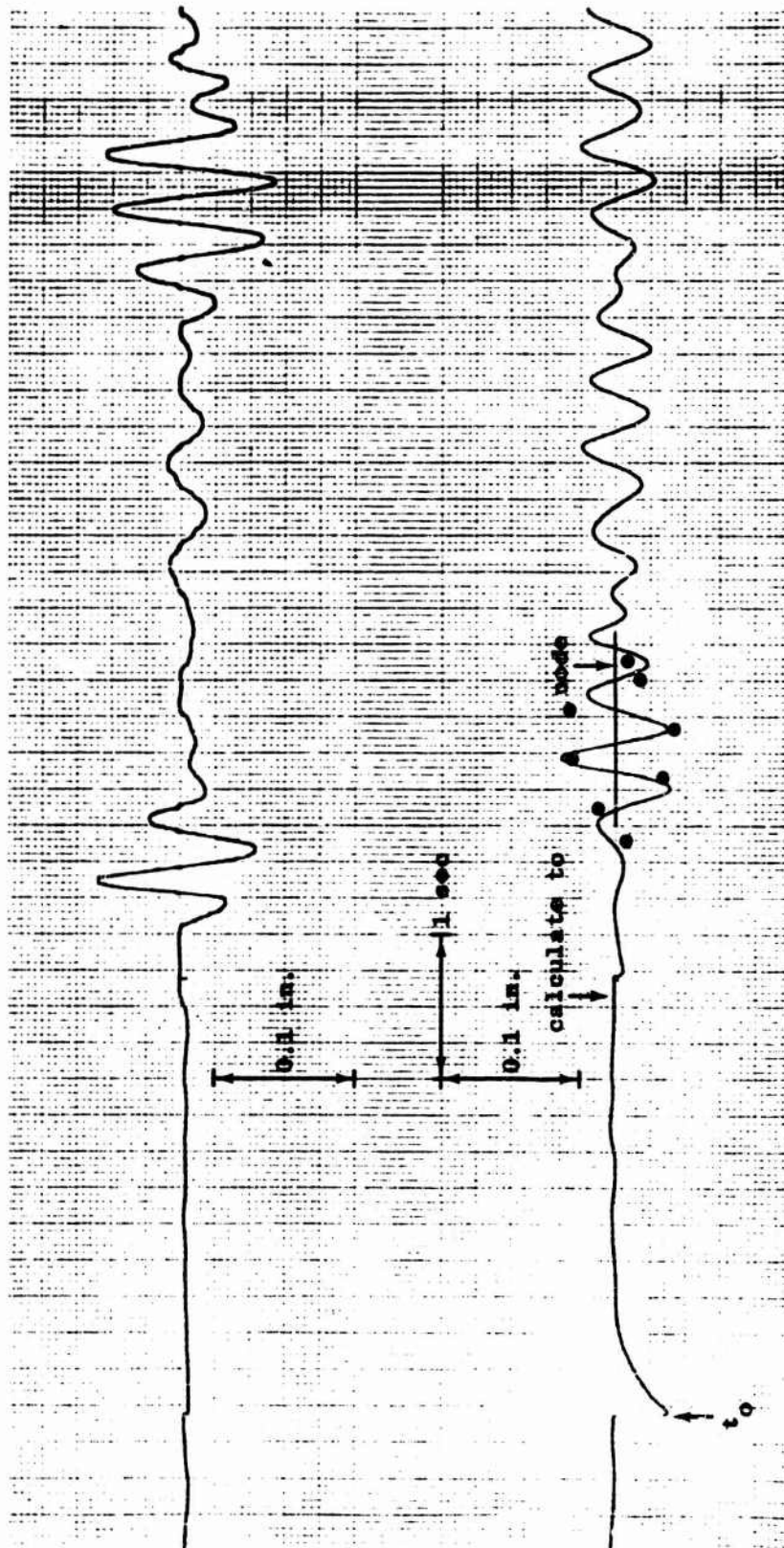
Fig. 51. Wave Gage Records, Shot 5R
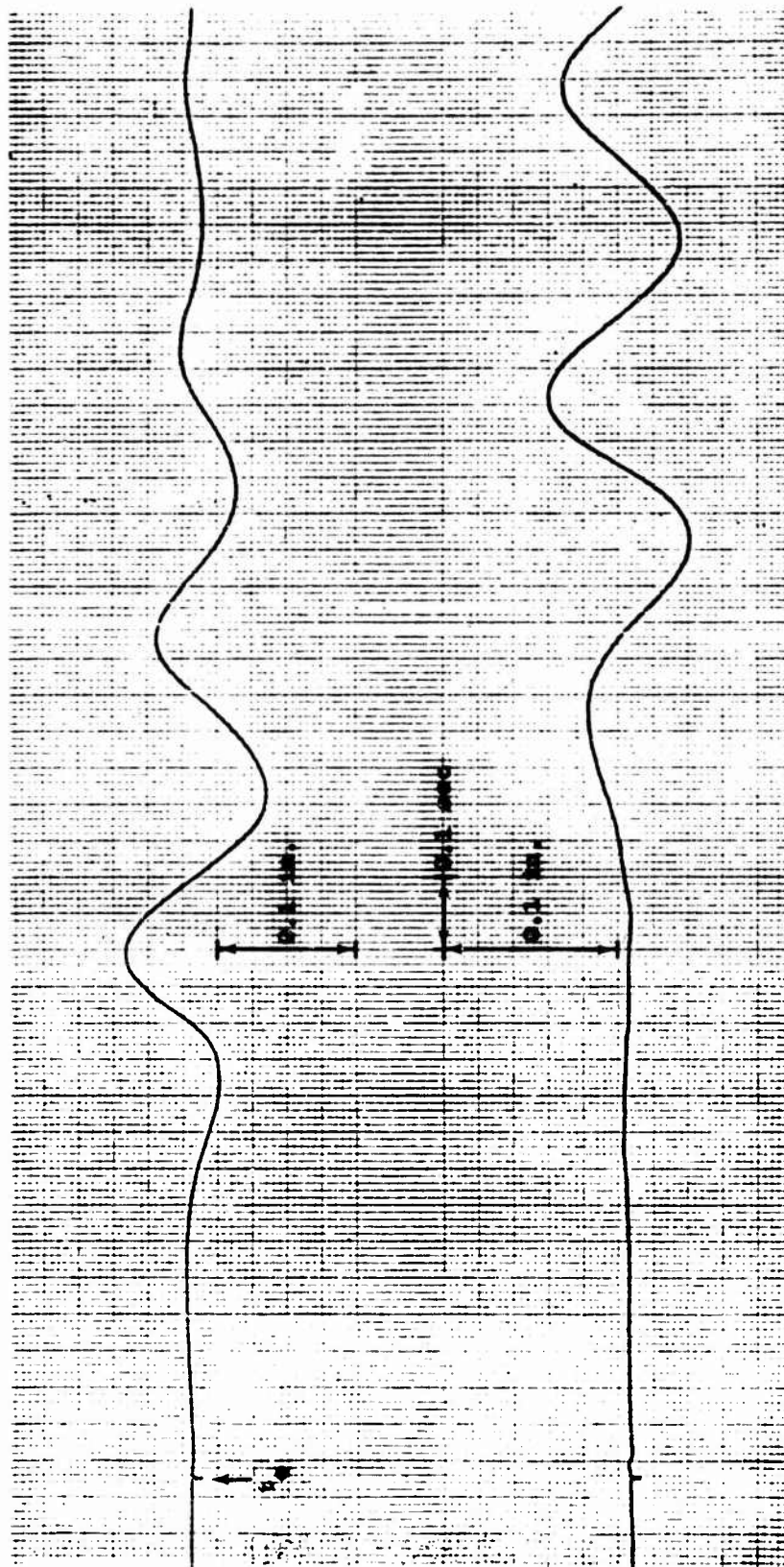
Fig. 52. Wave Gage Records, Shot 6
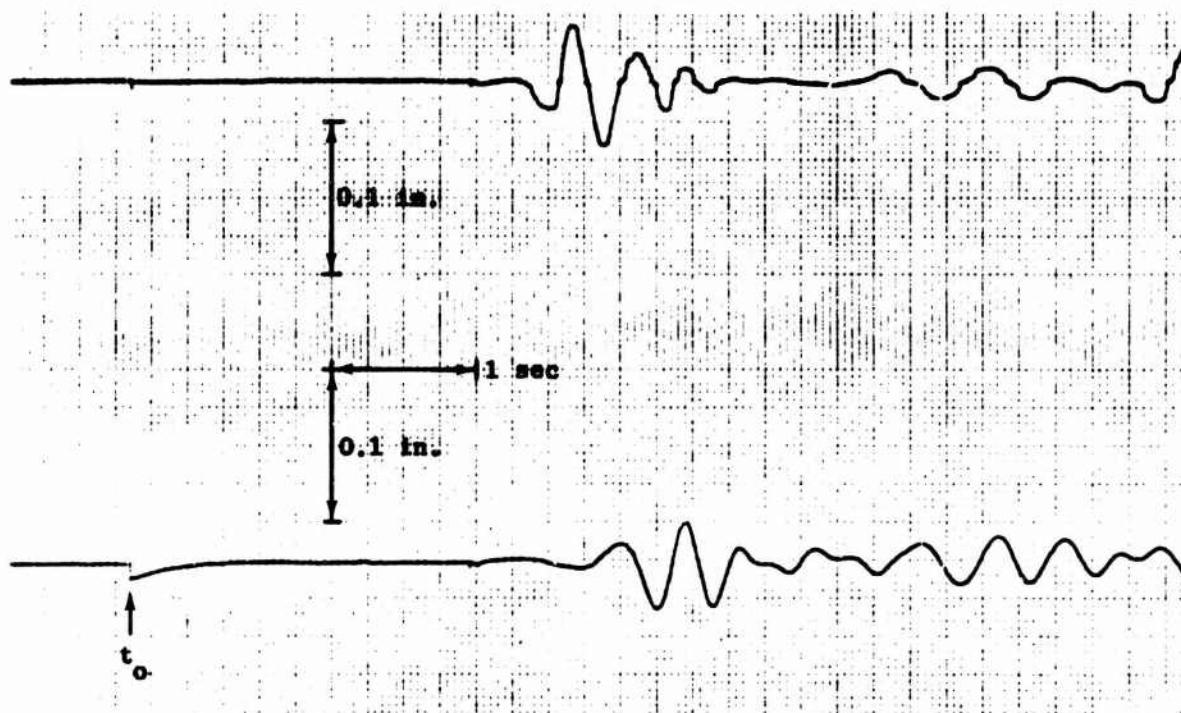
Fig. 53. Wave Gage Records, Shot 6R
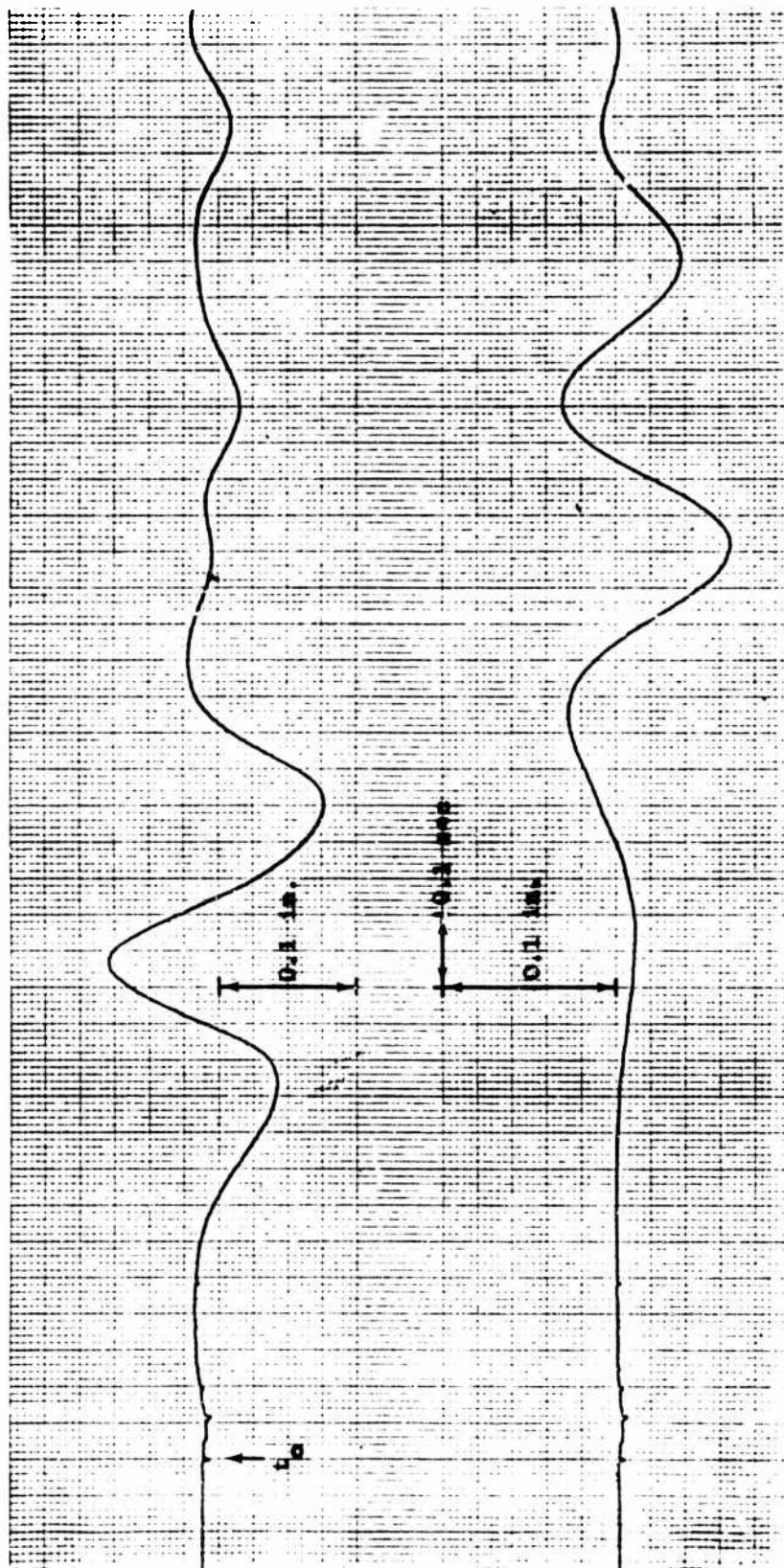
Fig. 54. Wave Gage Records, Shot 7
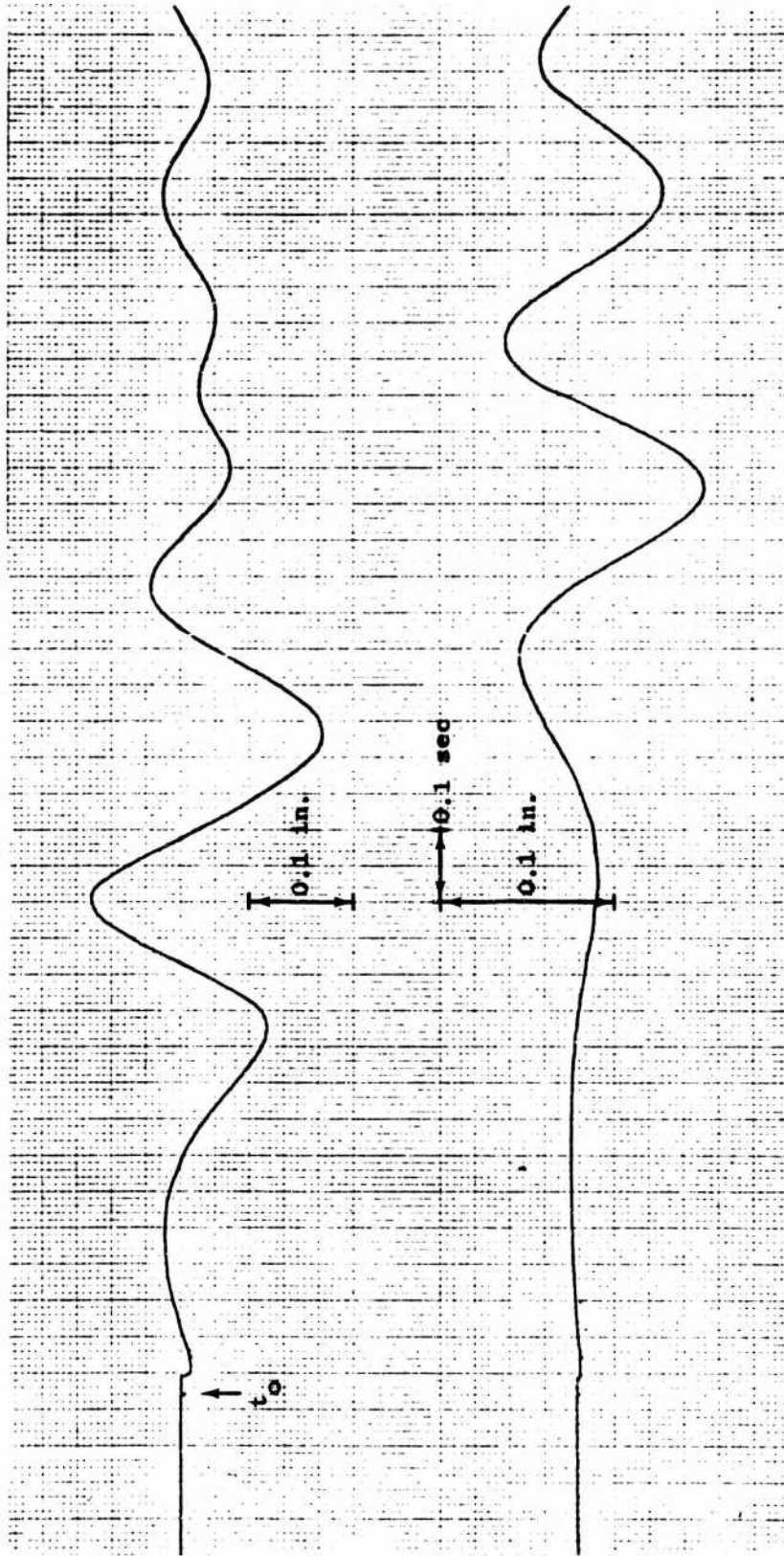
Fig. 55. Wave Gage Records, Shot 8

107

0.1 in.

0.1 sec

0.1 in.

t_o
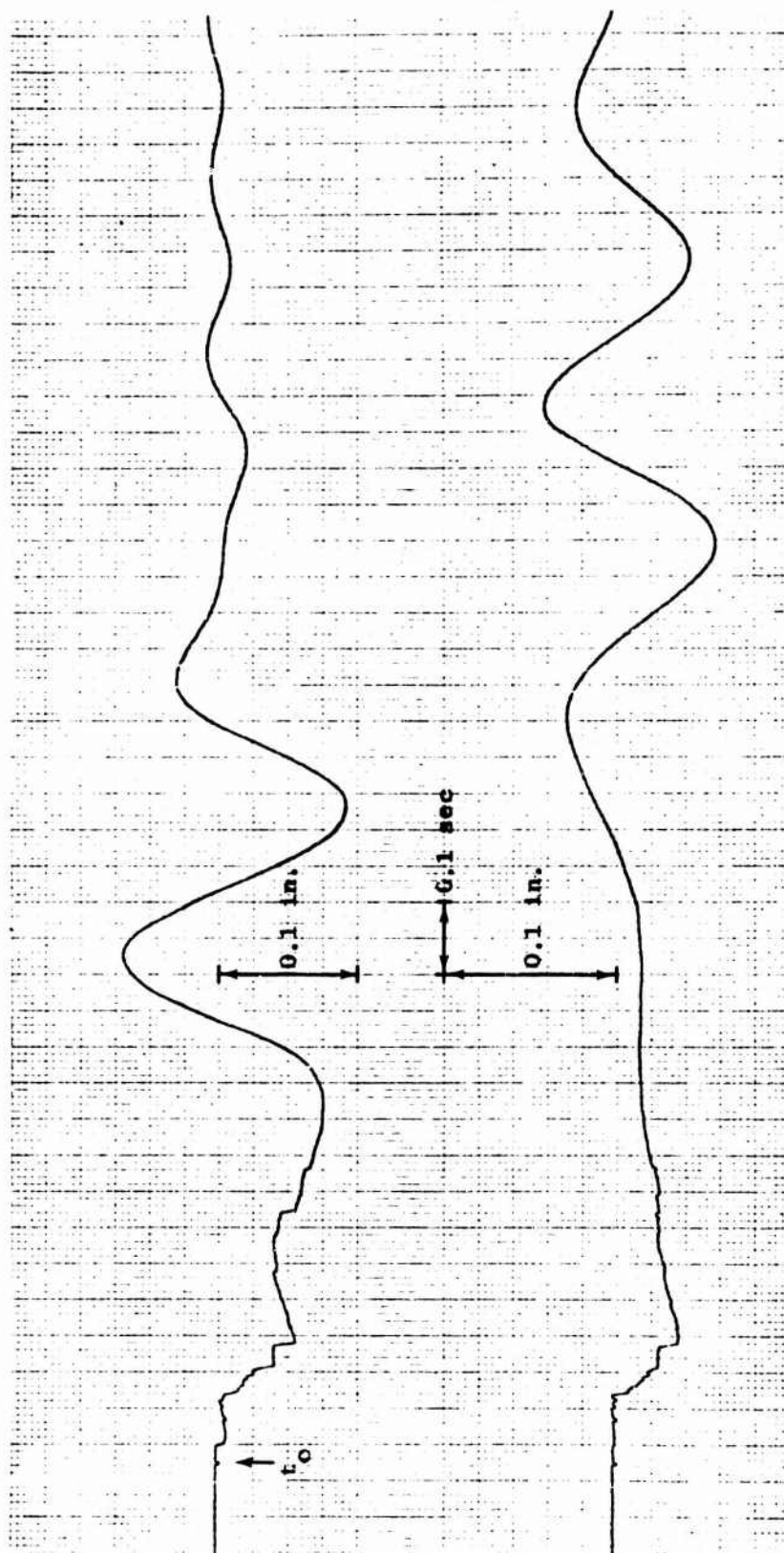
Fig. 56. Wave Gage Records, Shot 9
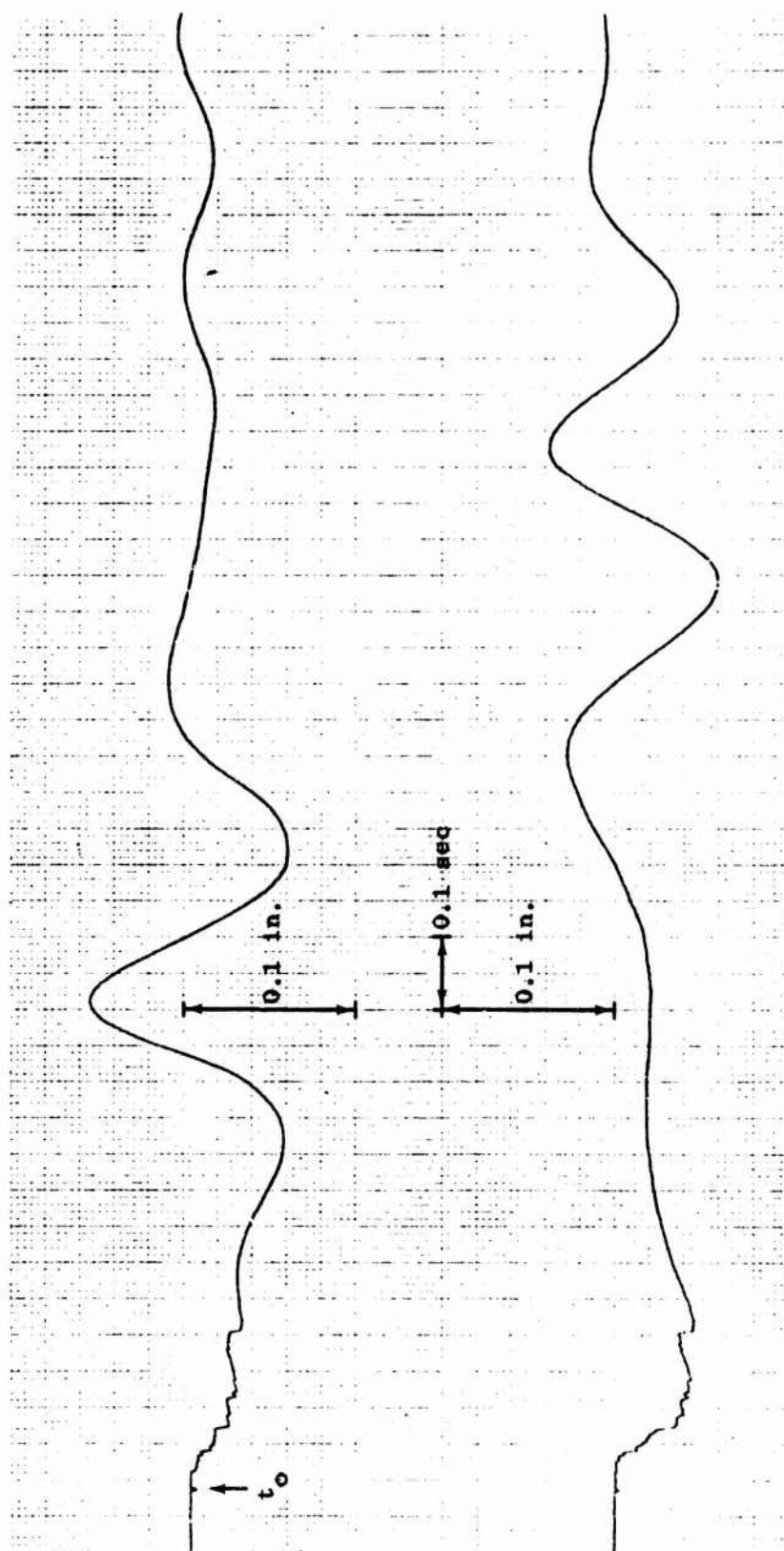
Fig. 57. Wave Gage Records, Shot 10
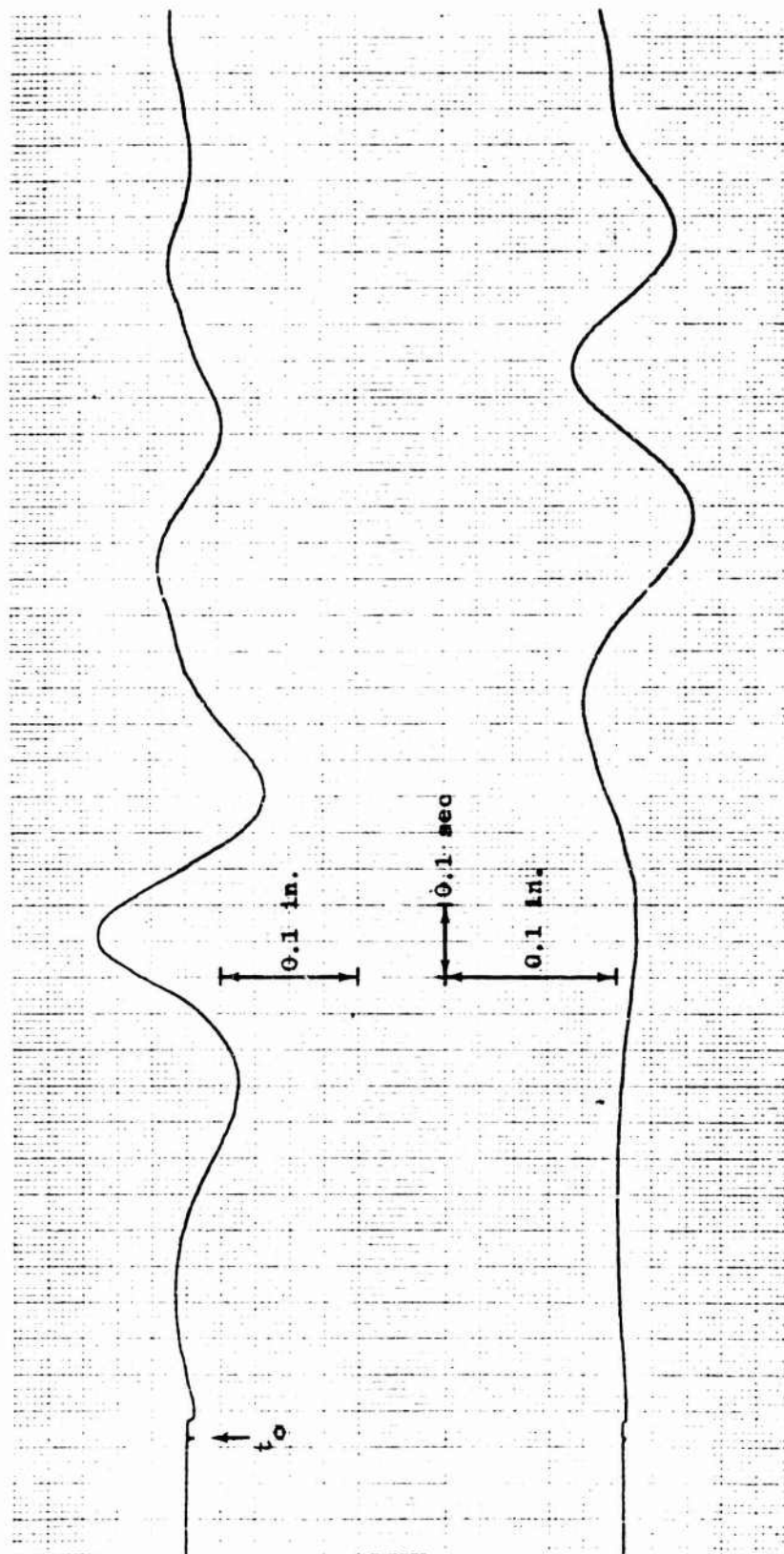
Fig. 58. Wave Gage Records, Shot 11

0.1 in.

0.1 sec

0.1 in.
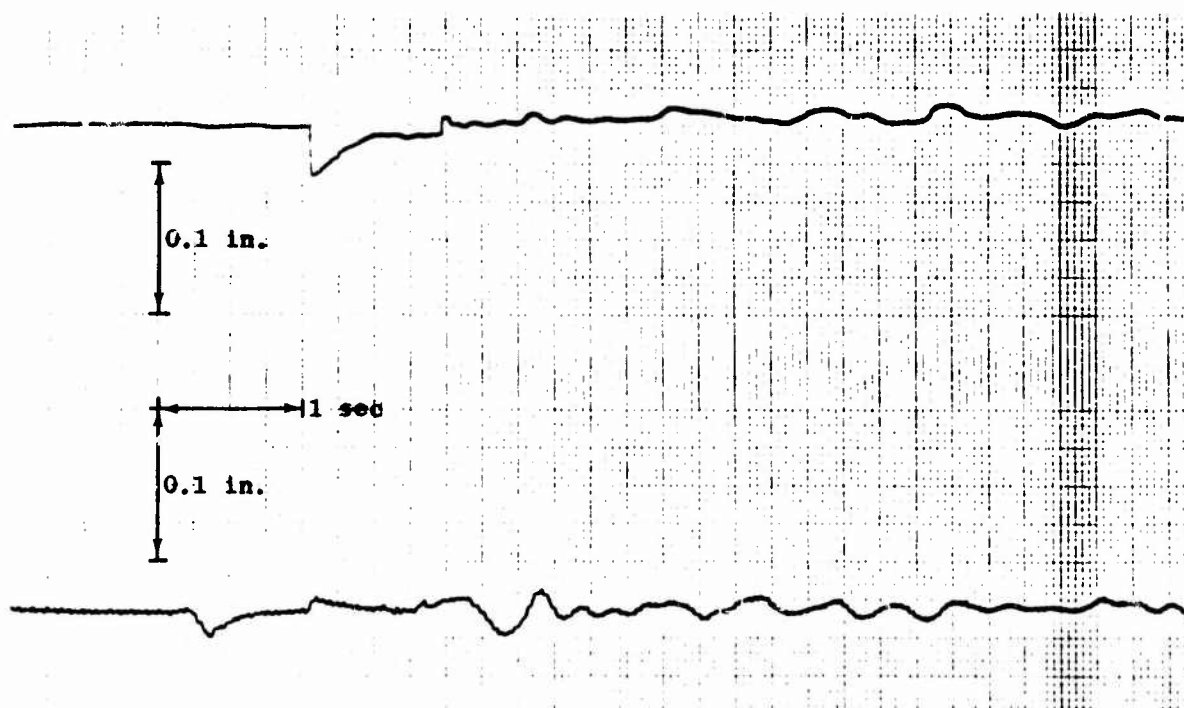
t_0

110
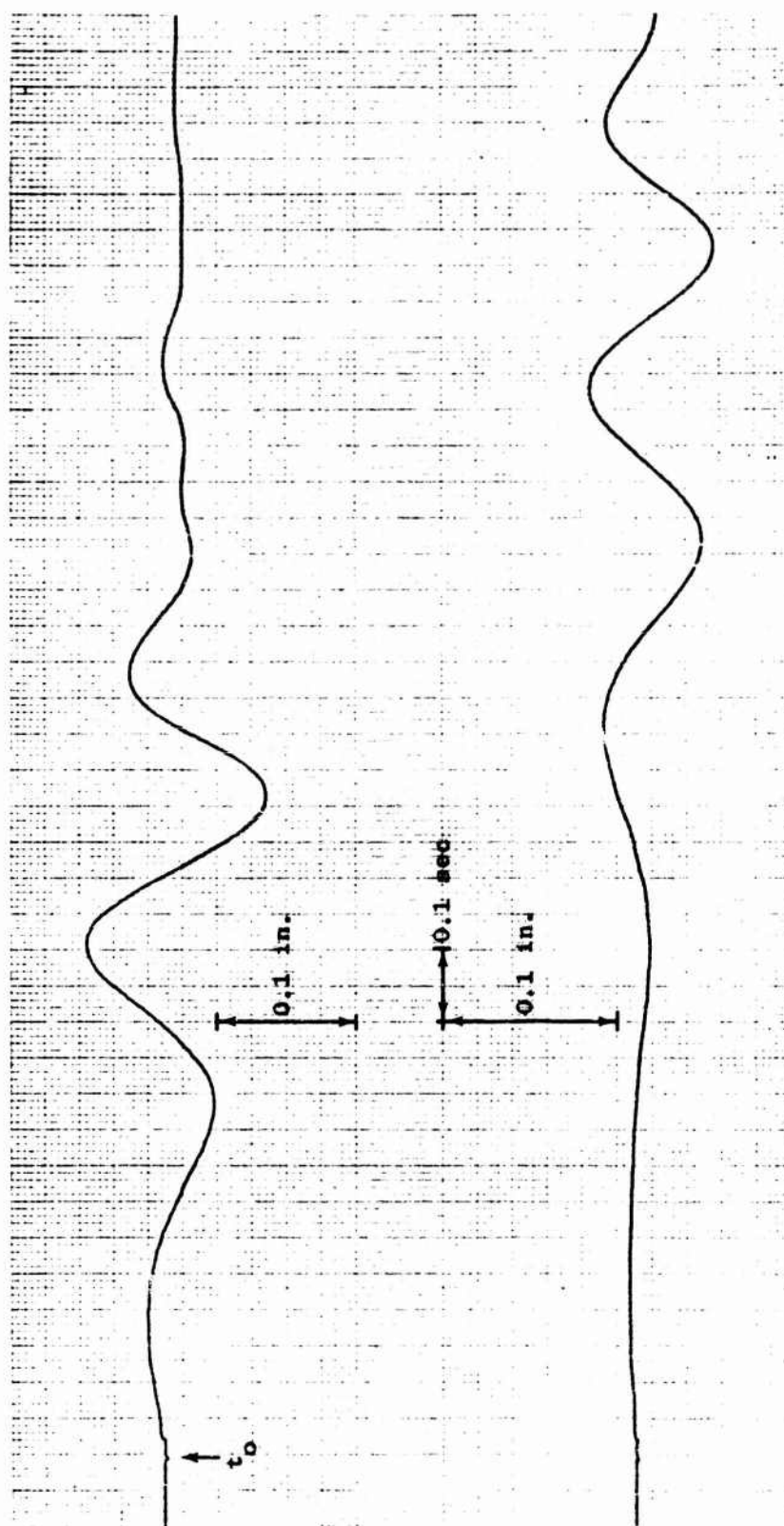
Fig. 59. Wave Gage Records, Shot 12
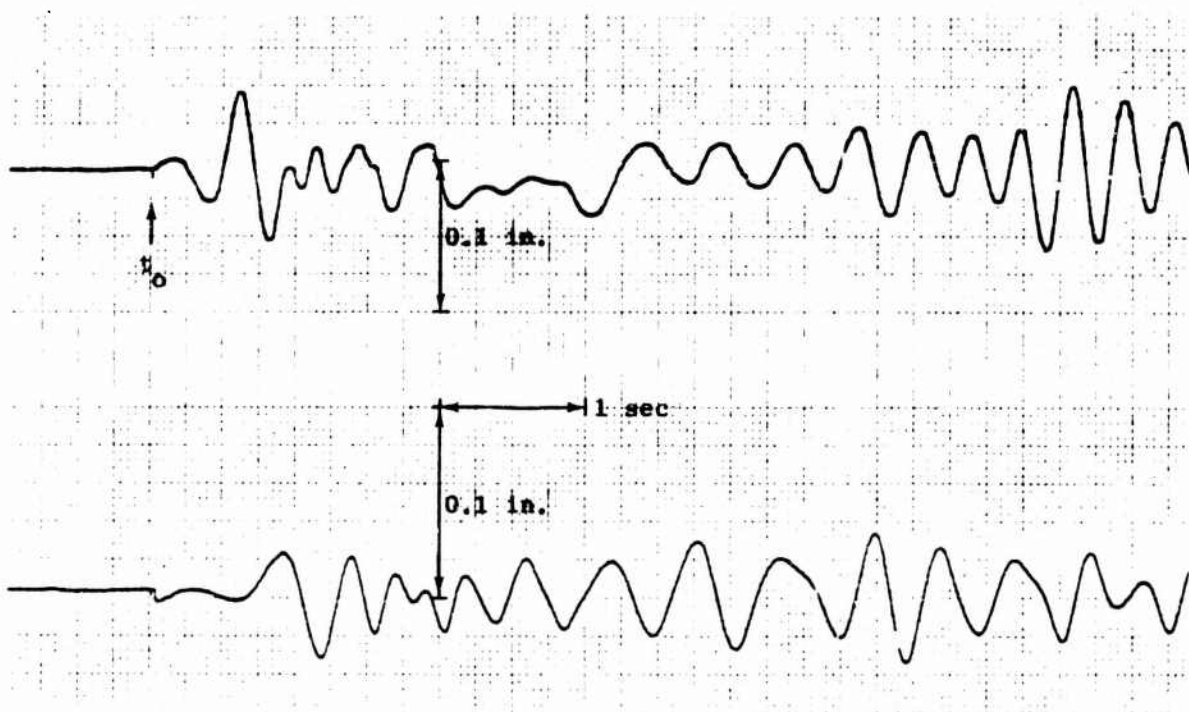
Fig. 60. Wave Gage Records, Shot 13
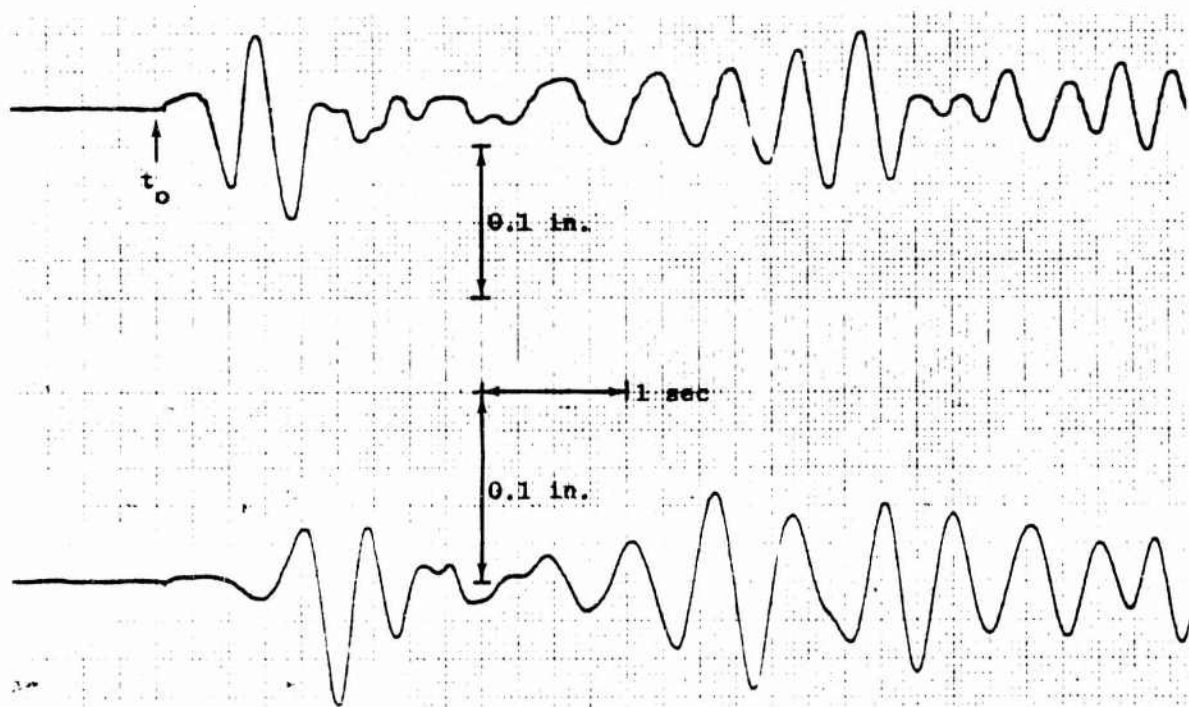
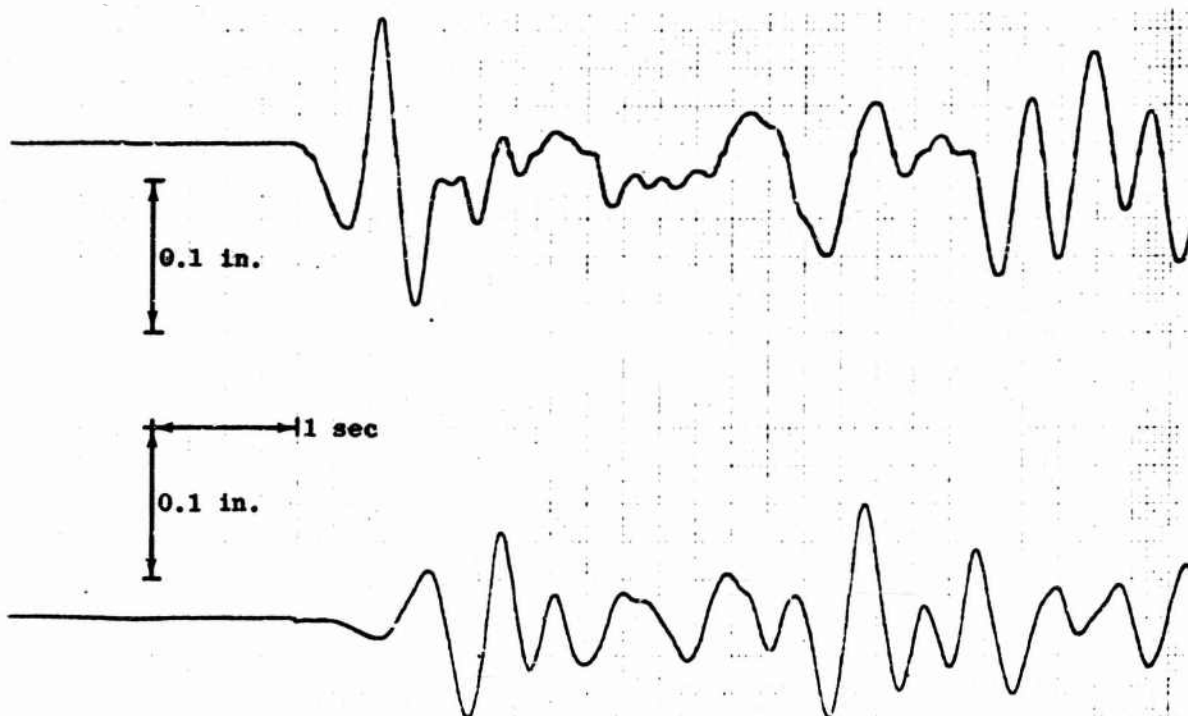

Fig. 61. Wave Gage Records, Shot 14
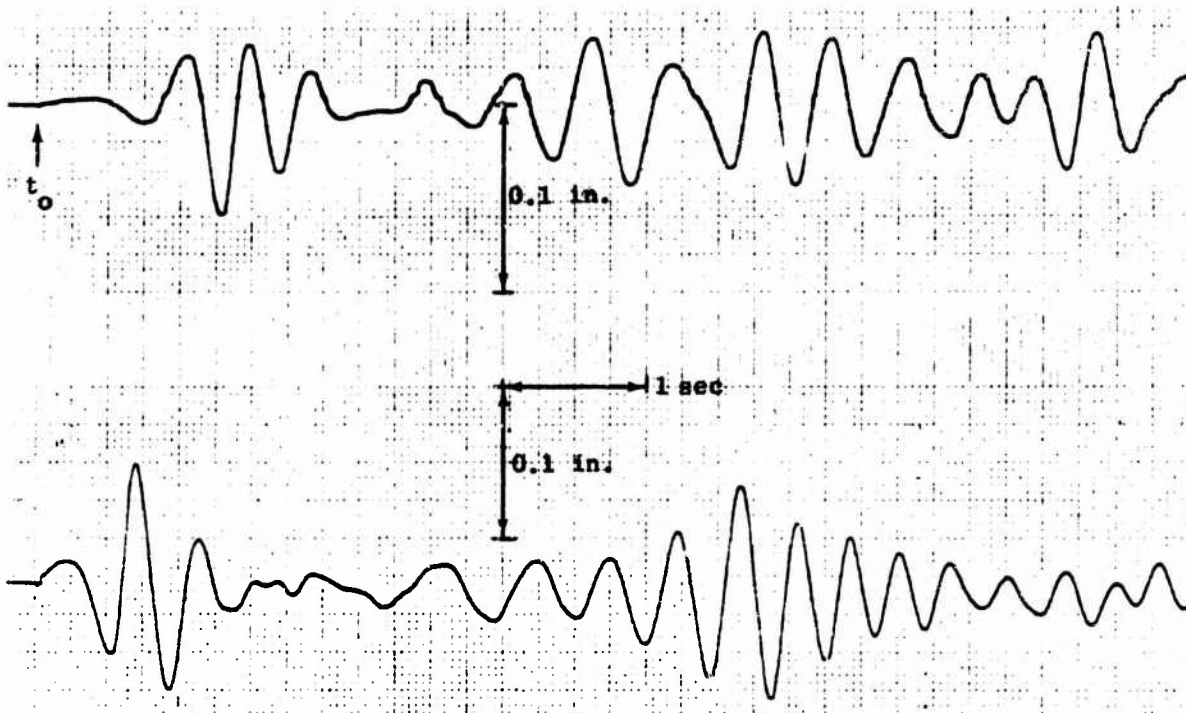
Fig. 62.   Wave Gage Records, Shot 15
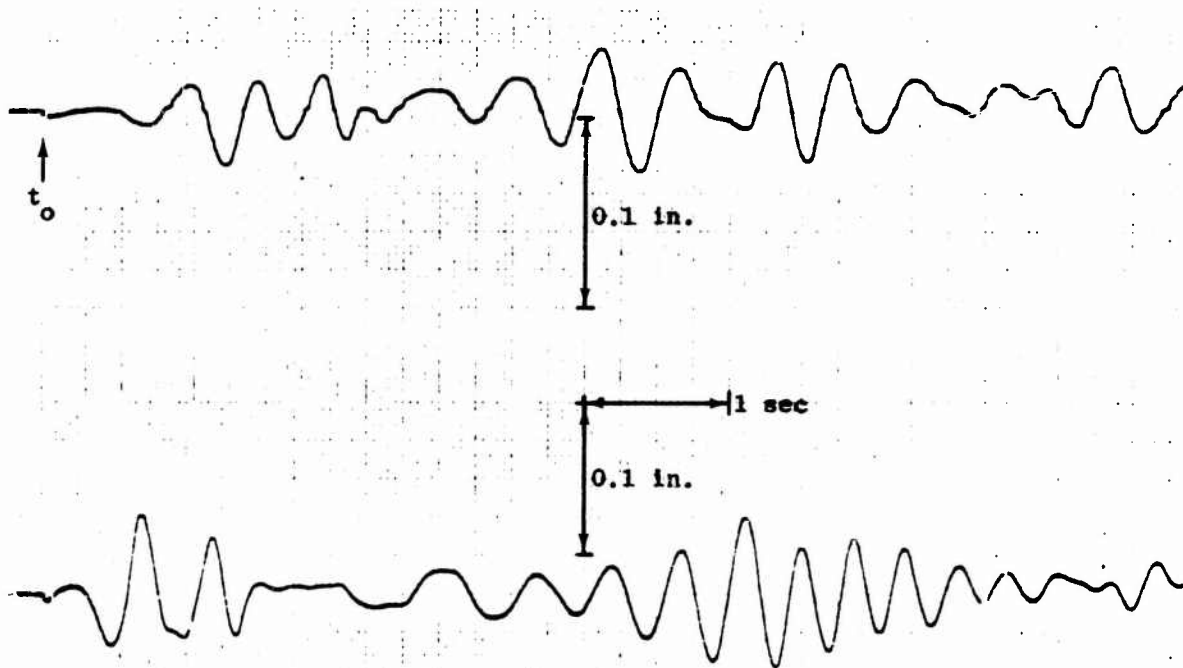
Fig. 63.   Wave Gage Records, Shot 16

113
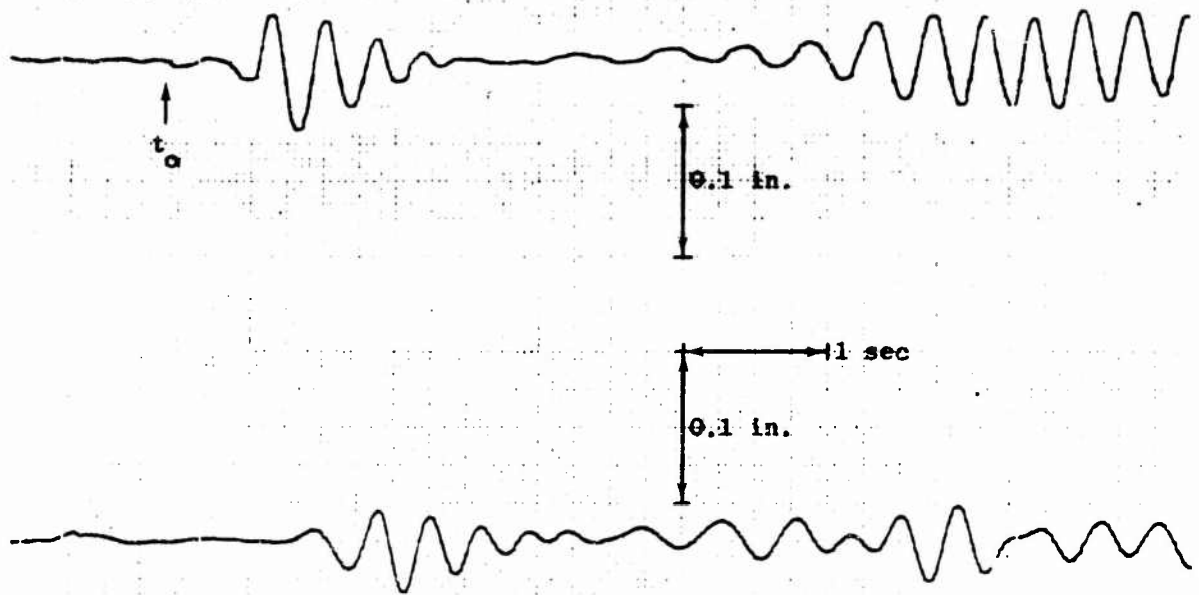
Fig. 64. Wave Gage Records, Shot 17
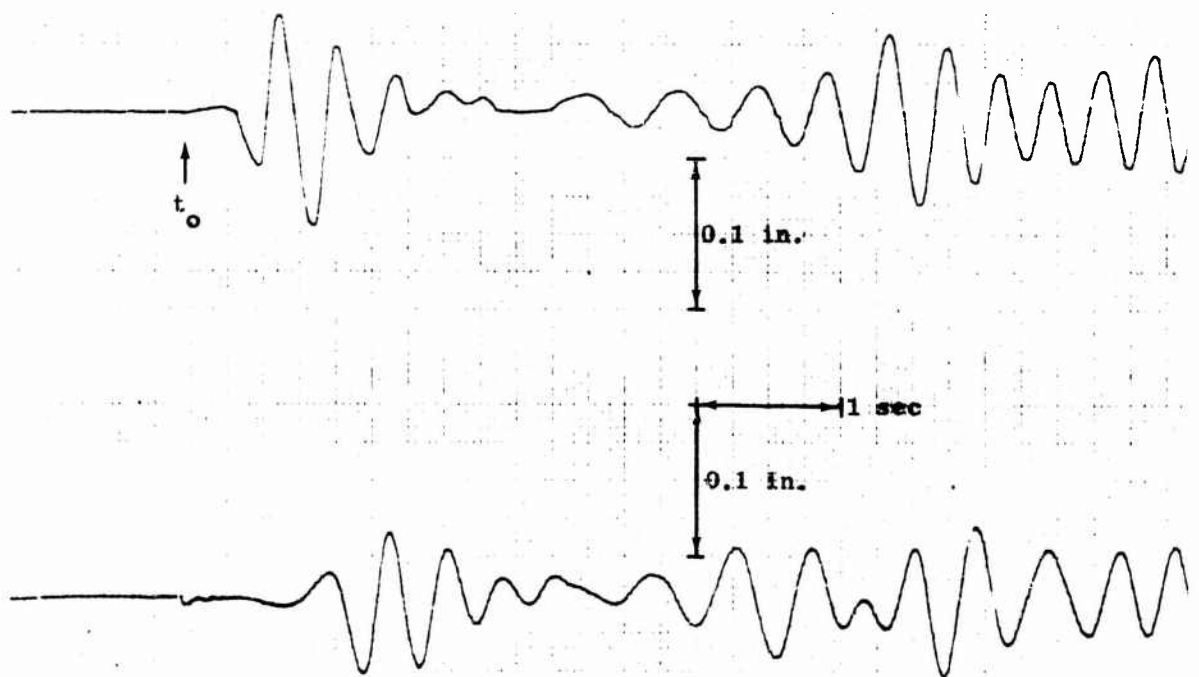
Fig. 65. Wave Gage Records, Shot 17R

114
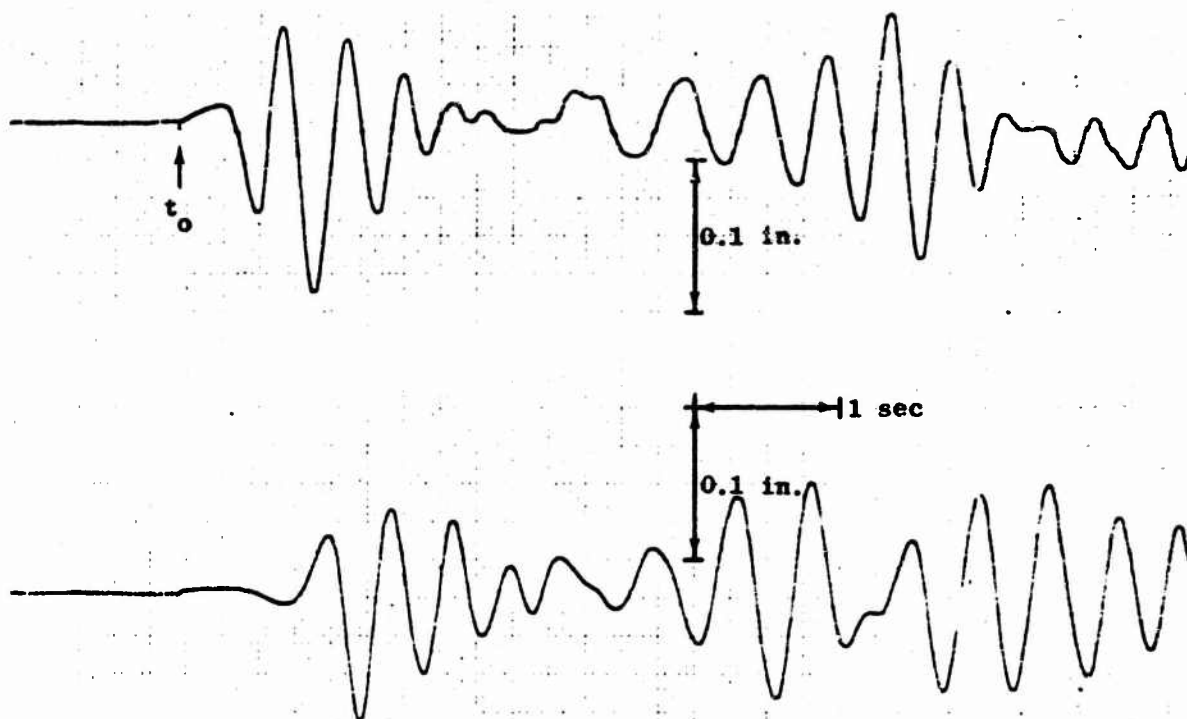
Fig. 66.   Wave Gage Records, Shot 18
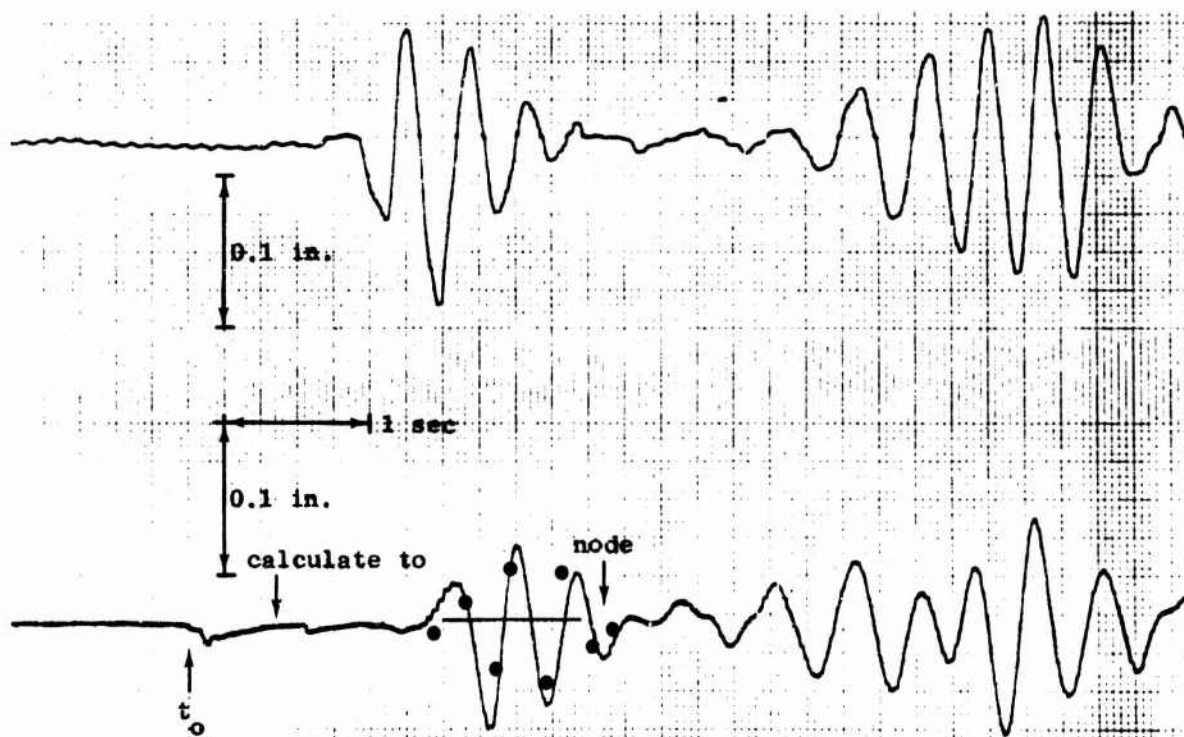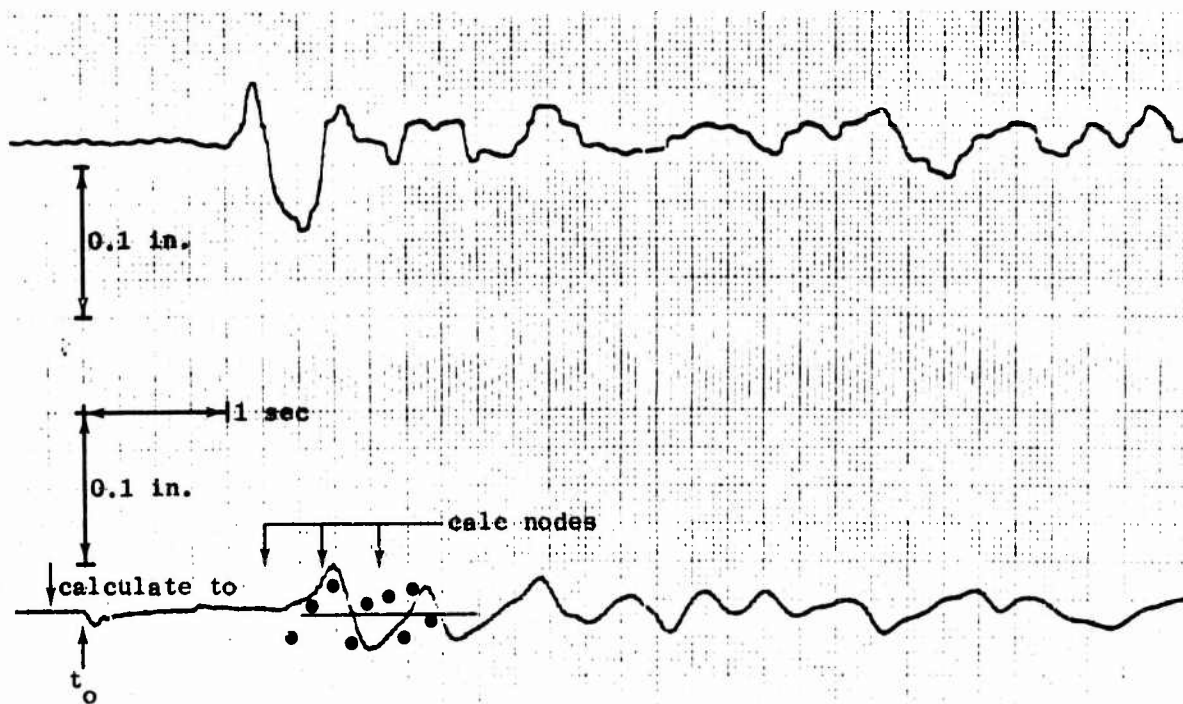
Fig. 67.   Wave Gage Records, Shot 18R

115
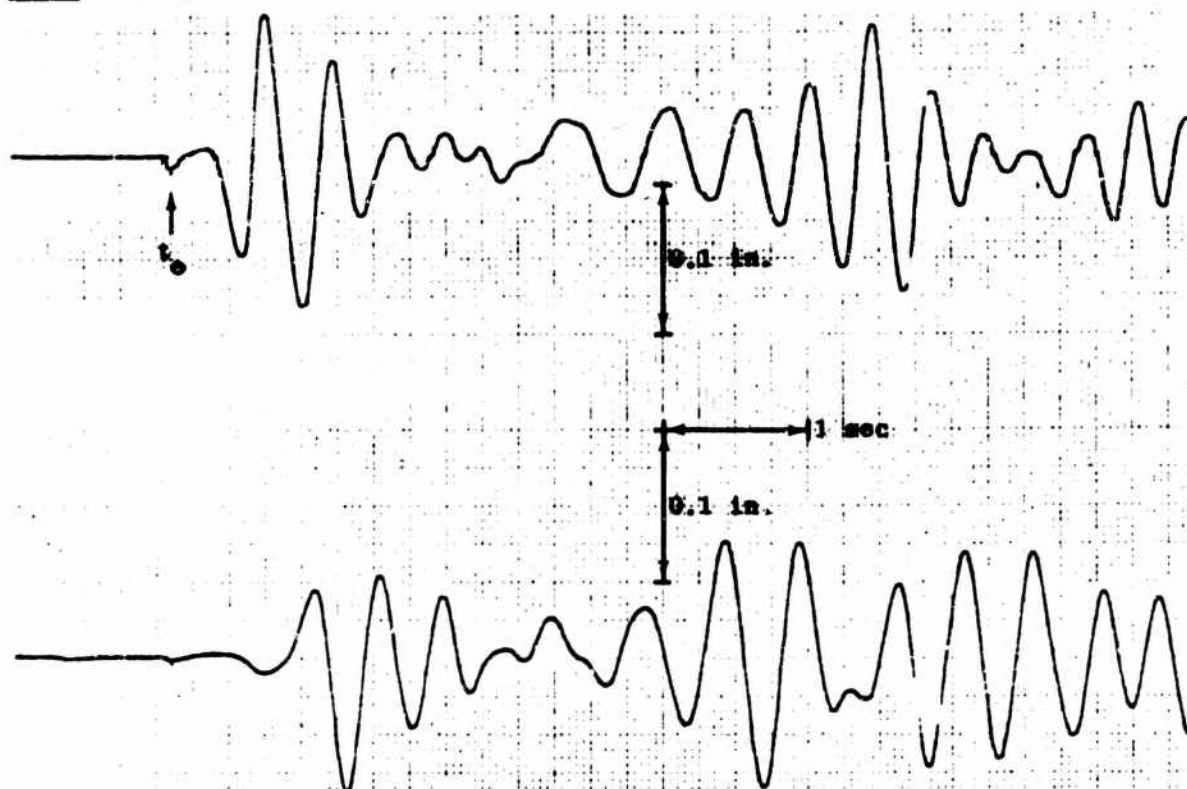
Fig. 68. Wave Gage Records, Shot 19
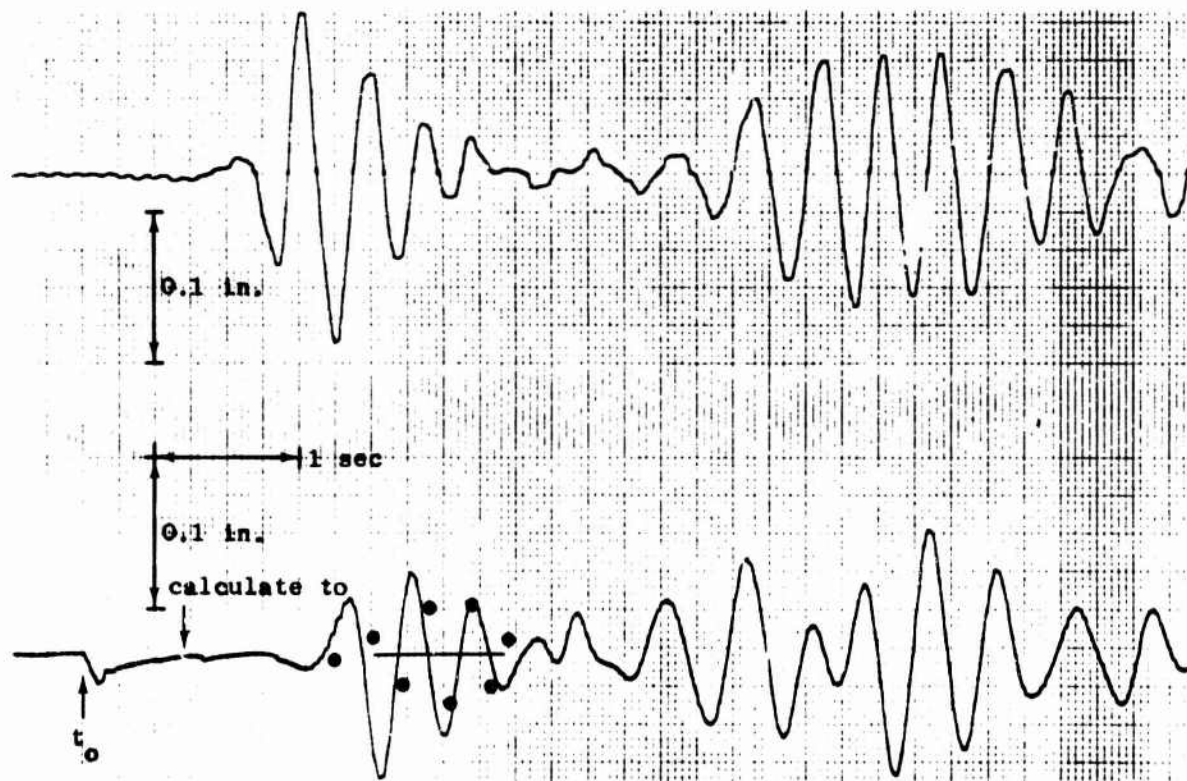
Fig. 69. Wave Gage Records, Shot 19R
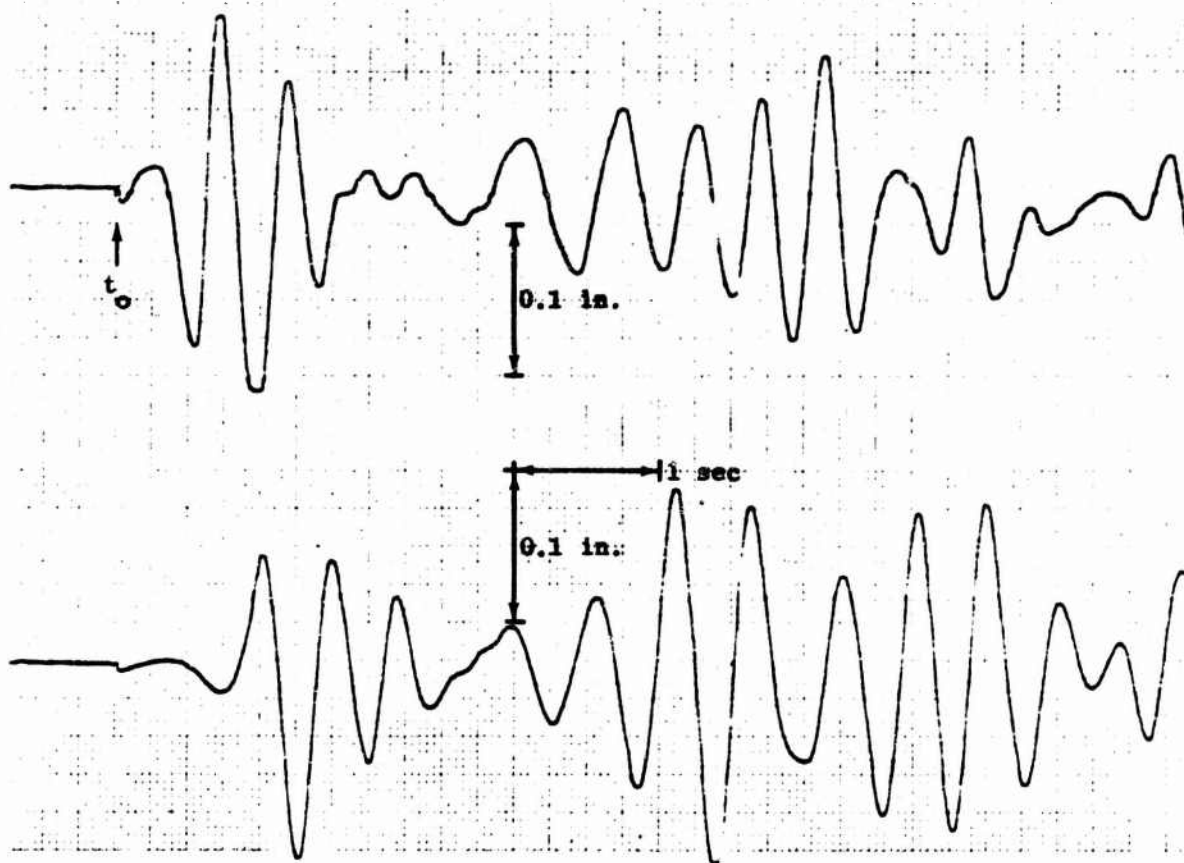
Fig. 70.   Wave Gage Records, Shot 20

0.1 in.

1 sec

0.1 in.
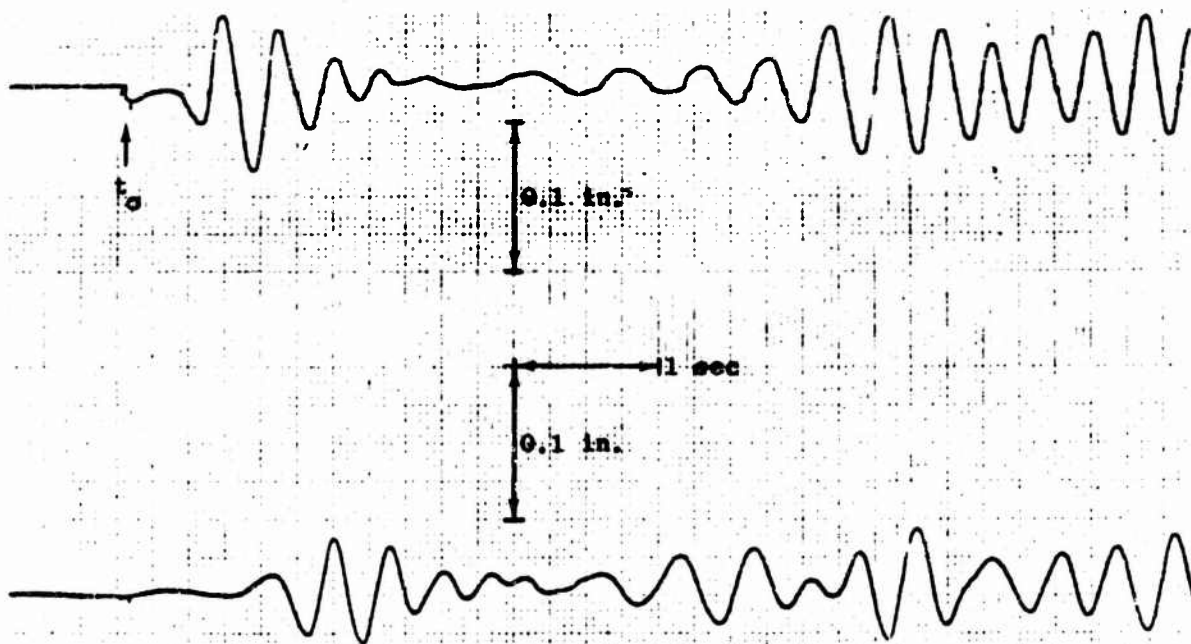
Fig. 71.   Wave Gage Records, Shot 21

0.1 in.

1 sec

0.1 in.
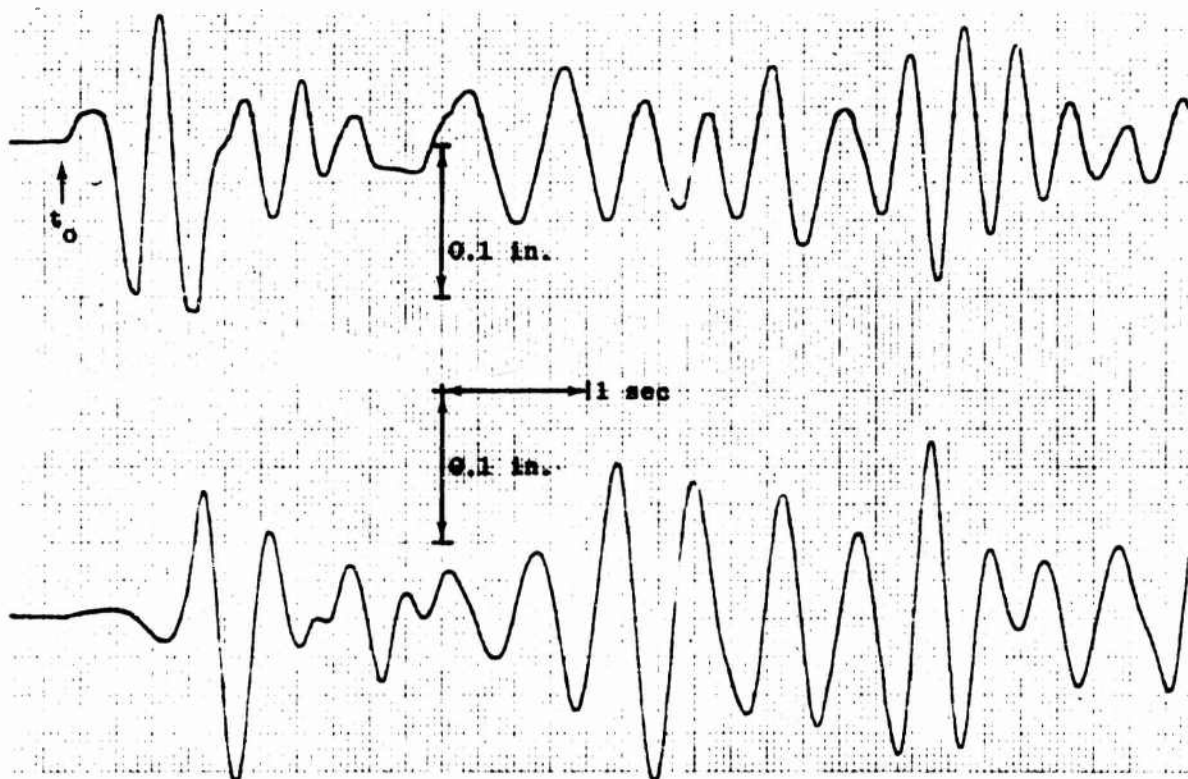
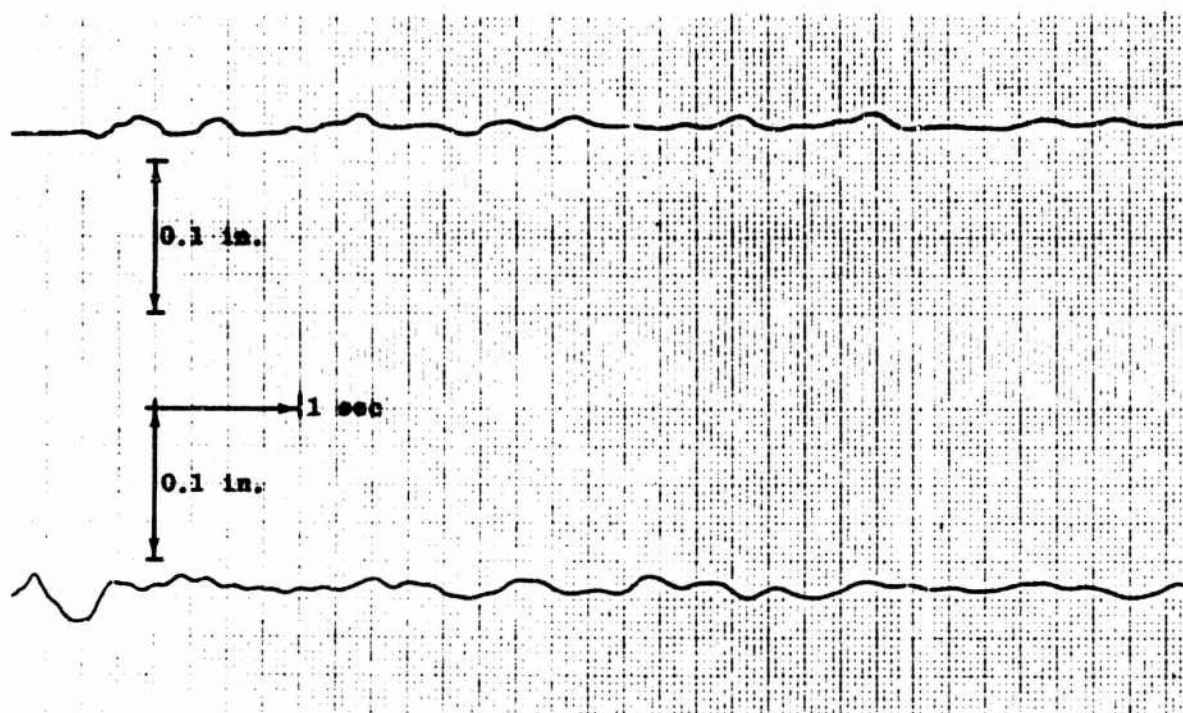Fig. 72.   Wave Gage Records, Shot 22

118
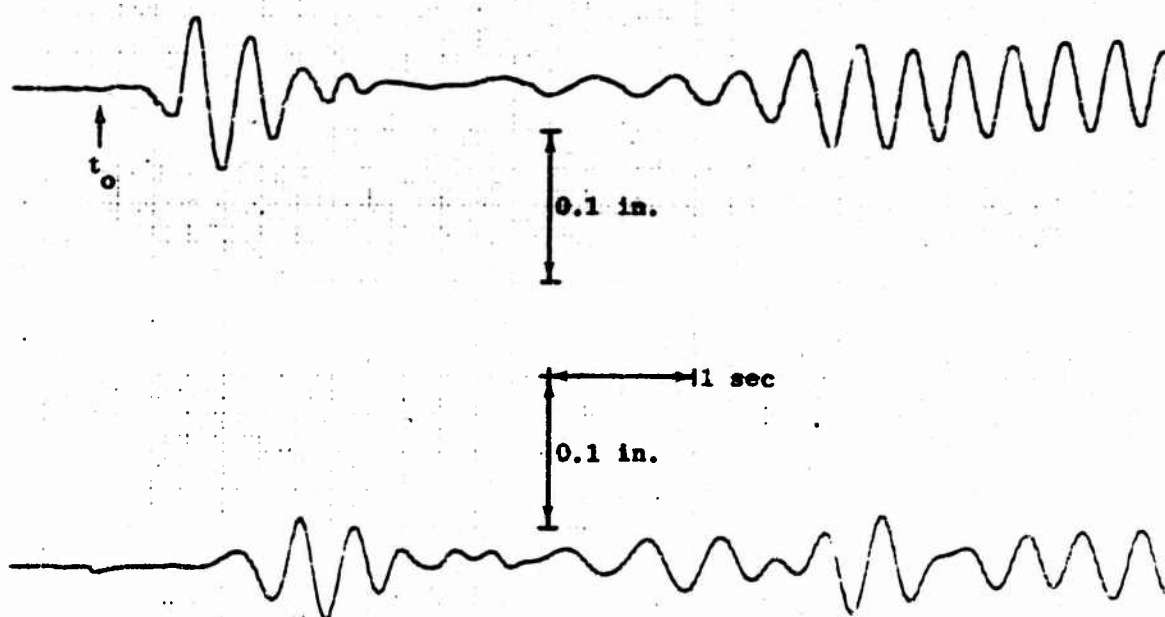
Fig. 73. Wave Gage Records, Shot 23
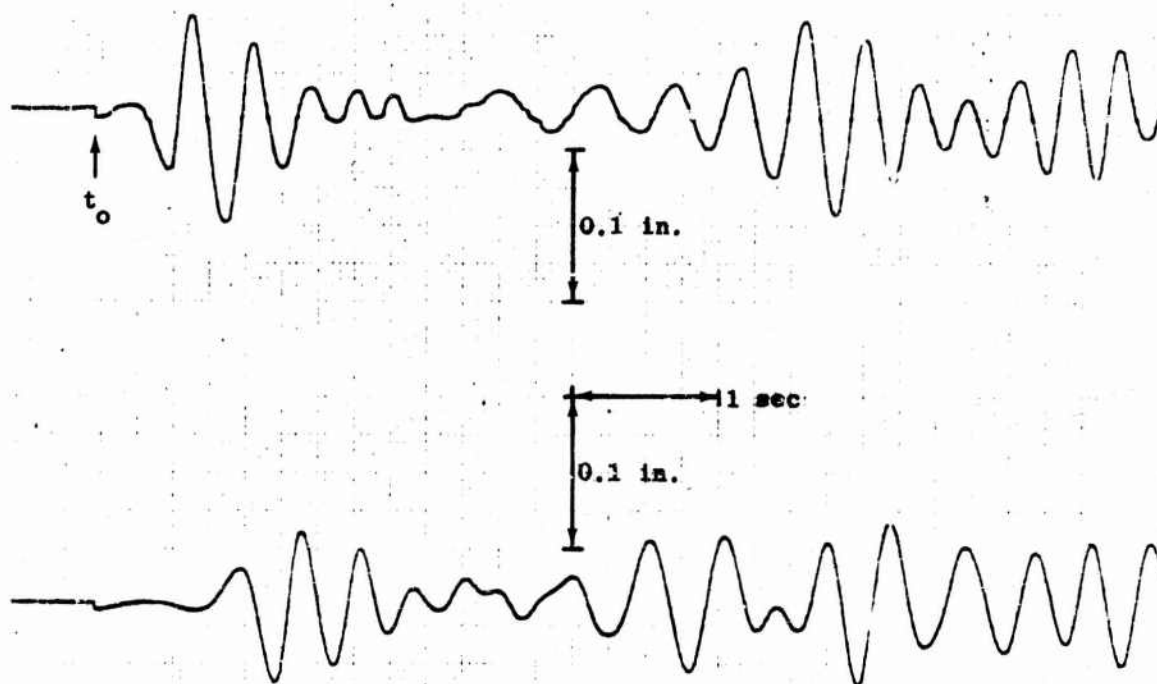
Fig. 74. Wave Gage Records, Shot 24

119

Fig. 75.   Wave Gage Records, Shot 25

Fig. 76.   Wave Gage Records, Shot 25R

120

Fig. 77. Wave Gage Records, Shot 26

Fig. 78. Wave Gage Records, Shot 26R
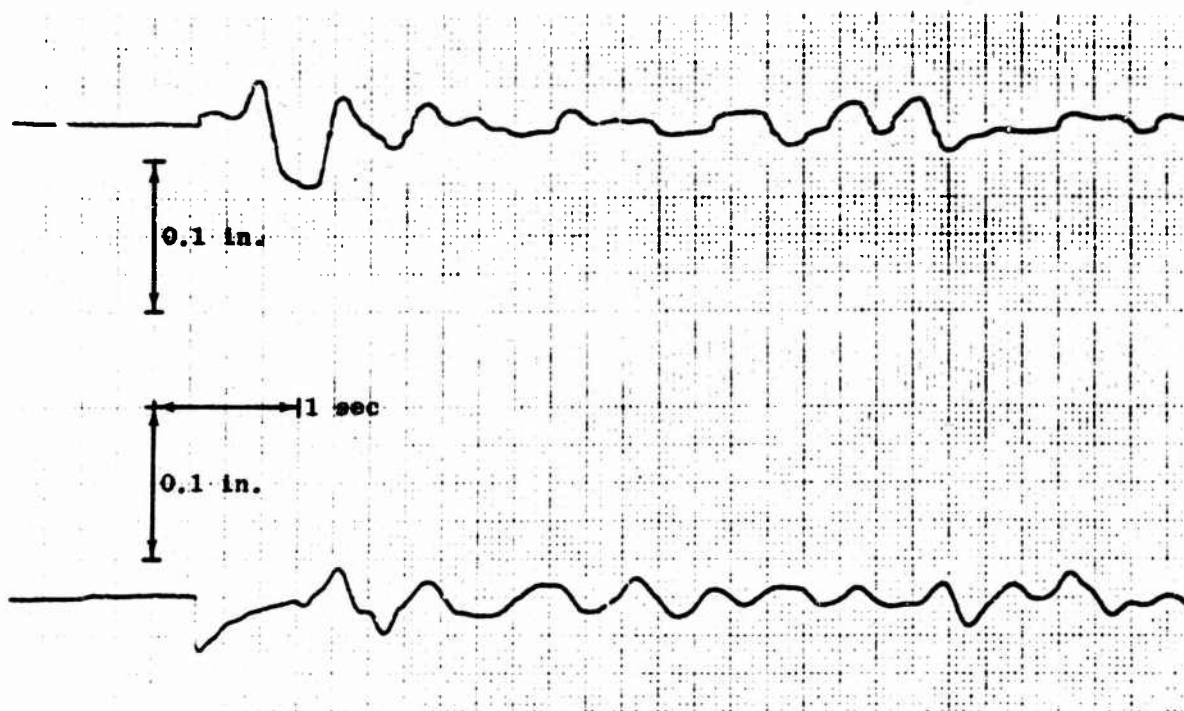
Fig. 79.   Wave Gage Records, Shot 30
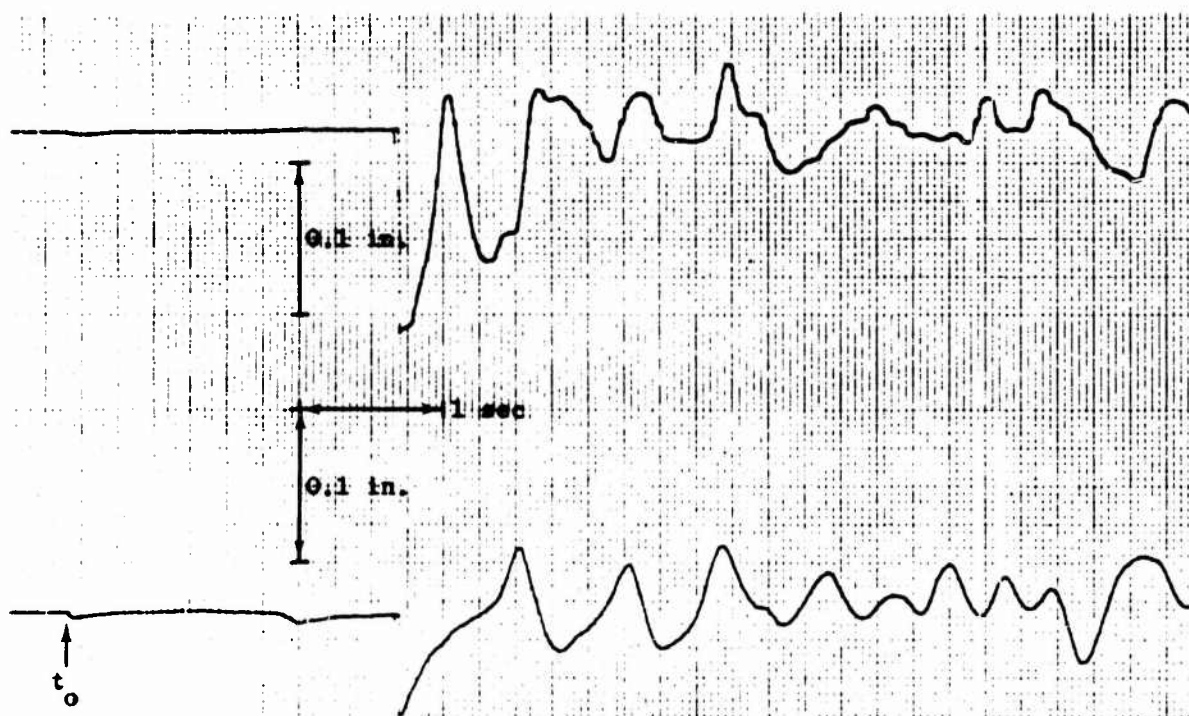

Fig. 80.   Wave Gage Records, Shot 31

Fig. 81. Wave Gage Records, Shot 34

Fig. 82. Wave Gage Records, Shot 38

123

Fig. 83.   Wave Gage Records, Shot 38R

Fig. 84.   Wave Gage Records, Shot 39

124
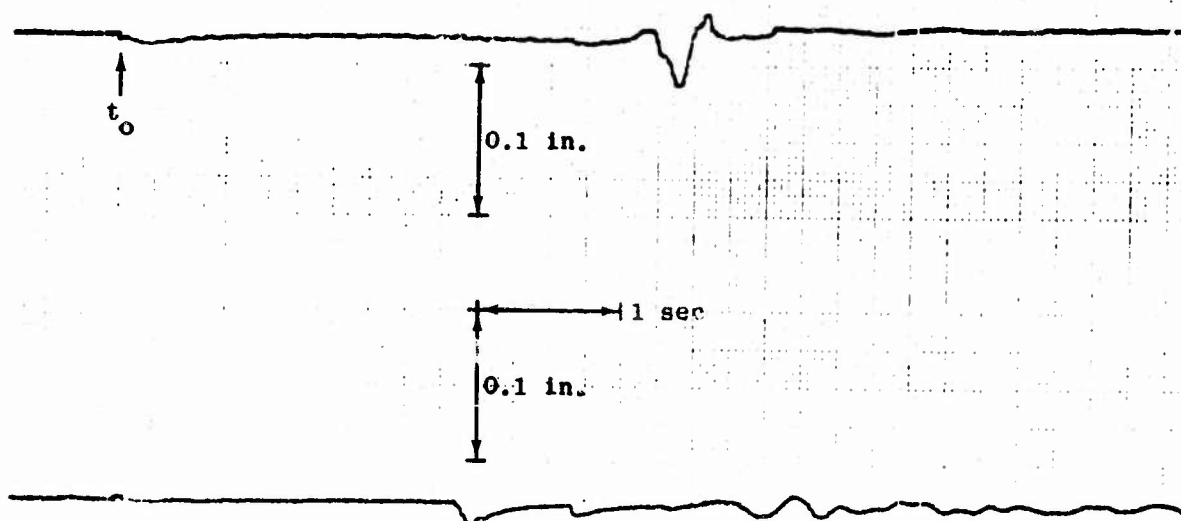
Fig. 85.   Wave Gage Records, Shot 40

Fig. 86.   Wave Gage Records, Shot 42

NOTE: 1. Range R_2 = 18 in.

2. Wire probe axis upward

3. Test numbers indicated
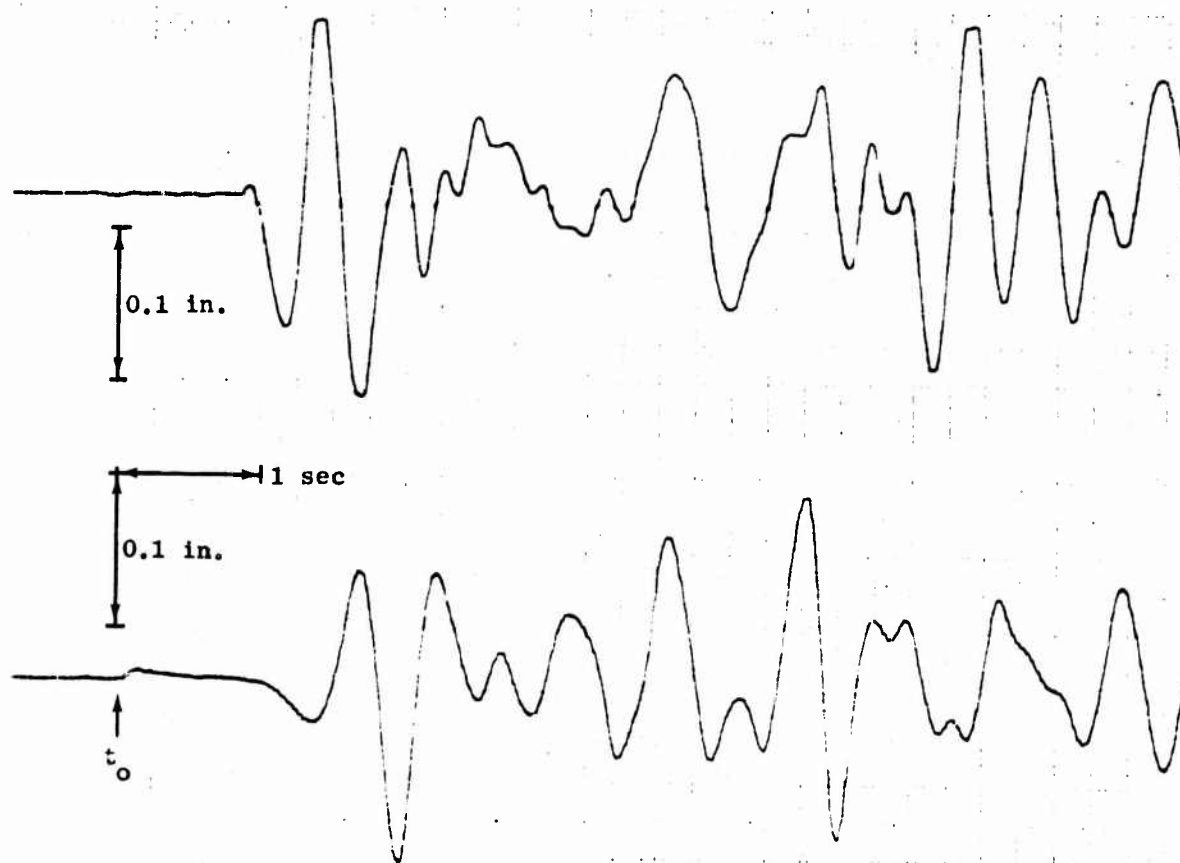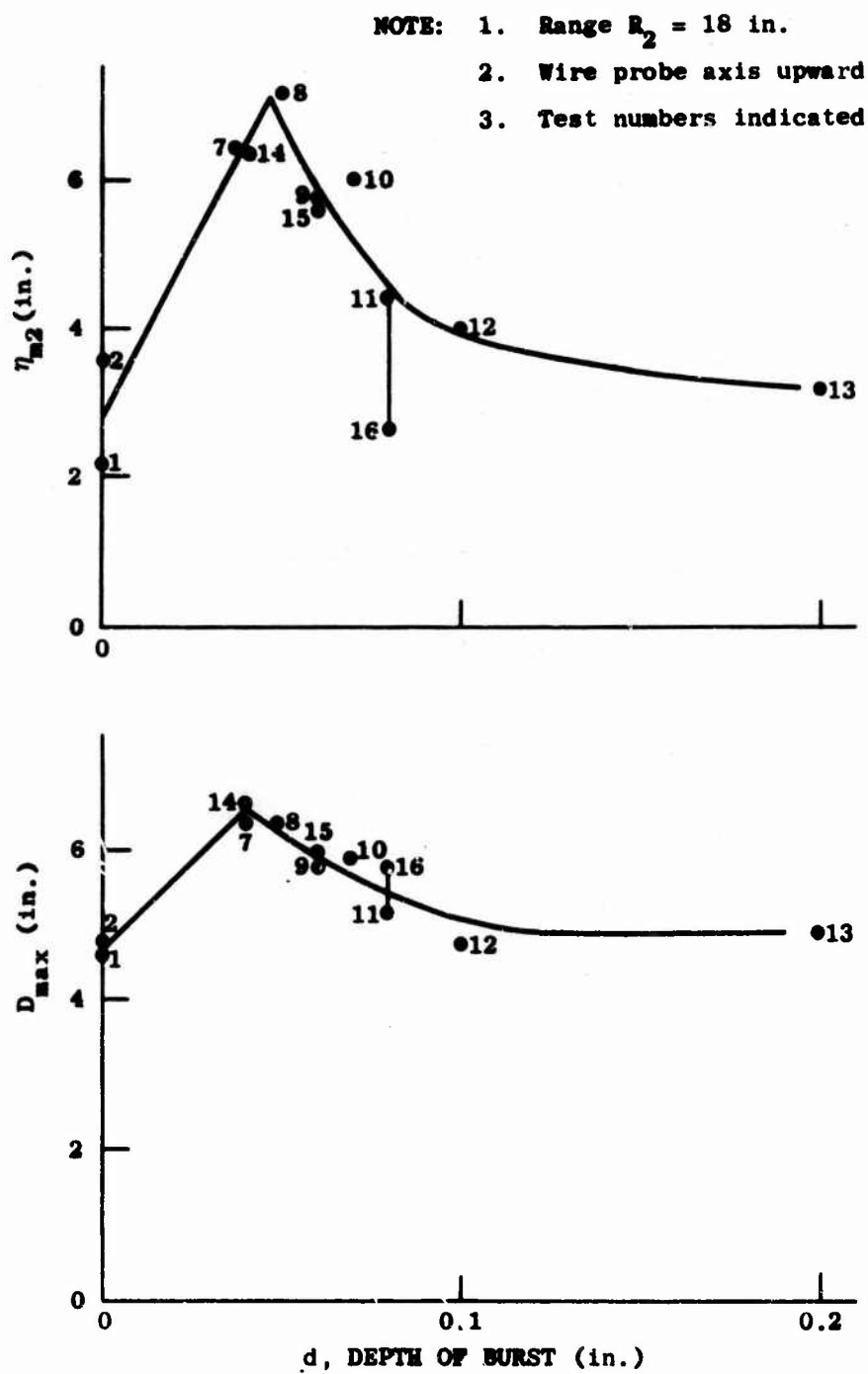

Fig. 87.   Peak Wave Height and Expanded Cavity Diameter vs Depth of
Burst at Normal Atmospheric Pressure in Deep Water

126

NOTE: 1. Range R_2 = 18 in.

2. Wire probe axis upward
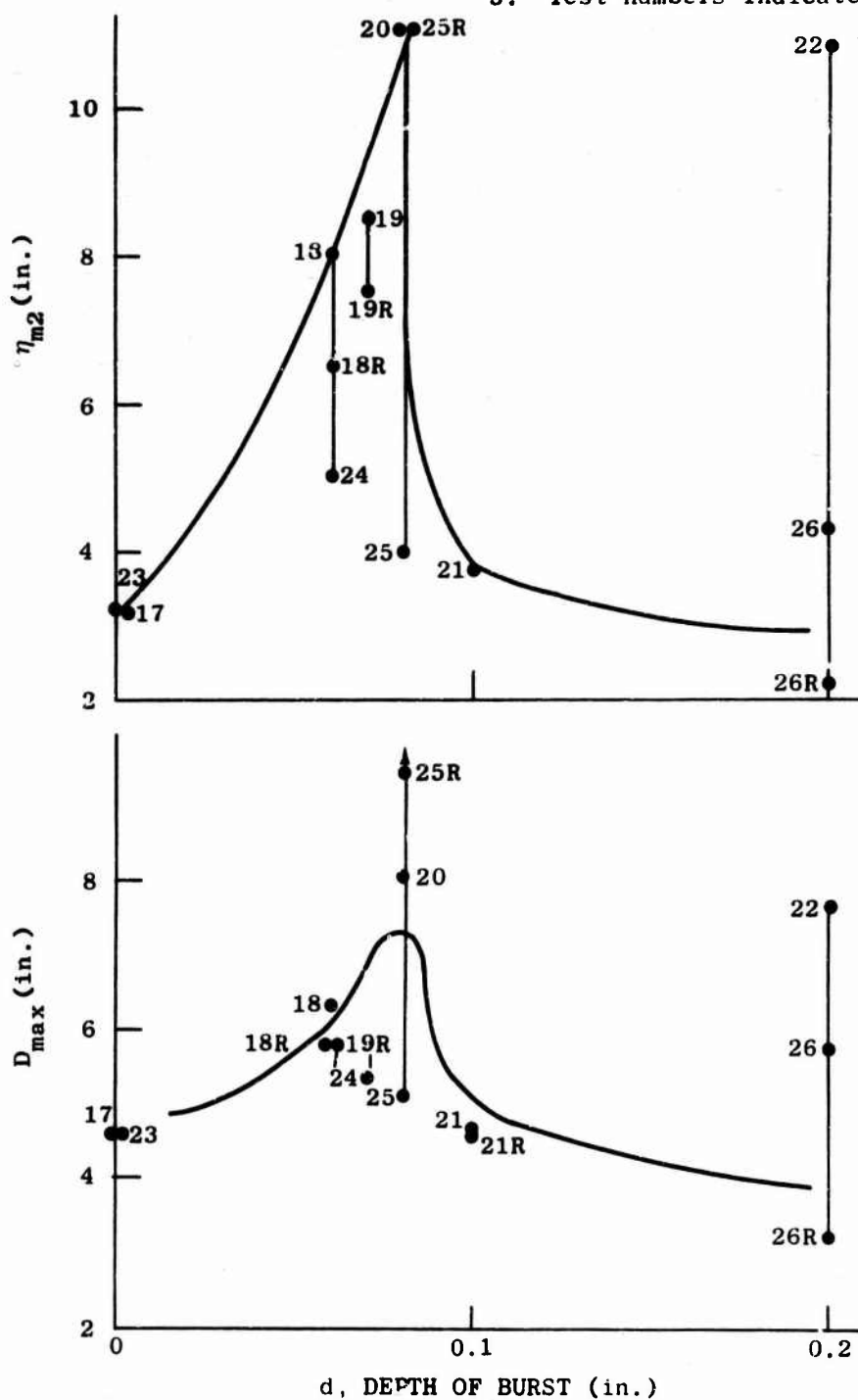
3. Test numbers indicated

Fig. 88. Peak Wave Height and Expanded Cavity Diameter vs Depth of Burst at Half Normal Atmospheric Pressure in Deep Water
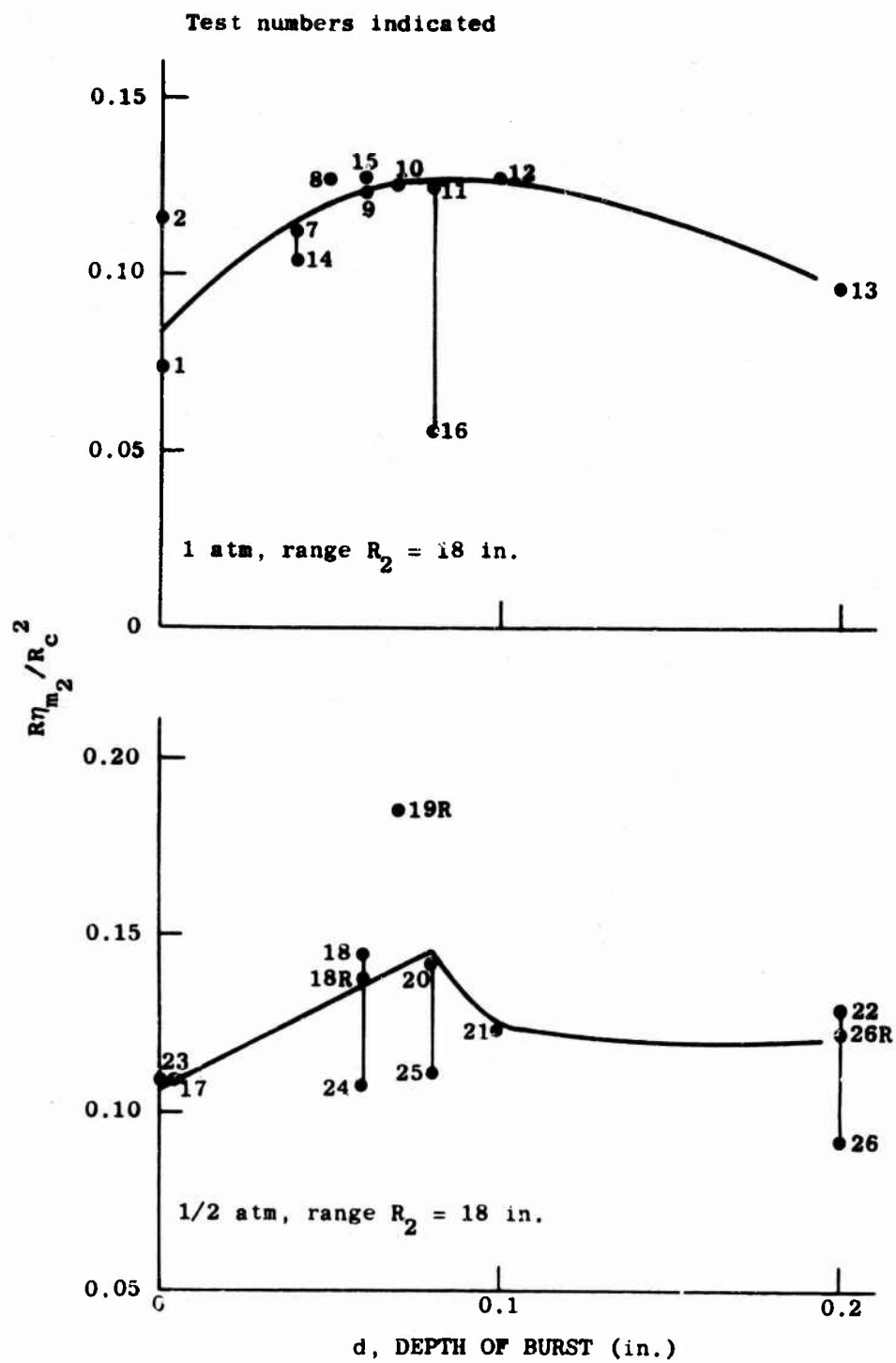
Test numbers indicated

Fig. 89. Dimensionless Peak Wave Height vs Depth of Burst in Deep Water

Section 8

REFERENCES

1. Kriebel, A. R., Hydrodynamic Data from Exploding Wires, URS 679-6, Contract N0014-67-0451, URS Research Company, April 1970.

2. Kriebel, A.R., Analysis of Water Waves Generated Explosively at the Upper Critical Depth, URS 679-1, Contract N0014-67-0451, URS Research Company, January 1968.

3. Kaplan, K., et al., A Study of Explosion-Generated Surface Water Waves, a series of 8 reports, URS 162-1 through 162-8, Contract Nonr-3143(00), URS Research Company, December 1963.

4. Kriebel, A.R., Cavities and Waves from Explosions in Shallow Water, URS 679-5, Contract N0014-67-0451, URS Research Company, October 1969.

5. Hendricks, J.W. and D.L. Smith, Above-and-Below Surface Effects of One-Pound Underwater Explosions, Hydra I, TR-480, NRDL, October 1960.

6. Walter, D.F., Explosion-Generated Wave Tests, Mono Lake, California, Ground and Aerial Photography, URS 654-2, Contract Nonr-4959(00), URS Research Company, January 1966.

7. Hudson, G.E., The Analysis of Data from Some Small Explosions in Shallow Water, Contract Nord 14663, College of Engineering Research Division, New York University, August 1956.